Astro/Phys 224 Spring 2012

Origin and Evolution of the Universe

Week 7

Galaxy Formation Simulations and SAMs

Joel Primack

University of California, Santa Cruz

The Bolshoi simulation

ART code

250Mpc/h Box
LCDM

σ_8 = 0.82
h = 0.70

8G particles
1kpc/h force resolution
1e8 Msun/h mass res

dynamical range 262,000
time-steps = 400,000

NASA AMES
supercomputing center
Pleiades computer
13824 cores
12TB RAM
75TB disk storage
6M cpu hrs
18 days wall-clock time

Cosmological parameters are consistent with the latest observations

Force and Mass Resolution are nearly an order of magnitude better than Millennium-I

Force resolution is the same as Millennium-II, in a volume 16x larger

Halo finding is complete to $V_{circ} > 50$ km/s, using both BDM and ROCKSTAR halo finders

Bolshoi and MultiDark halo catalogs were released in September 2011 at Astro Inst Potsdam; Merger Trees will soon be available

BOLSHOI
Merger Tree
Peter Behroozi, et al.

Time: 13664 Myr Ago
Timestep Redshift: 14.083
Radius Mode: Rvir
Focus Distance: 6.1
Aperture: 40.0
World Rotation: (216.7, 0.06, -0.94, -0.34)
Trackball Rotation: (0.0, 0.00, 0.00, 0.00)
Camera Position: (0.0, 0.0, -6.1)

1000 Mpc/h

BIG BOLSHOI

7 kpc/h resolution, complete to Vcirc > 170 km/s

Anatoly Klypin, Stefan Gottloeber, Joel Primack, Gustavo Yepes, et al.

Zoom-in on the Largest Cluster in **BIG BOLSHOI**

Anatoly Klypin, Stefan Gottloeber, Joel Primack, Gustavo Yepes, et al.

MultiDark Hydro Simulation of Largest Cluster in **BIG BOLSHOI**

Anatoly Klypin, Stefan Gottloeber, Joel Primack, Gustavo Yepes, et al.

UNDERSTANDING GALAXY CORRELATIONS

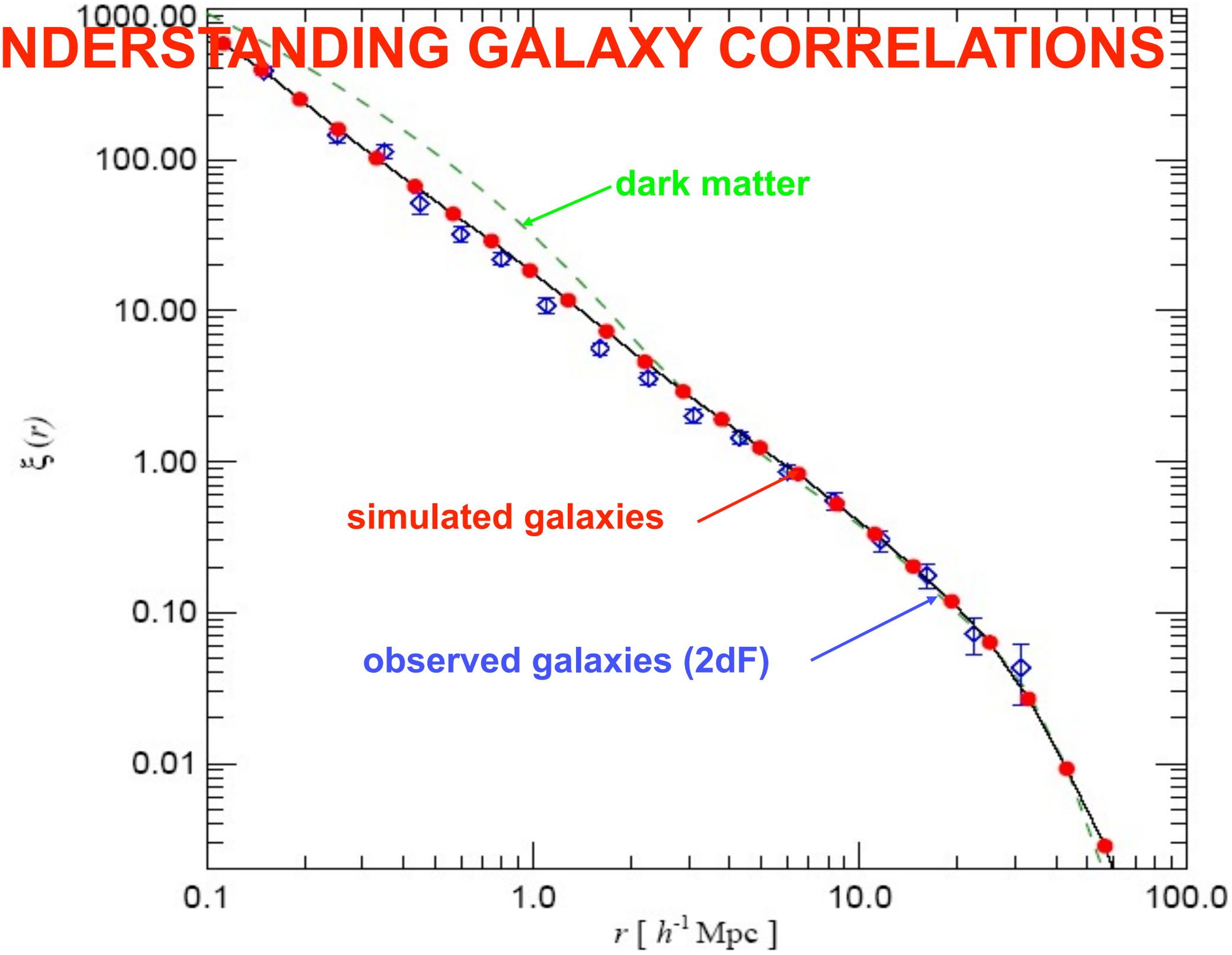

Galaxy 2-point correlation function at the present epoch.

Springel et al. 2005

ΛCDM + HAM* PREDICTS EVOLUTION IN THE GALAXY CORRELATION FUNCTION

$\xi_{gg}(r)$

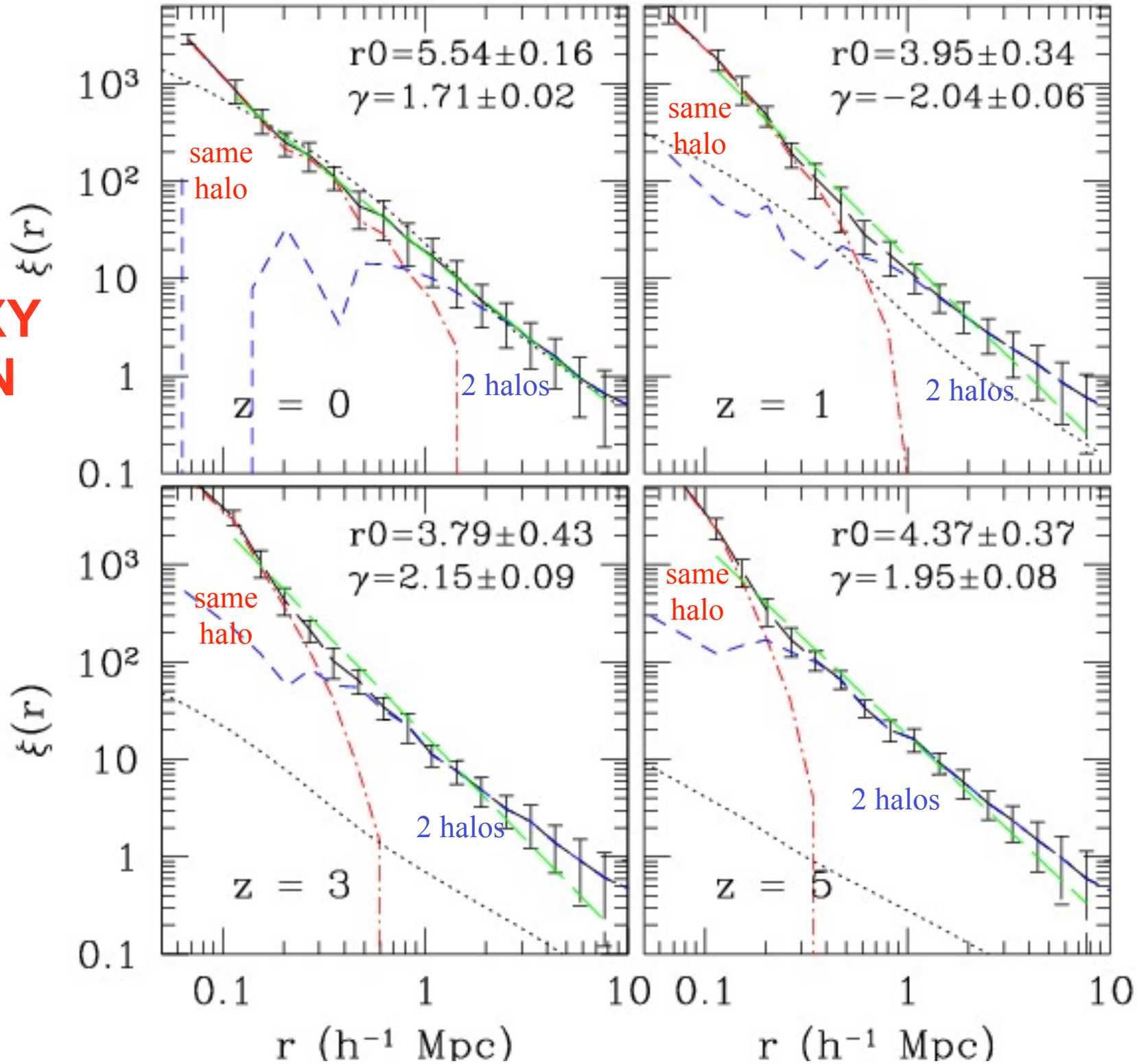

* HAM = halo abundance matching

FIG. 8.— Evolution of the two-point correlation function in the $80h^{-1}$ Mpc simulation. The solid line with error bars shows the clustering of halos of the fixed number density $n = 5.89 \times 10^{-3}h^3$ Mpc^{-3} at each epoch. The error-bars indicate the "jack-knife" one sigma errors and are larger than the Poisson error at all scales. The dot-dashed and dashed lines show the corresponding one- and two-halo term contributions. The long-dashed lines show the power-law fit to the correlation functions in the range of $r = [0.1 - 8h^{-1}$ Mpc$]$. Although the correlation functions can be well fit by the power law at $r \gtrsim 0.3h^{-1}$ Mpc in each epoch, at $z > 0$ the correlation function steepens significantly at smaller scales due to the one-halo term.

Kravtsov, Berlind, Wechsler, Klypin, Gottloeber, Allgood, & Primack 2004

Galaxy clustering in SDSS at z~0 agrees with ΛCDM predictions

$n(>V_{\mathrm{max,acc}})=n(>L)$

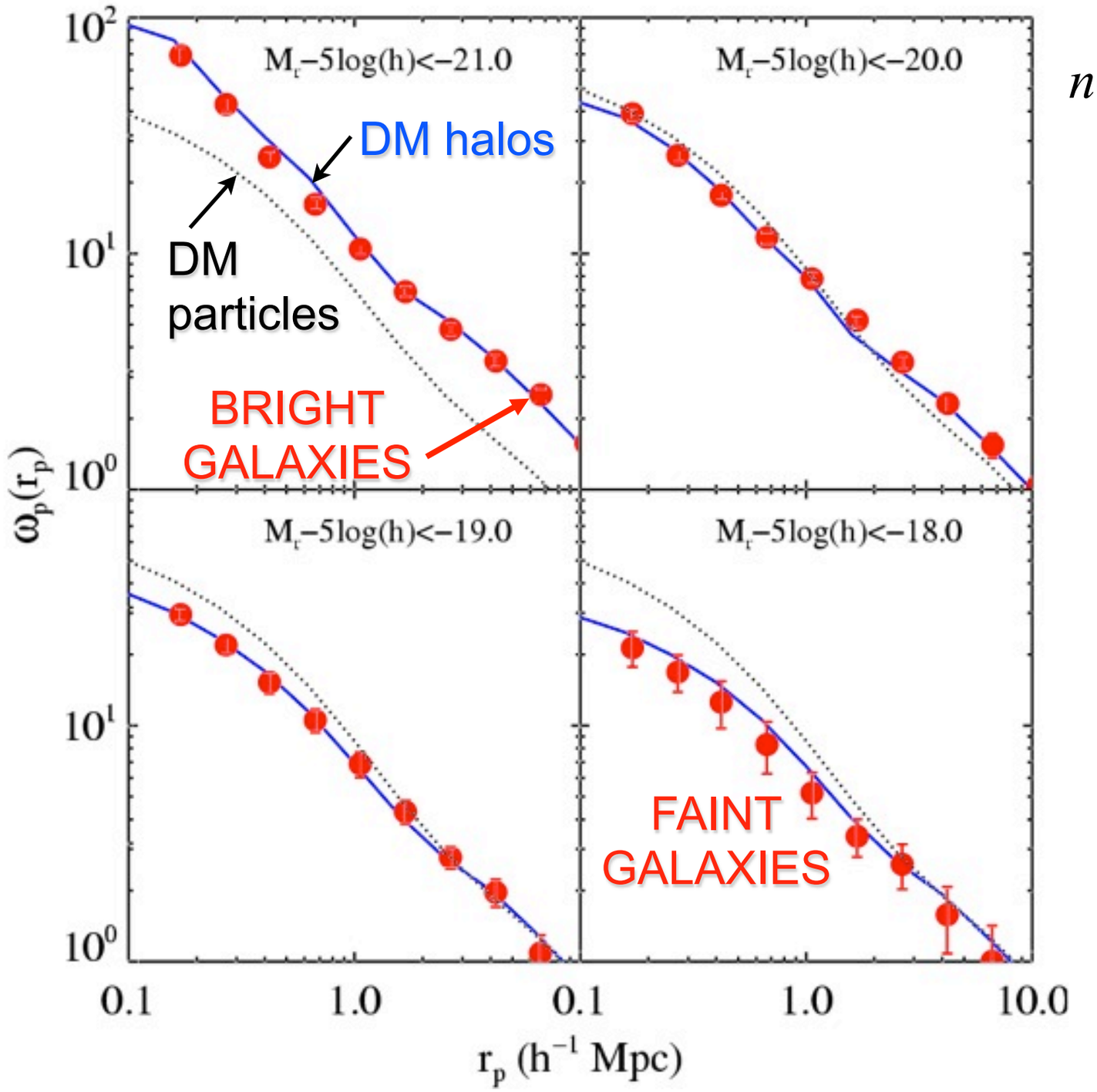

projected 2-point correlation function

projected separation

Conroy, Wechsler & Kravtsov 2006, ApJ 647, 201

and at redshift z~1 (DEEP2)!

$$n(>V_{\mathrm{max,acc}})=n(>L)$$

projected 2-point correlation function

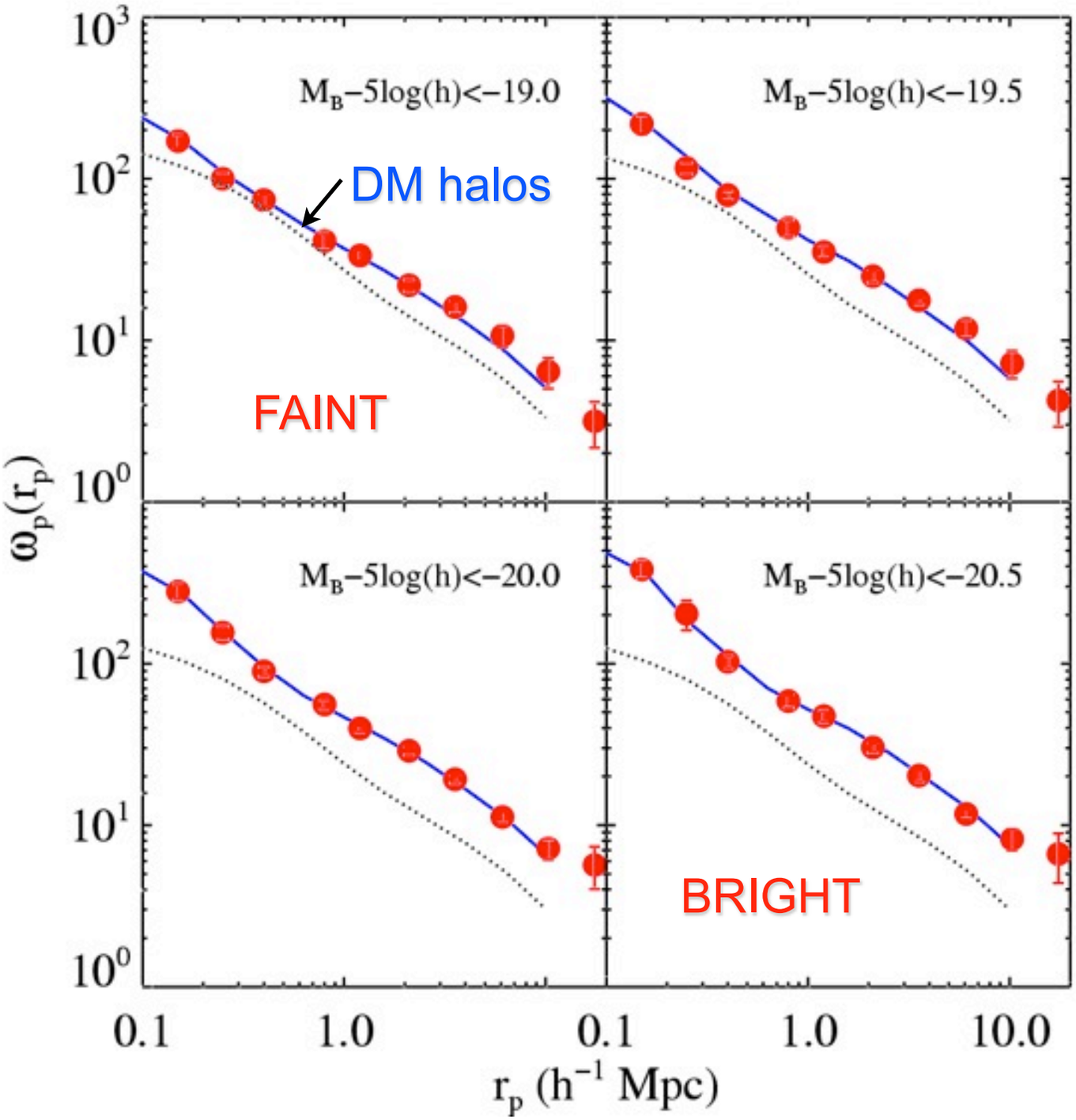

projected separation

Conroy, Wechsler & Kravtsov 06

and at z~4-5 (LBGs, Subaru)!!

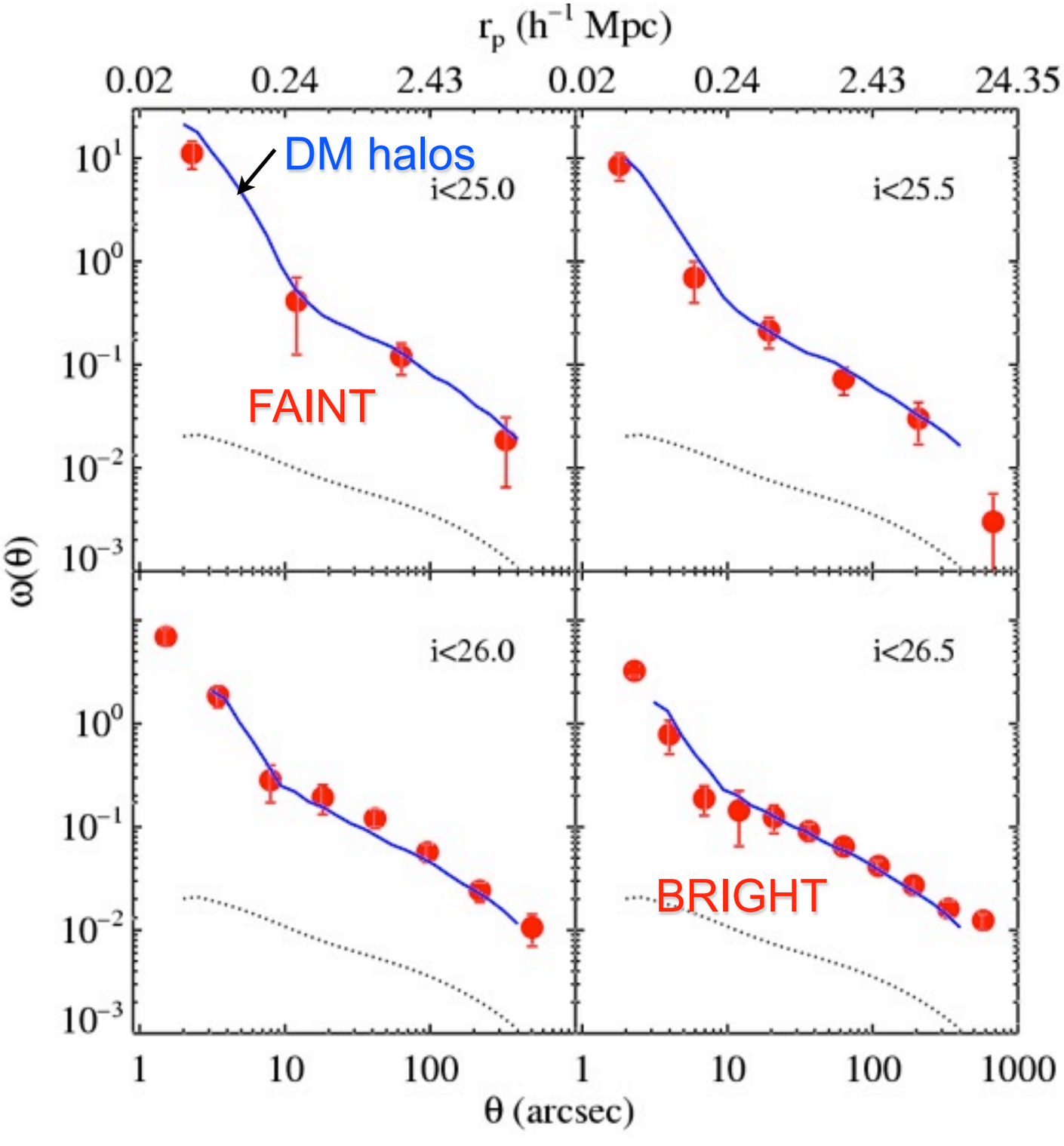

$n(>V_{\mathrm{max,acc}})=n(>L)$

angular 2-point correlation function

projected separation

Conroy, Wechsler & Kravtsov 06

GRAVITATIONALLY CONSISTENT HALO CATALOGS AND MERGER TREES FOR PRECISION COSMOLOGY

PETER S. BEHROOZI, MICHAEL T. BUSHA, RISA H. WECHSLER
Physics Department, Stanford University; Department of Particle and Particle Astrophyiscs, SLAC National Accelerator Laboratory; Kavli Institute for Particle Astrophysics and Cosmology Stanford, CA 94305

ANATOLY KLYPIN
Astronomy Department, New Mexico State University, Las Cruces, NM, 88003

JOEL PRIMACK
Department of Physics, University of California at Santa Cruz, Santa Cruz, CA 95064

Draft version January 28, 2011

Preliminary

ABSTRACT

We present a new algorithm for generating merger trees and halo catalogs which explicitly ensures consistency of halo properties (mass, position, velocity, radius) across timesteps. We use this algorithm to generate merger trees for two large simulations (Bolshoi and Consuelo) and discuss the relative consistency of two halo finders (BDM and SUBFIND). Finally, we use the merger trees thus generated to examine the question of when satellite halos reached their peak mass. We find that the peak mass for infalling halos occurs at roughly 3 $R_{\rm vir}$ of the final host halo, which suggests that dark matter stripping occurs even before halos cross the virial radius of a larger halo.

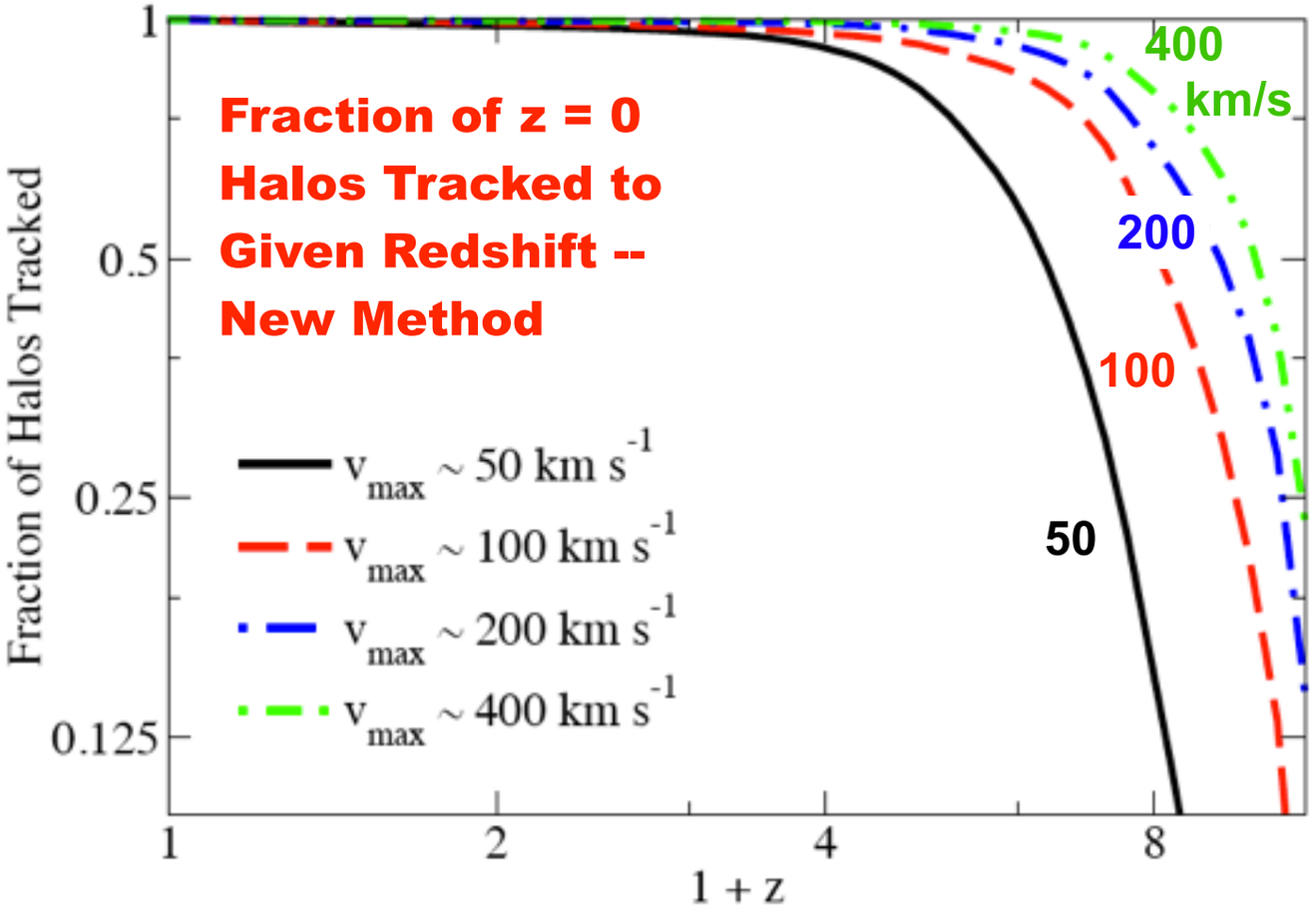

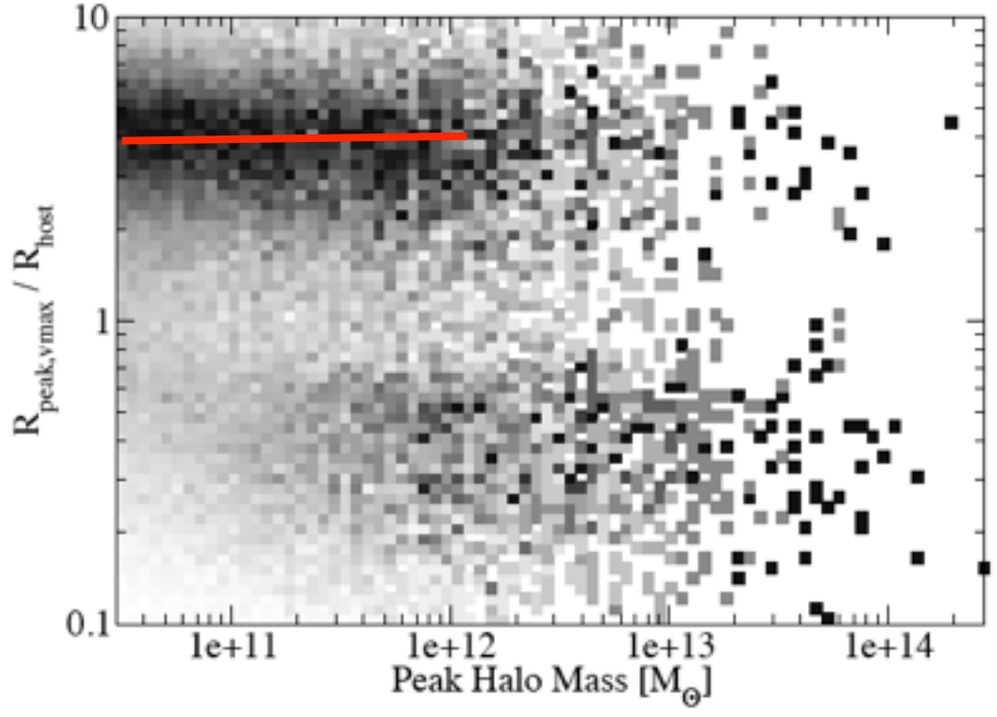

FIG. 9.— Scatter plot of $R_{\rm peak}/R_{\rm host}$ as a function of subhalo mass at $z = 0$ in Bolshoi. $R_{\rm peak}$ is the distance from the final host at which the subhalo had its maximum $v_{\rm max}$; $R_{\rm host}$ is the radius of the current host halo at the epoch of peak subhalo $v_{\rm max}$. The region below a ratio of 1 is largely populated by subhalos which were not tracked outside of the virial radius; see Figure 7.

Halo Abundance Matching

Trujillo-Gomez, Klypin, Primack, & Romanowsky ApJ 2011

To investigate the statistics of galaxies and their relation to host DM halos as predicted by the LCDM model, we predicted the properties of our model galaxies using the following Halo Abundance Matching (HAM) procedure:

1. Using the merger tree of each DM halo and subhalo, obtain V_{acc} = the peak value of the circular velocity over the history of the halo (this is typically the maximum circular velocity of the halo when the halo is first accreted). Perform abundance matching of the velocity function of the halos to the LF of galaxies to obtain the luminosity of each model galaxy.

2. Perform abundance matching of the velocity function to the stellar mass function of galaxies to obtain the stellar mass of each model galaxy.

3. Use the observed gas-to-stellar mass ratio as a function of stellar mass to assign cold gas masses to our model galaxies. The stellar mass added to the cold gas mass becomes the total baryonic mass.

4. Using the density profiles of the DM halos, obtain the circular velocity at 10 kpc (V_{10}) from the center of each halo. Multiply the DM mass, as it comes from simulations, by the factor $(1 - f_{bar})$, where f_{bar} is the cosmological fraction of baryons. This is the dark-matter-only contribution. Add the contribution to V_{10} of the baryon mass from step 3 assuming it is enclosed within a radius of 10 kpc.

5. Optionally implement the BFFP86 correction to V_{10} due to the adiabatic contraction of the DM halos from the infall of the baryon component to the center.

Bolshoi $w_p(r_p)$ by Halo Abundance Matching vs. SDSS Observations

The correlation function of SDSS galaxies vs. Bolshoi galaxies using halo abundance matching, with scatter using our stochastic abundance matching method. This results in a better than 20% agreement with SDSS. *Top left:* correlation functinon in three magnitude bins, showing Poisson uncertainties as thin lines. *Remaining panels:* correlation function in each luminosity bin compared with SDSS galaxies (points with error bars: Zehavi et al. 2010).

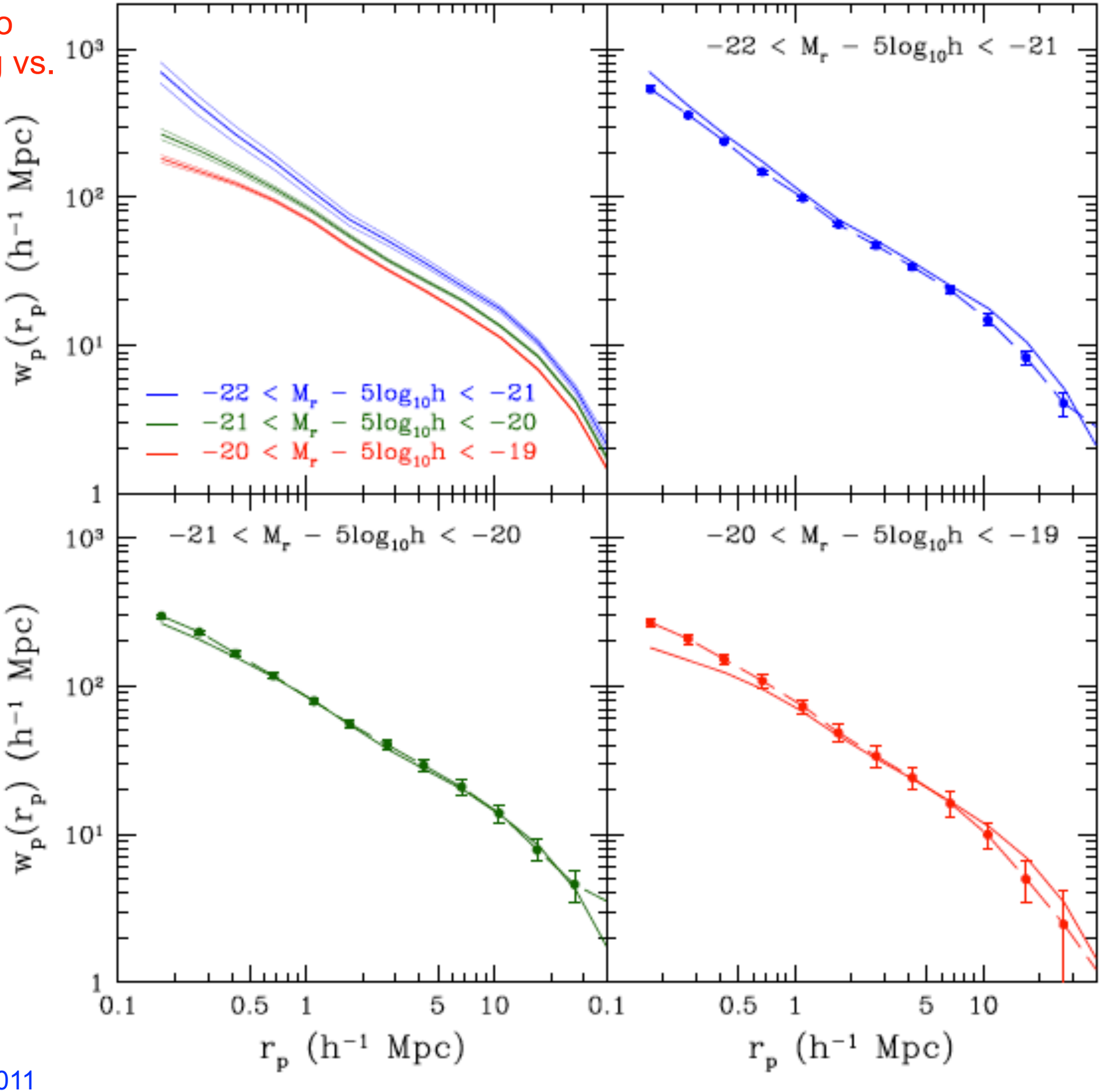

Trujillo-Gomez, Klypin, Primack, & Romanowsky 2011

Millennium-I and II $w_p(r_p)$ by SAM vs. SDSS Observations

——— MS

---------- MS-II

The correlations are seriously overestimated at small separations for lower masses because the high σ_8 = 0.90 produces too many massive halos, which contain pairs of such subhalos.

Guo, White, et al. 2011 MN

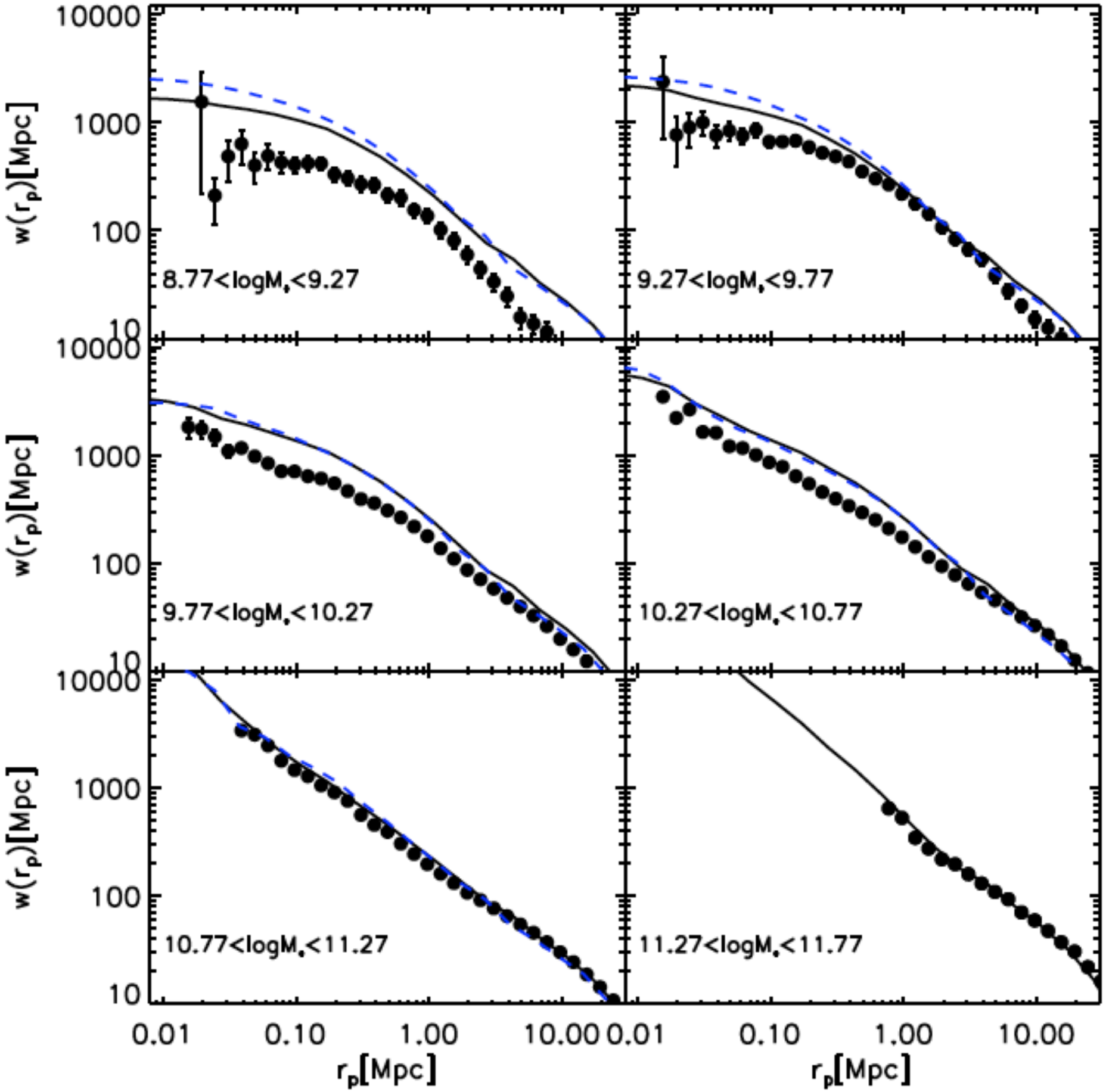

The Milky Way has two large satellite galaxies,
the small and large Magellanic Clouds

The Bolshoi simulation predicts the likelihood of this

Statistics of MW-satellite analogs

Liu, Gerke & Wechsler

- Search SDSS DR7 Co-Add data to look for analogues of the LMC/SMC in extragalactic hosts
- SDSS Co-Add Data:
  - Stripe-82 in the SDSS was observed ~370 times, complete to observed magnitude limit $M_r = 23.6$ over ~270 sq. deg; main sample spectroscopy (mostly) complete down to $M_r = 17.77$
  - Photometric redshifts calculated for the remaining objects using a template method.
    - Training/validation set taken from CNOC2, SDSS main, and DEEP2 samples.
    - Measured scatter: $\Delta z = 0.02$
  - 23,000 spectroscopic galaxy (non-QSO) candidates in Stripe 82 with $m_r < 17.77$
- Magnitude Cuts:
  - Identify all objects with absolute $^{0.1}M_r = -20.73 \pm 0.2$ and observed $m_r < 17.6$
  - Lets us probe out to $z = 0.15$, a volume of roughly 500 $(Mpc/h)^3$
  - leaves us with 3,200 objects.
- Isolation Criteria: exclude objects in clusters, since those are likely biased -- exclude candidates with neighbors brighter than itself within a cylinder defined by:
  - radial distance 1000 km/s -- the velocity dispersion of a typical cluster and $\Delta z \approx 0.01$ at our relevant redshifts.
  - projected angular distance $R_{iso} = 0.7$ Mpc
  - leaves us with 1,332 hosts.

Statistics of MW bright satellites: SDSS data vs. Bolshoi simulation

- Apply the same absolute magnitude and isolation cuts to Bolshoi+SHAM galaxies as to SDSS:
  - Identify all objects with absolute $^{0.1}M_r = -20.73 \pm 0.2$ and observed $m_r < 17.6$
  - Probe out to z = 0.15, a volume of roughly 500 (Mpc/h)^3
  - leaves us with 3,200 objects.
- Comparison of Bolshoi with SDSS observations is in close agreement, well within observed statistical error bars.

# of Subs	Prob (obs)	Prob (sim)
0	60%	61%
1	22%	25%
2	13%	8.1%
3	4%	3.2%
4	1%	1.4%
5	0%	0.58%

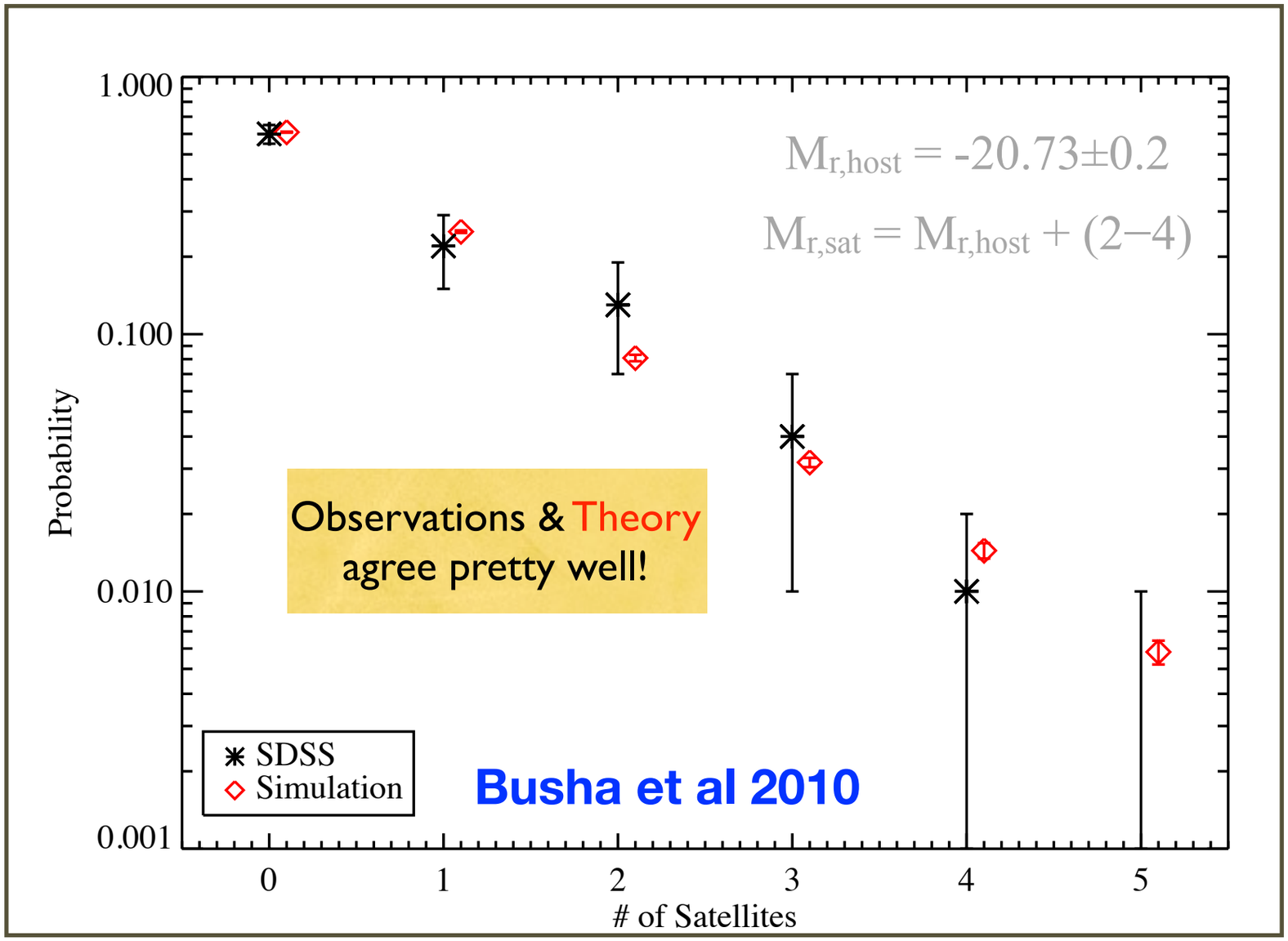

Every case agrees within observational errors!

Risa Wechsler

SMALL-SCALE STRUCTURE IN THE SDSS AND ΛCDM: ISOLATED $\sim L_*$ GALAXIES WITH BRIGHT SATELLITES

ERIK J. TOLLERUD[1], MICHAEL BOYLAN-KOLCHIN[1,2], ELIZABETH J. BARTON[1], JAMES S. BULLOCK [1], CHRISTOPHER Q. TRINH[3,1]

Draft version March 11, 2011

Similarly good agreement with SDSS for brighter satellites with spectroscopic redshifts compared with Millennium-II using abundance matching.

We use a volume-limited spectroscopic sample of isolated galaxies in the Sloan Digital Sky Survey (SDSS) to investigate the frequency and radial distribution of luminous ($M_r \lesssim -18.3$) satellites like the Large Magellanic Cloud (LMC) around $\sim L_*$ Milky Way analogs and compare our results object-by-object to ΛCDM predictions based on abundance matching in simulations. We show that 12% of Milky Way-like galaxies host an LMC-like satellite within 75 kpc (projected), and 42% within 250 kpc (projected). This implies $\sim 10\%$ have a satellite within the distance of the LMC, and $\sim 40\%$ of L_* galaxies host a bright satellite within the virialized extent of their dark matter halos. Remarkably, the simulation reproduces the observed frequency, radial dependence, velocity distribution, and luminosity function of observed secondaries exceptionally well, suggesting that ΛCDM provides an accurate reproduction of the observed Universe to galaxies as faint as $L \sim 10^9 L_\odot$ on ~ 50 kpc scales. When stacked, the observed projected pairwise velocity dispersion of these satellites is $\sigma \simeq 160\ \mathrm{km\,s^{-1}}$, in agreement with abundance-matching expectations for their host halo masses. Finally, bright satellites around L_* primaries are significantly *redder* than typical galaxies in their luminosity range, indicating that environmental quenching is operating within galaxy-size dark matter halos that typically contain only a single bright satellite. This redness trend is in stark contrast to the Milky Way's LMC, which is unusually blue even for a field galaxy. We suggest that the LMC's discrepant color might be further evidence that it is undergoing a triggered star-formation event upon first infall.

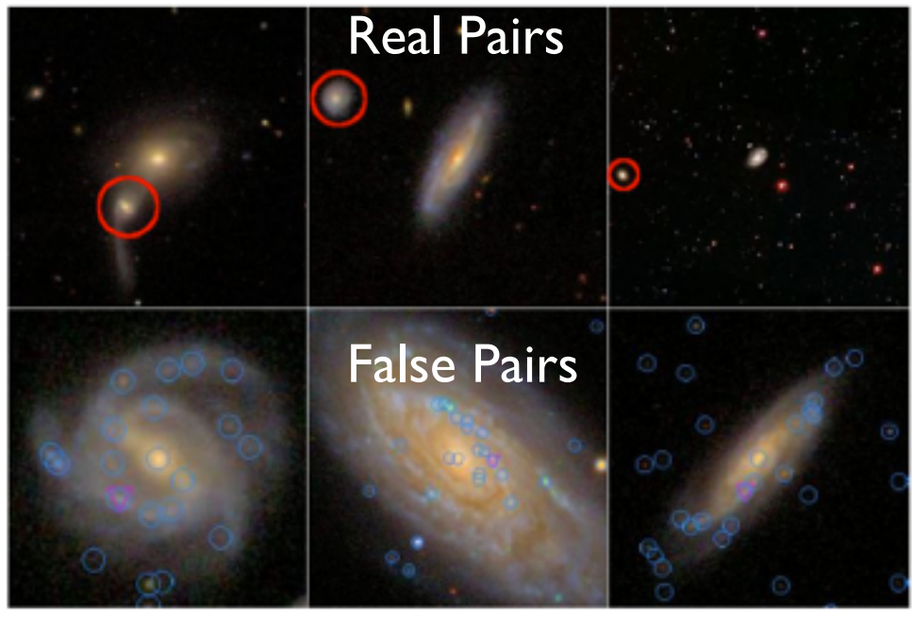

FIG. 1.— Examples of SDSS primary/secondary pairs in the clean sample (upper) and false pairs (lower). Secondaries identified by our criteria (see text) are marked with red circles (upper panels) or magenta triangles (lower panels). The upper three are all in the clean sample (have redshifts close to the primary) and span a range of projected separations. For the lower three images, blue circles are SDSS pipeline photometric objects, clearly showing the identification of HII regions as photometric objects. For these same lower three, the secondaries are clearly HII regions in the primary (or satellites that are indistinguishable from HII regions). We visually identify and remove all pairs of this kind from our sample.

Good agreement between simulated and observed pairwise velocities

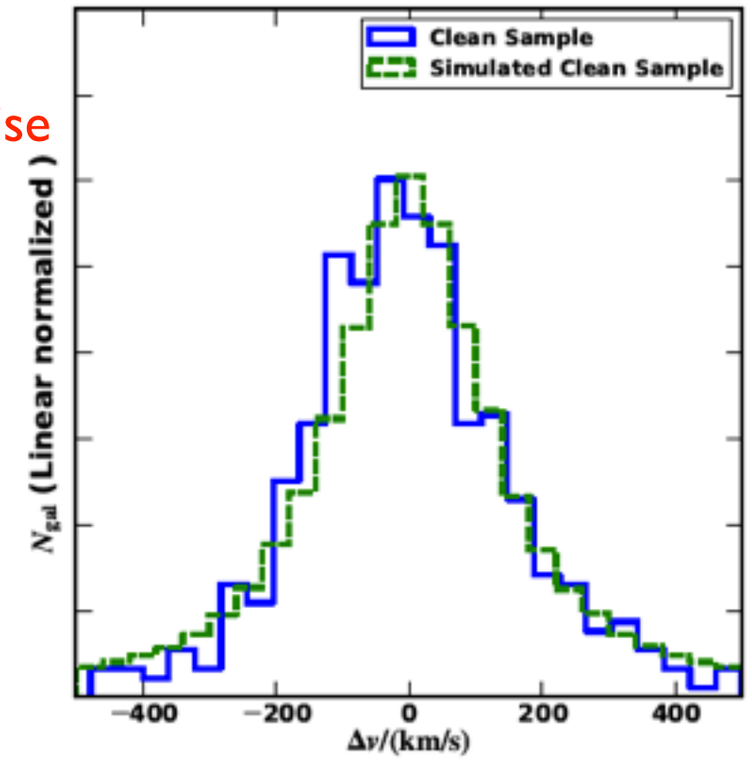

FIG. 6.— Distribution of $\Delta v \equiv c(z_{\rm pri} - z_{\rm sec})$ for the clean sample (solid blue histogram), the clean-like sample from MS-II (dashed green). The KS test yields $p_{\rm KS} = 33\%$. The pairwise velocity dispersion in the observed sample is $\sigma = 161\ \mathrm{km\,s^{-1}}$.

STELLAR MASS – HALO MASS RELATION

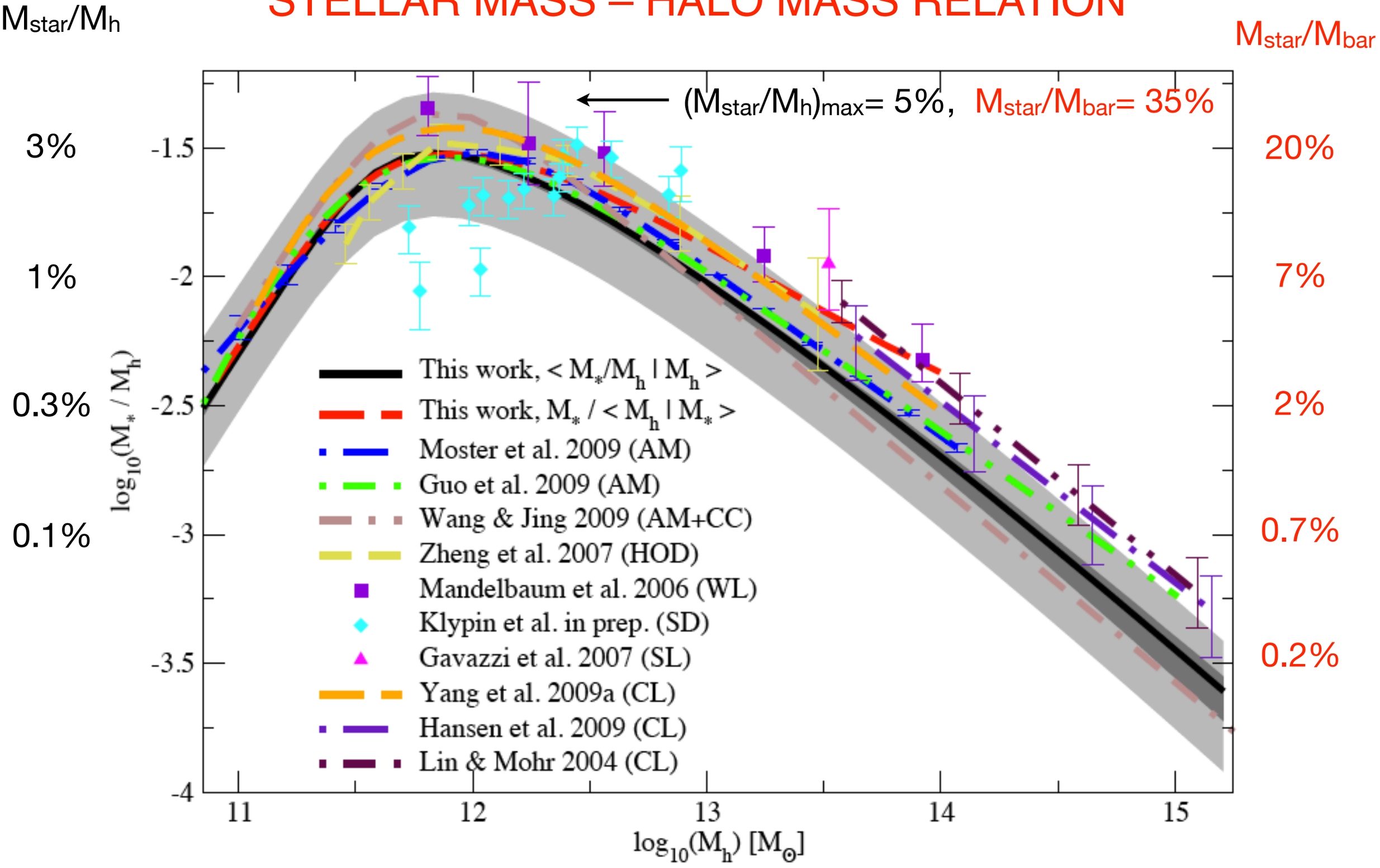

Comparison of best-fit model of Behroozi, Conroy, Wechsler (2010) at $z = 0.1$ to previously published results.

STELLAR MASS – HALO MASS RELATION

M_{star}/M_h

M_{star}/M_{bar}

At higher redshifts

3%

1%

0.3%

0.1%

20%

7%

2%

0.7%

0.2%

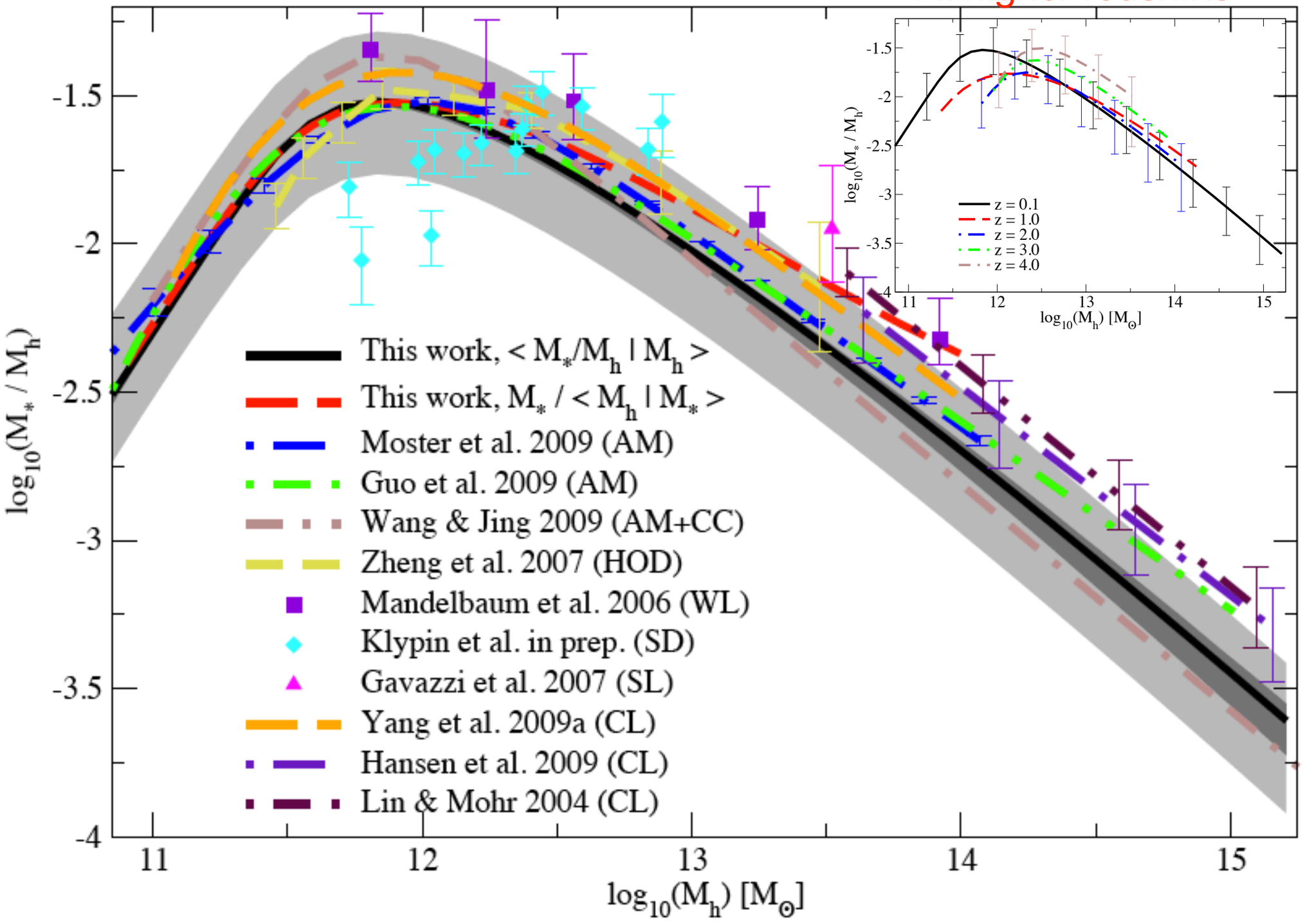

Comparison of best-fit model of Behroozi, Conroy, Wechsler (2010) at $z = 0.1$ to previously published results.

Bolshoi Sub-Halo Abundance Matching

Luminosity-Velocity Relation

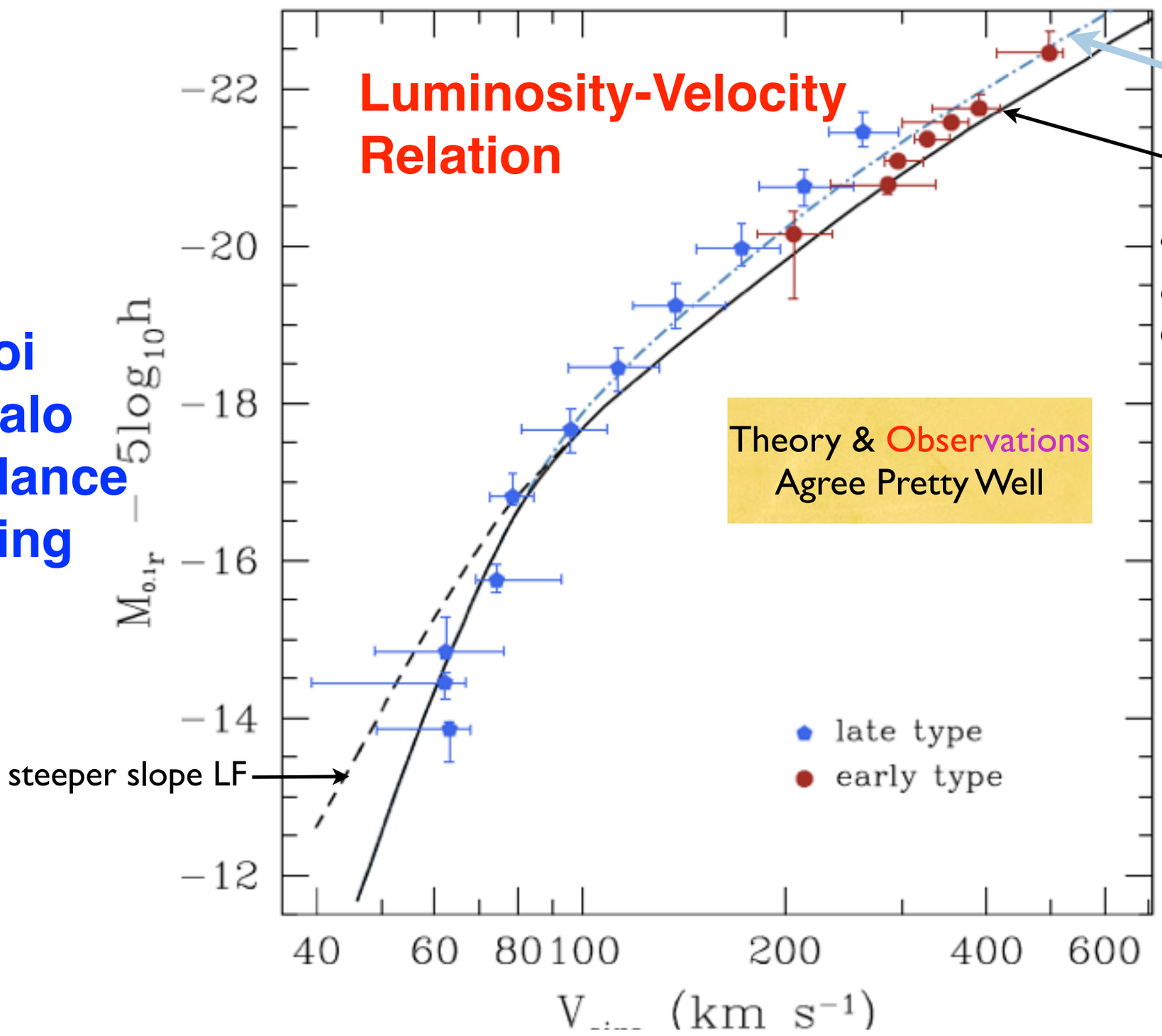

median Vcirc without AC

median Vcirc with AC

"AC" = Adiabatic Contraction of dark matter halos when baryons cool & condense to halo centers, following Blumenthal, Faber, Flores, & Primack 1986

Theory & Observations Agree Pretty Well

Trujillo-Gomez, Klypin, Primack, & Romanowsky arXiv: 1005.1289 ApJ

Fig. 4.— Comparison of the observed LuminosityVelocity relation with the predictions of the ΛCDM model. The solid curve shows the median values of $^{0.1}r$-band luminosity vs. circular velocity for the model galaxy sample. The circular velocity for each model galaxy is based on the peak circular velocity of its host halo over its entire history, measured at a distance of 10 kpc from the center including the cold baryonic mass and the standard correction due to adiabatic halo contraction. The dashed curve show results for a steeper ($\alpha = -1.34$) slope of the LF. The dot-dashed curve shows predictions after adding the baryon mass but without adiabatic contraction. Points show representative observational samples.

Bolshoi Sub-Halo Abundance Matching

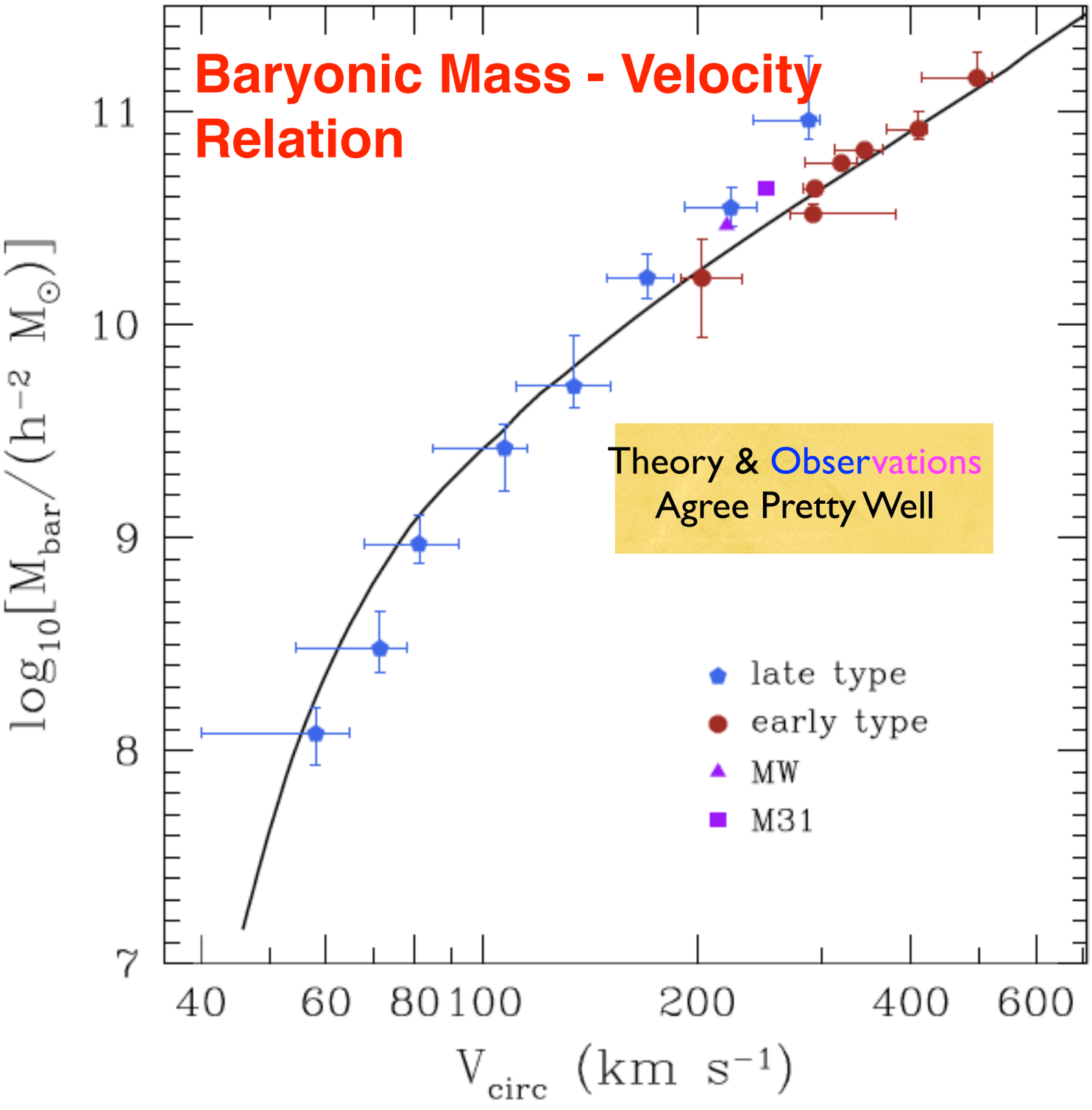

Trujillo-Gomez, Klypin, Primack, & Romanowsky arXiv: 1005.1289 ApJ

Fig. 10.— Mass in cold baryons as a function of circular velocity. The solid curve shows the median values for the ΛCDM model using halo abundance matching. The cold baryonic mass includes stars and cold gas and the circular velocity is measured at 10 kpc from the center while including the effect of adiabatic contraction. For comparison we show the individual galaxies of several galaxy samples. Intermediate mass galaxies such as the Milky Way and M31 lie very close to our model results.

Bolshoi Sub-Halo Abundance Matching

Discrepancy due to incomplete observations or ΛCDM failure?

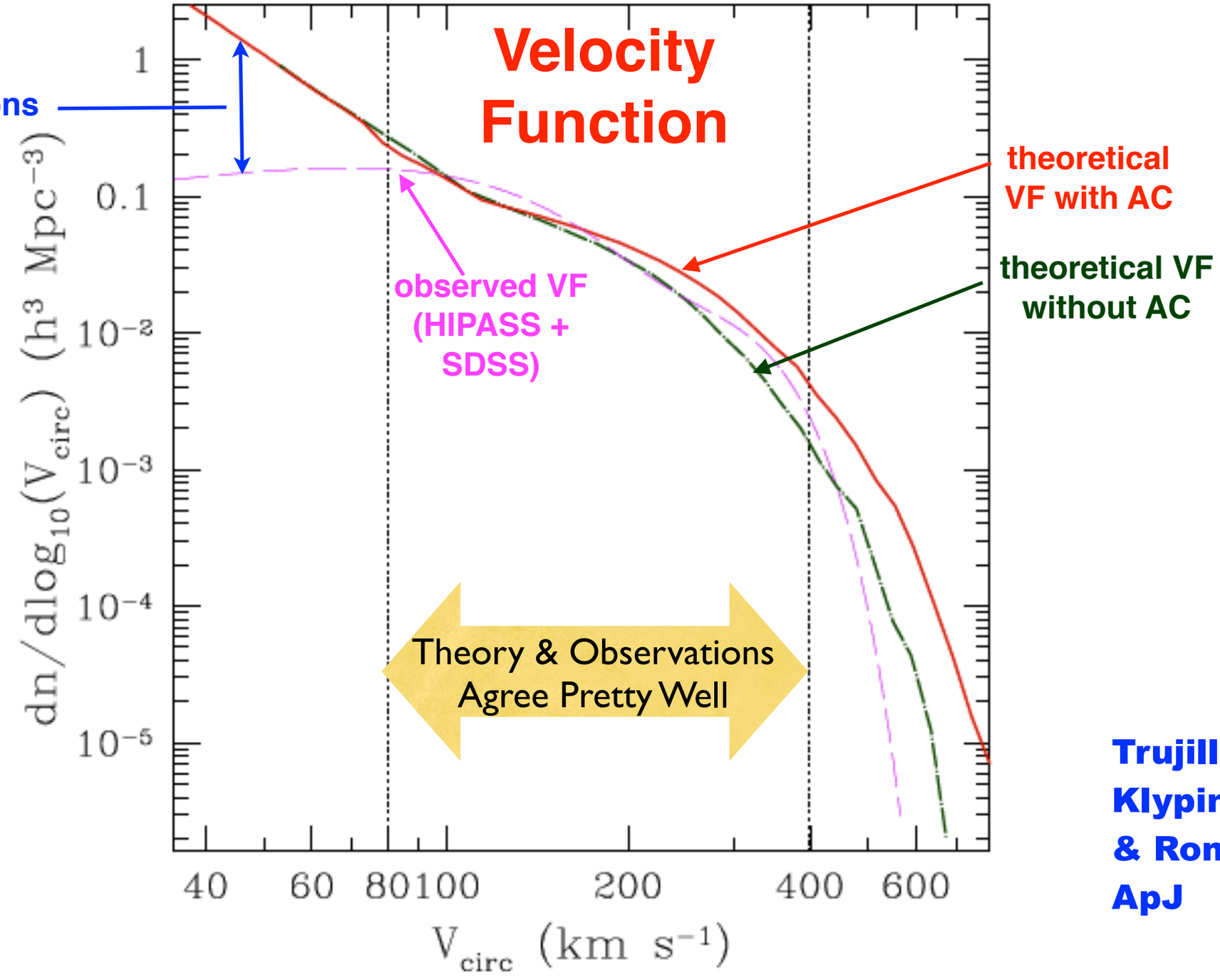

Trujillo-Gomez, Klypin, Primack, & Romanowsky ApJ

Fig. 11.— Comparison of theoretical (dot-dashed and thick solid curves) and observational (dashed curve) circular velocity functions. The dot-dashed line shows the effect of adding the baryons (stellar and cold gas components) to the central region of each DM halo and measuring the circular velocity at 10 kpc. The thick solid line is the distribution obtained when the adiabatic contraction of the DM halos is considered. Because of uncertainties in the AC models, realistic theoretical predictions should lie between the dot-dashed and solid curves. Both the theory and observations are highly uncertain for rare galaxies with $V_{\rm circ} > 400$ km s^{-1}. Two vertical dotted lines divide the VF into three domains: $V_{\rm circ} > 400$ km s^{-1} with large observational and theoretical uncertainties; < 80 km s^{-1} $< V_{\rm circ} < 400$ km s^{-1} with a reasonable agreement, and $V_{\rm circ} < 80$ km s^{-1}, where the theory significantly overpredicts the number of dwarfs.

Klypin, Karachentsev, Nasonova 2012

Deeper Local Survey -- better agreement with ΛCDM but still more halos than galaxies below 50 km/s

Local Volume: D <10Mpc

Total sample: 813 galaxies
Within 10Mpc: 686
M_B<-13 N=304
M_B<-10 N=611

80-90% are spirals or dIrr (T>0)

Accuracy of distances are 8-10%

80% with D<10Mpc have HI linewidths

Vrot =
150x10^(-(20.5+M_B)/8.5)km/s

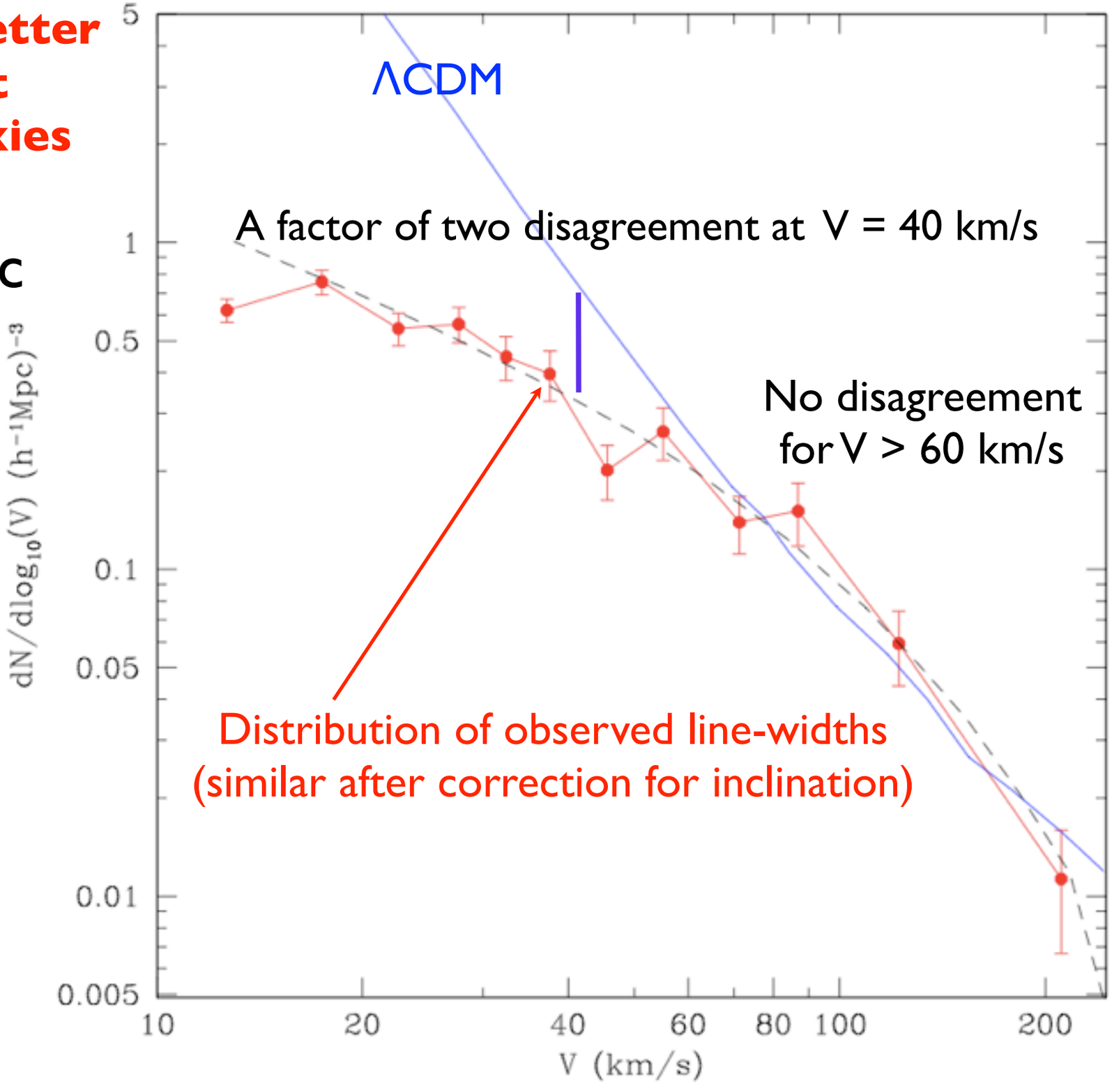

Bolshoi simulations - recent progress

- Anatoly Klypin has improved his BDM halofinder. It now finds the spin parameter, concentration, and shape and orientation of all halos. It also produces catalogs for both "virial" and overdensity-200 halo definitions. Results on all 180 stored timesteps of the Bolshoi simulation will be finished in a week or so. Peter Behroozi has written a new phase-space halofinder that finds subhalos better in the central regions of larger halos.

- All catalogs are finished for BigBolshoi-1 (MultiDark), which has the same cosmology as Bolshoi in a volume 64x larger. It has 7 kpc/h resolution, and is complete to Vcirc > 170 km/s (so all MWy-size halos are found). BigBolshoi simulations can now be run and analyzed in one week; two more are planned to get statistics for BOSS. Merger trees are coming soon.

- A new miniBolshoi simulation is runing now. It will have a force resolution of about 100 pc and a mass resolution of about 10^6 M_{sun} and it will be complete to 15 km/s or better. We will have complete merger histories and substructure for hundreds of MWy-size halos.

- All catalogs are available at Astrophysicalishes Institut Potsdam: http://www.multidark.org/MultiDark/ (You have to get an account there.) We hope to have more up soon, including merger trees.

ΛCDM vs. Downsizing

ΛCDM:

hierarchical formation
(small things form first)

"Downsizing":

massive galaxies are old, star formation moves to smaller galaxies

small structures → large structures

early → late

large galaxies → small galaxies

ΛCDM vs. Downsizing

ΛCDM:

hierarchical formation
(small things form first)

"Downsizing":

massive galaxies are old, star formation moves to smaller galaxies

=

=

mass assembly

simulations (DM)

How are these processes related?

star formation history

semi-analytic models

present-day structure

current stellar population

Formation of galaxies and large-scale structure with cold dark matter

Blumenthal, Feber, Primack, & Rees -- Nature 311, 517 (1984)

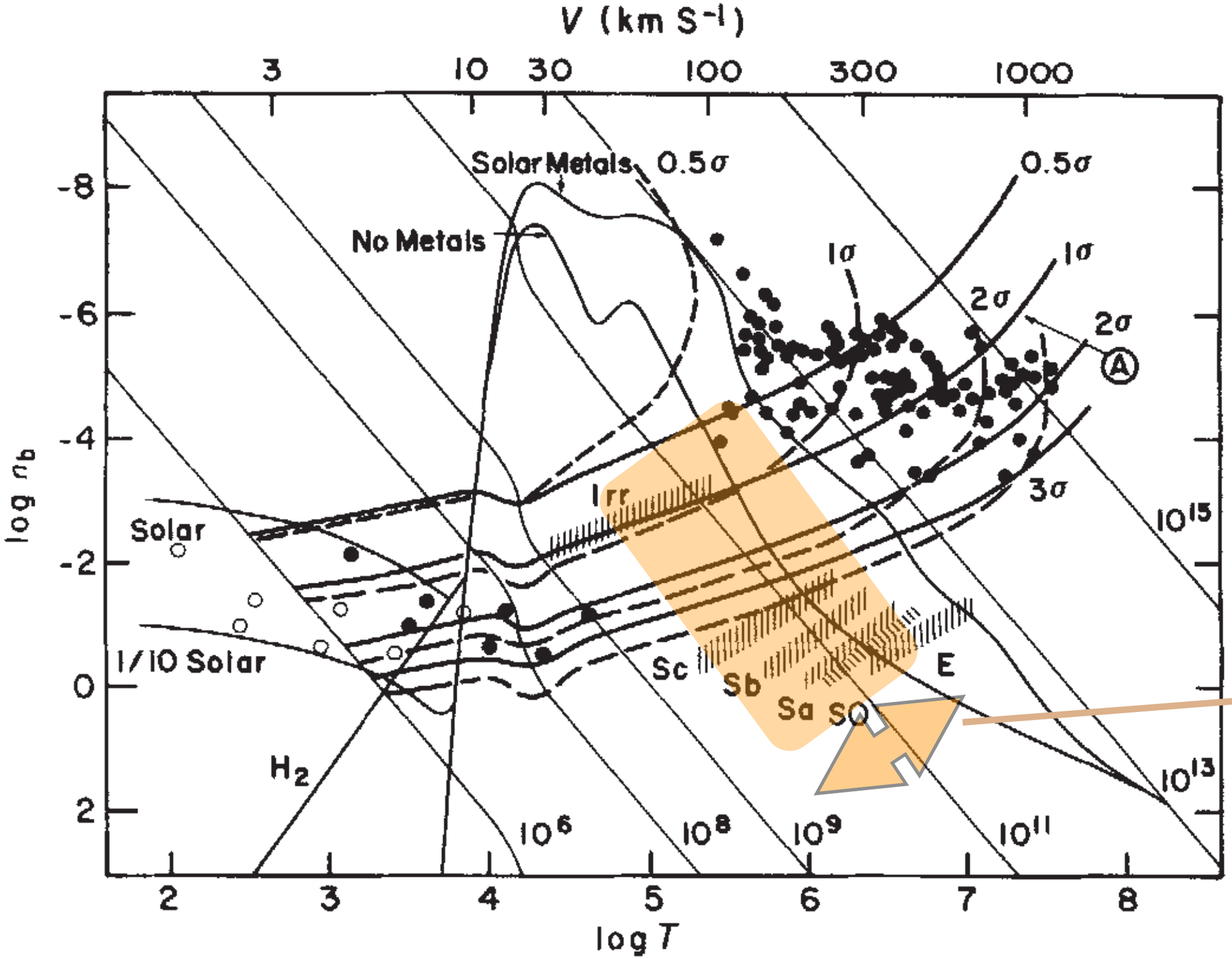

Star Forming Band: 10^{10} - 10^{12} Msun

Fig. 3 Baryon density n_b versus three-dimensional, r.m.s. velocity dispersion V and virial temperature T for structures of various size in the Universe. The quantity T is $\mu V^2/3k$, where μ is mean molecular weight ($\approx$0.6 for ionized, primordial H+He) and k is Boltzmann's constant.

Key assumption:

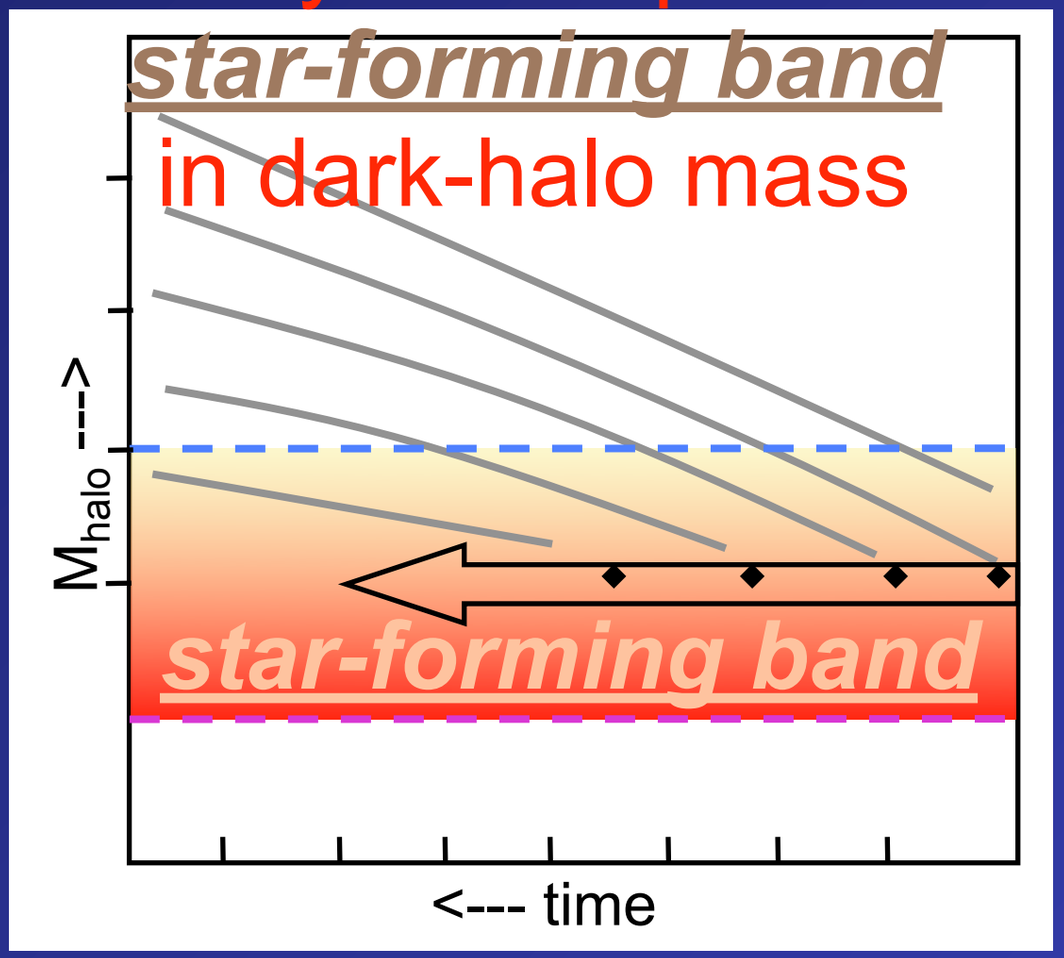

Implications and Predictions of the Model

1) Each halo has a unique dark-matter growth path and associated stellar mass growth path.

2) Stellar mass follows halo mass until M_{halo} crosses M_{crit}.

SAMs: $M_{star} < 0.05\ M_{halo}$

3) A ***mass sequence*** comes from the fact that different halo masses enter the star-forming band at different times. A galaxy's position is determined by its ***entry redshift*** into the band. More massive galaxies enter earlier. Thus:

$$z_{entry} \leftrightarrow M_{halo} \leftrightarrow M_{star}$$

Sandy Faber

Implications and Predictions of the Model

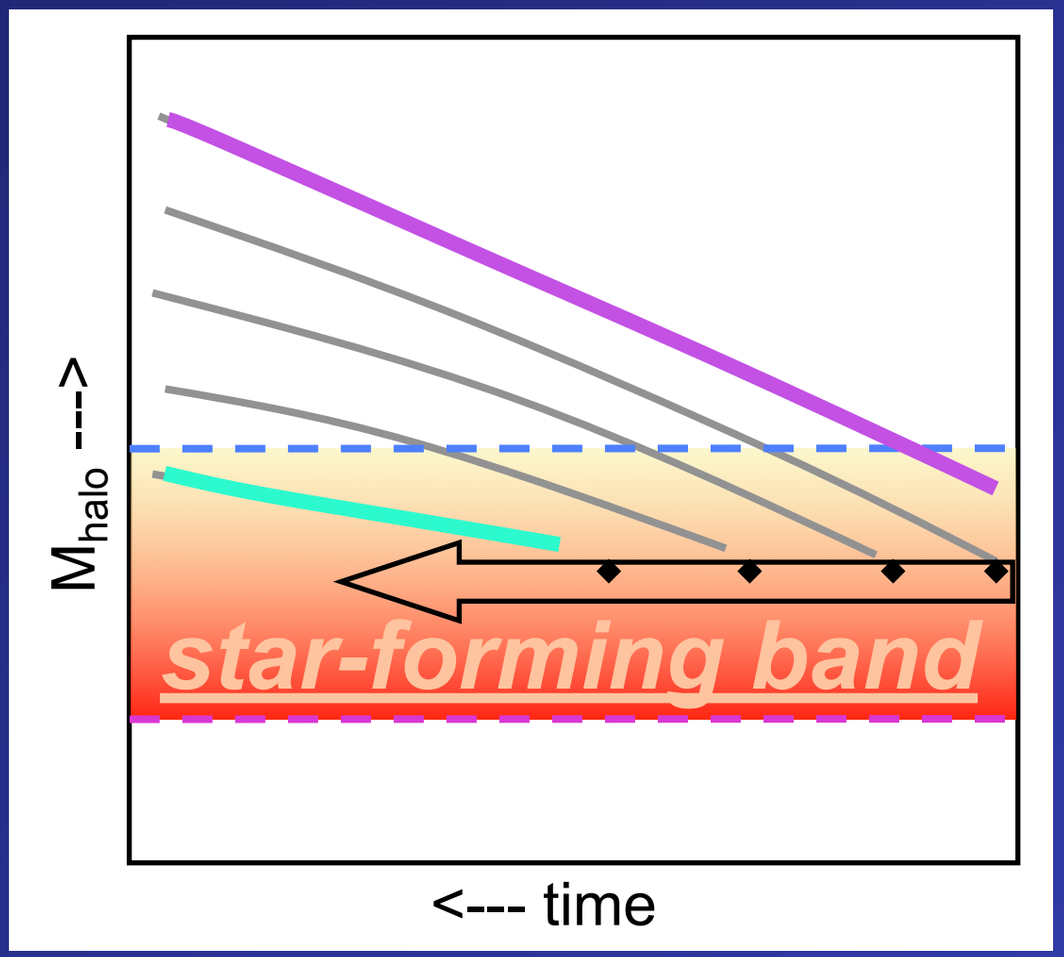

Massive galaxies:

- Started forming stars early.
- Shut down early.
- Are red today.
- Populate dark halos that are much more massive than their stellar mass.

Small galaxies:

- Started forming stars late.
- Are still making stars today.
- Are blue today.
- Populate dark halos that match their stellar mass.

"Downsizing"

Star formation is a wave that started in the largest galaxies and swept down to smaller masses later (Cowie et al. 1996).

Sandy Faber

Galaxy Formation Theory

Primordial fluctuations grow due to inflation.

Baryons trace the DM distribution in scales larger than the Jeans length

e.g. Rees & Ostriker 1977, White & Rees 1978, White & Frenk 1991, Kauffmann et al. 1993, Cole et al. 1994, Somerville & Primack 1999, Sommerville et al. 1998, Birnboim & Dekel 2003

Dark matter undergoes gravitational collapse (no pressure support) and generates at cosmic web

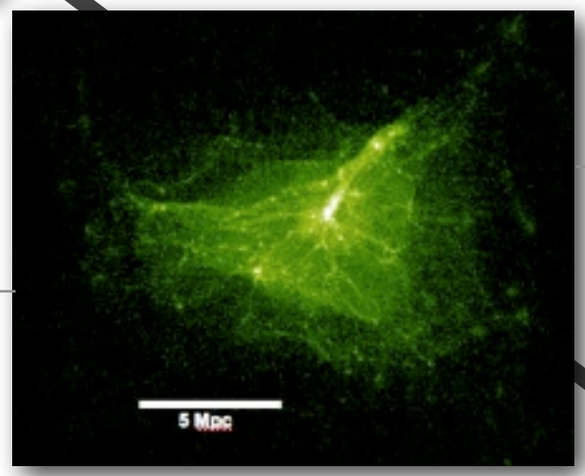

Governato et al. 2007

The angular momentum of the halo is acquired through cosmological torques

Question: How is the angular momentum of the dark matter related to that of the stars? Is it the same?

Baryonic material accretes onto the dark matter potentials via hot/cold accretion.

Supersonic gas accreting at $T < T_{vir}$ is shocked near R_{vir} when $t_{cool} > t_{dyn}$ and at smaller radii if $t_{cool} < t_{dyn}$

Bertshinger 1985, Book & Benson 2010

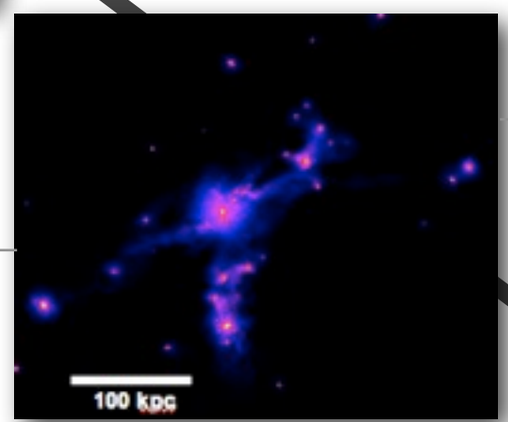

Governato et al. 2007

In halos of mass $M < 10^{11}\ M_{\odot}$ (pristine gas) shocks cannot form near R_{vir} and cold gas can accrete through filaments

Birnboim & Dekel 2003

Dissipative processes *cool* the shocked gas: atomic, Compton, molecular hydrogen cooling

Other processes *heat* gas: photo-heating, feedback, preheating, thermal conduction

Conservation of angular momentum during collapse produces disks. Feedback removes low angular momentum material

Can ΛCDM Simulations Form Realistic Galaxies?

The Angular Momentum Problem

Cooling was too effective particularly in low-mass halos at early times.

Navarro & Steinmetz

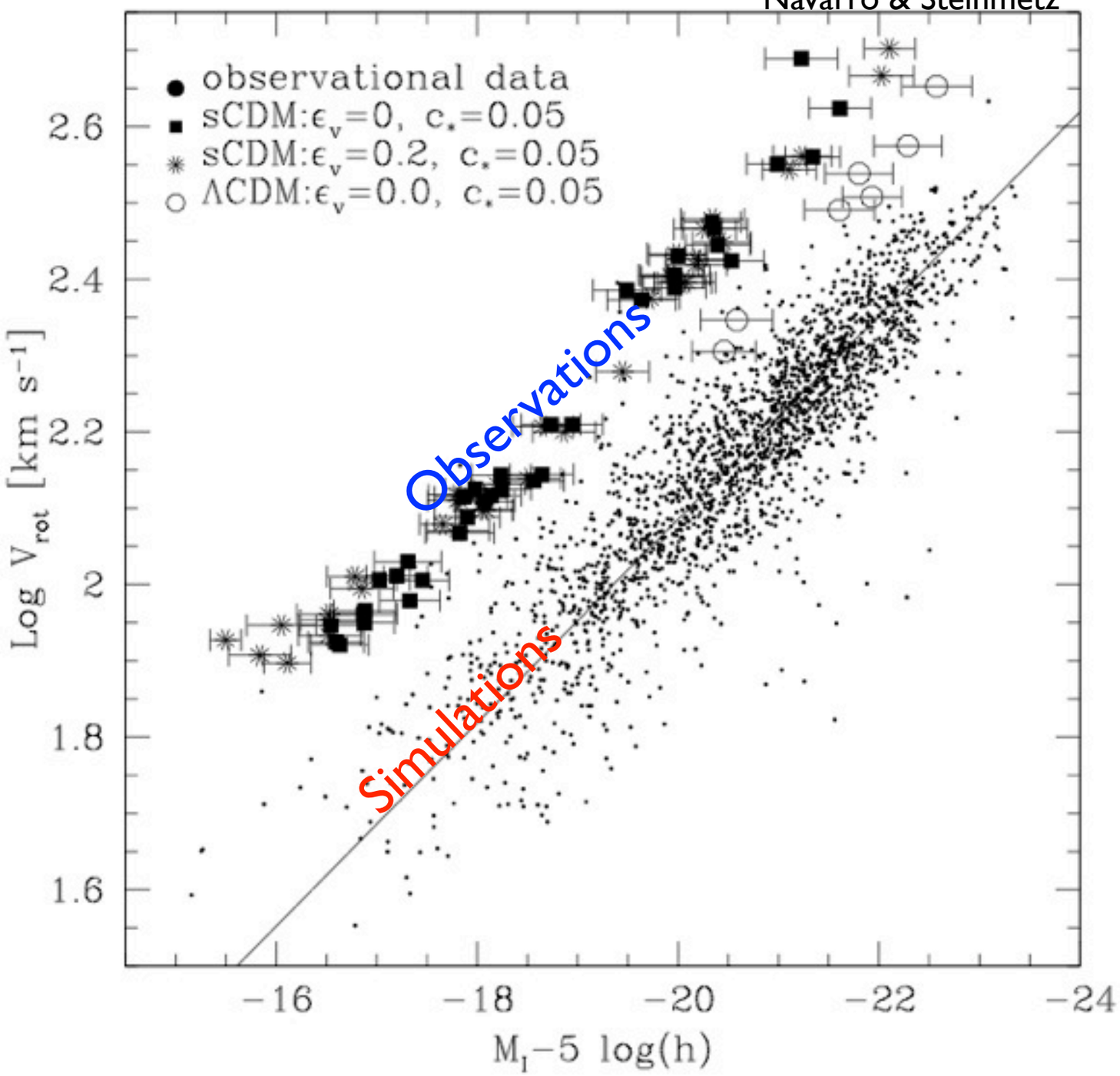

"Agreement between model and observations appears to demand substantial revision to the CDM scenario or to the manner in which baryons are thought to assemble and evolve into galaxies in hierarchical universes."

Navarro & Steinmetz 2000 ApJ

The Angular Momentum Catastrophe

In practice it is not trivial to form galaxies with massive, extended disks and small spheroids.
The angular momentum content of the disk determined its final structure.

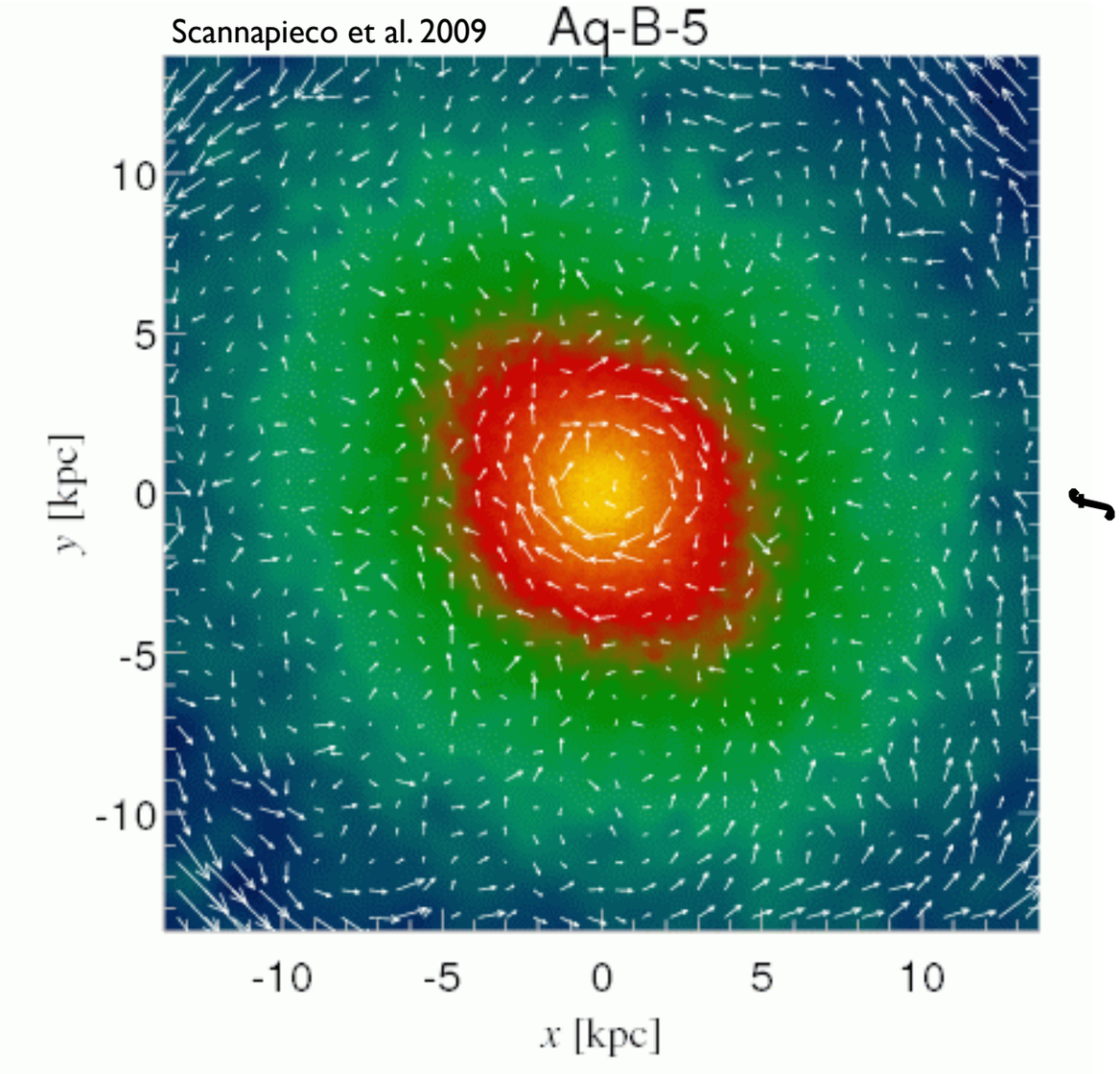

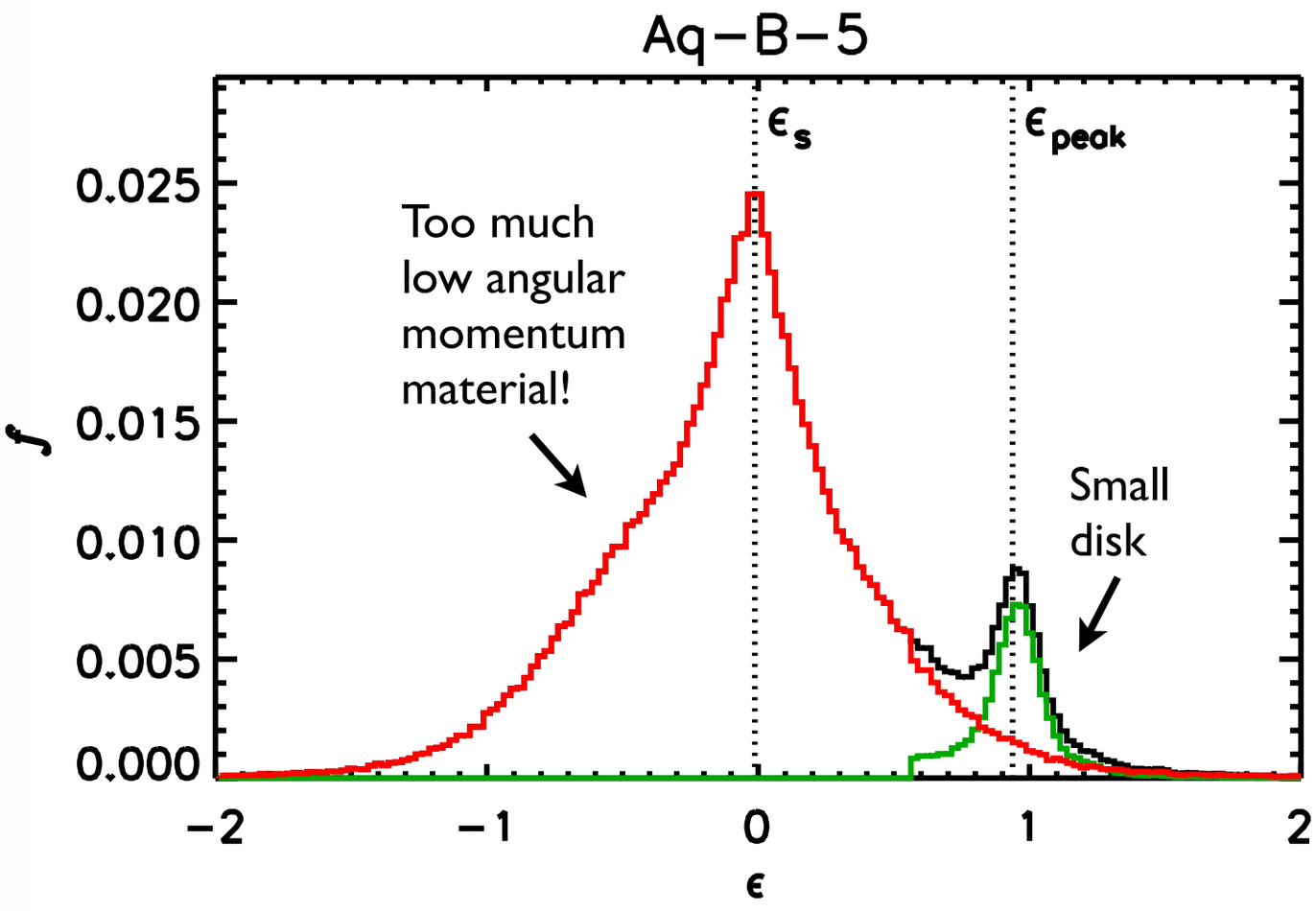

Solution: Stop cooling via SN feedback, AGN, preheating, etc.

z=90.73

Eris

Simulation
Guedes et al.

Structural Properties: Eris Bulge-to-Disk Ratio

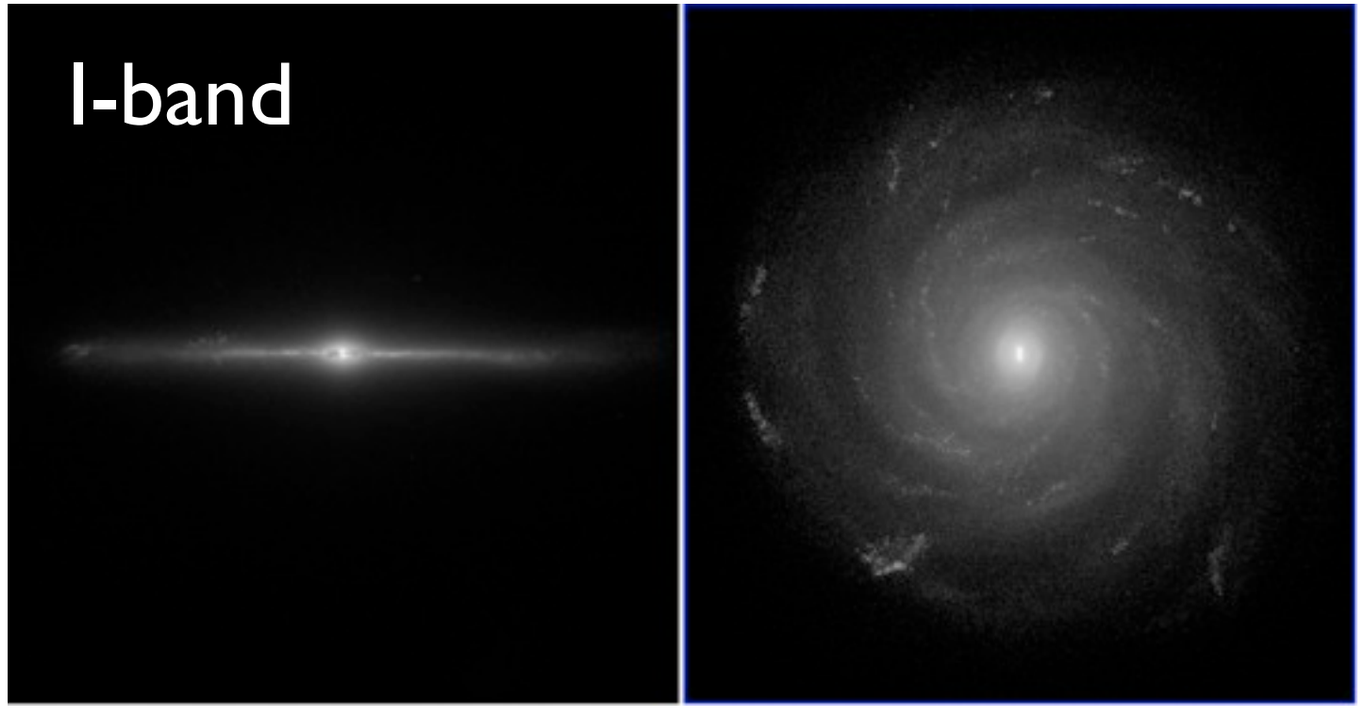

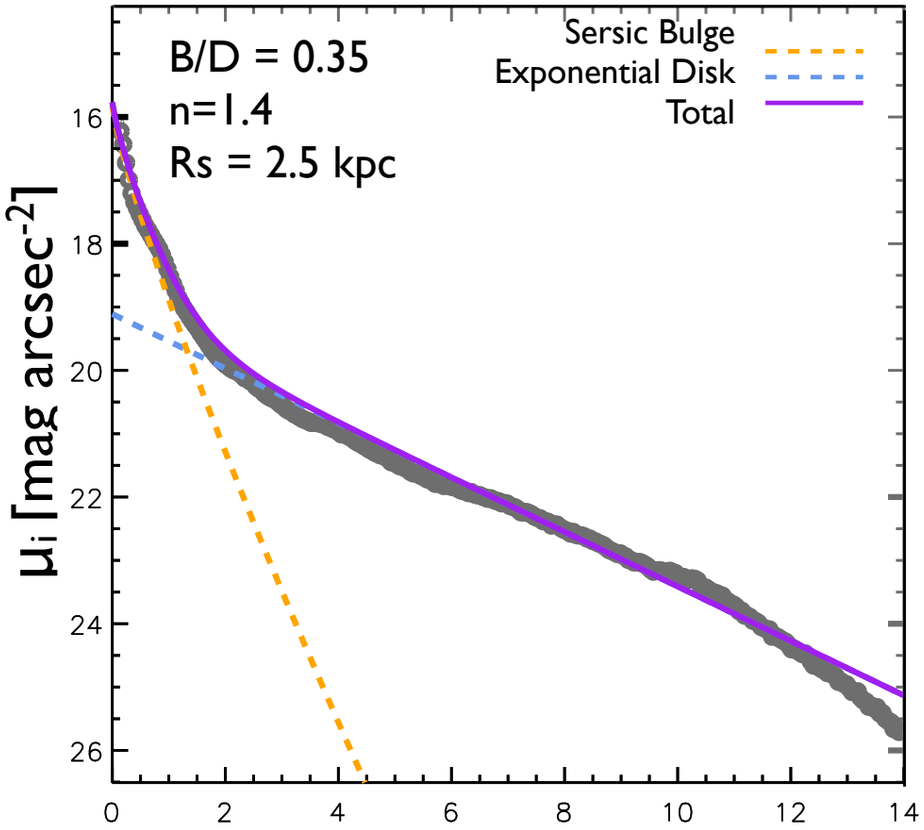

Ganda et al. 2006, 2009

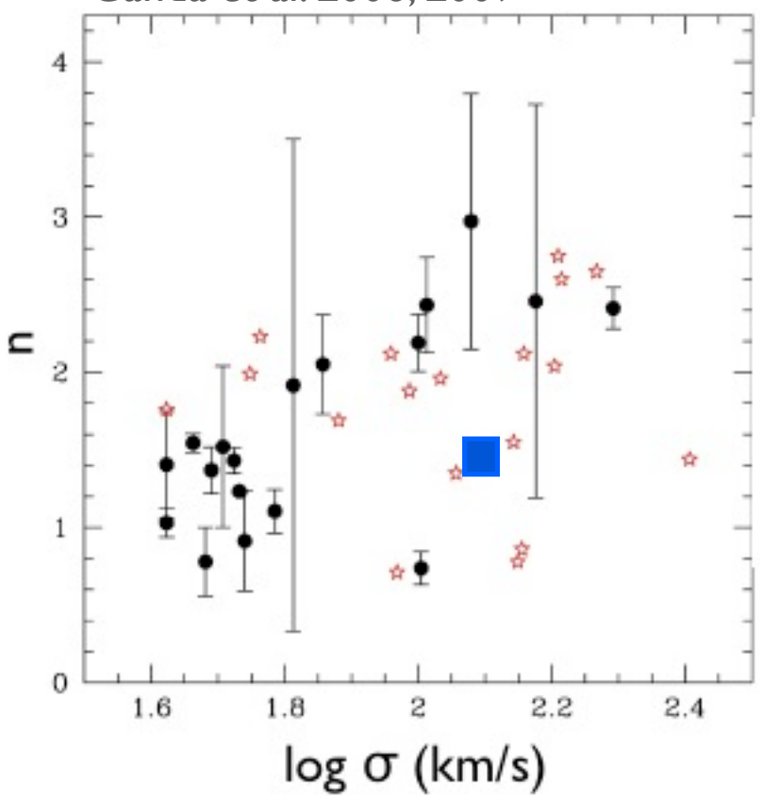

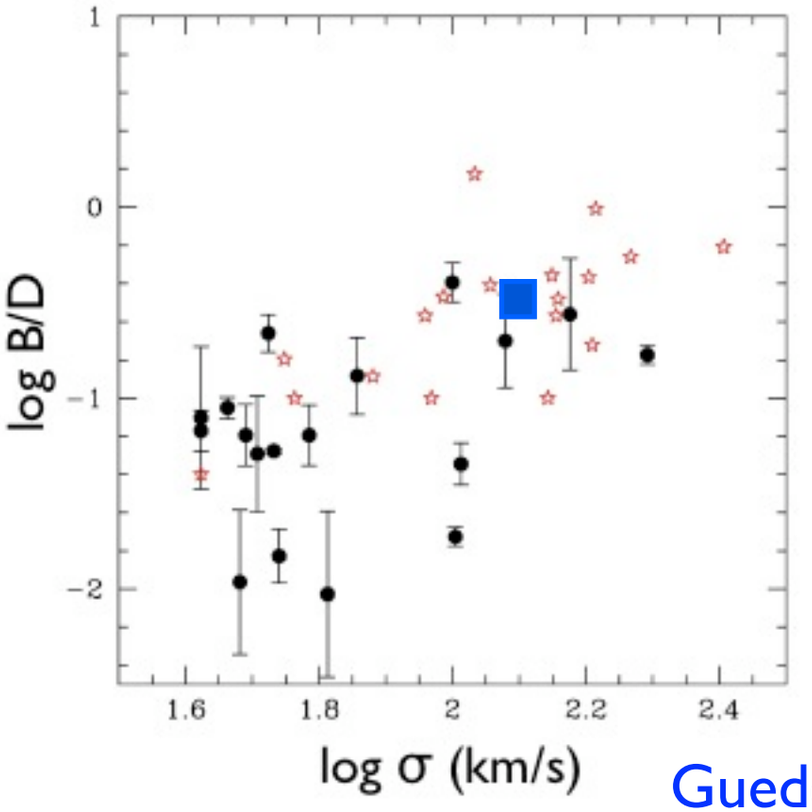

Photometric decomposition in i-band using Galfit (Peng et al. 2002)

- ● Late-type spirals
- ☆ Early-type spirals
- ■ Eris

Guedes, Callegari, Madau, Mayer 2011 ApJ

No Angular Momentum Problem in the Eris Simulation

Simulations tend to produce too many stars at the center, which translates into steeply rising rotation curves.

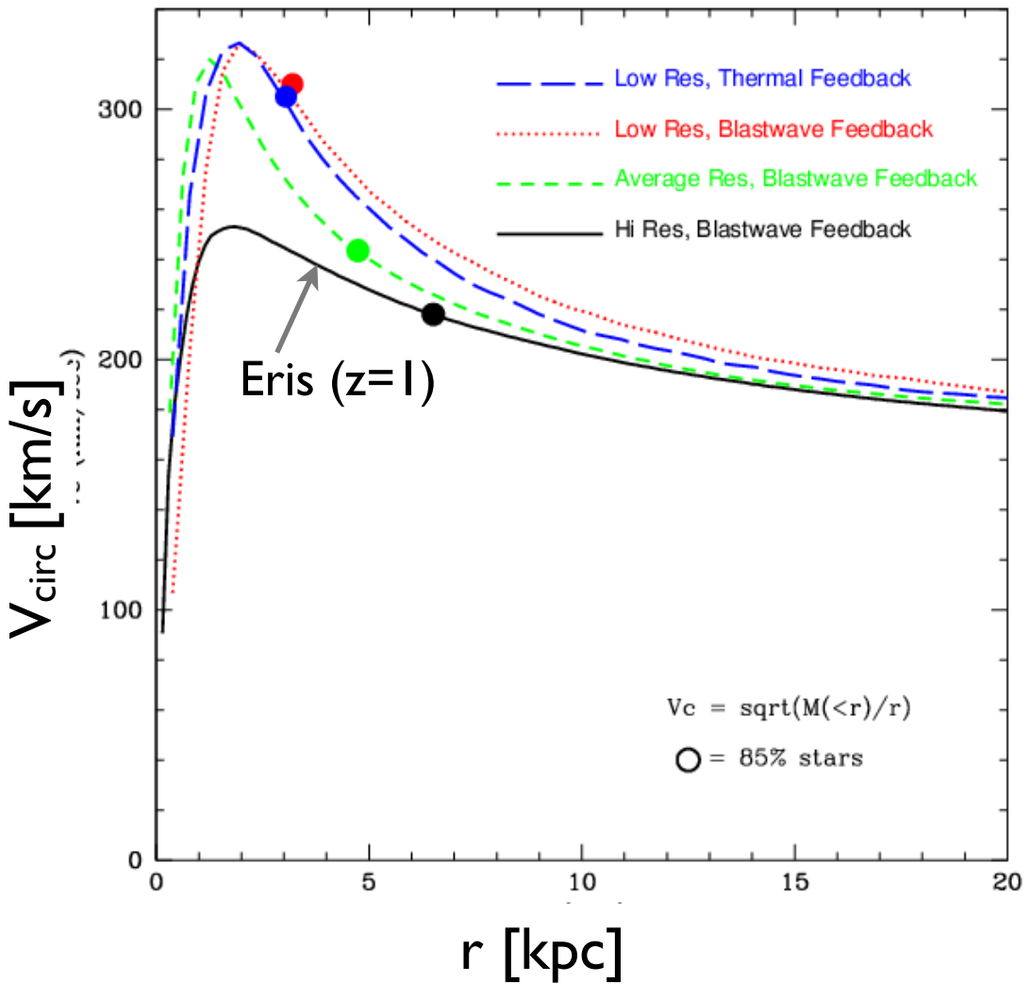

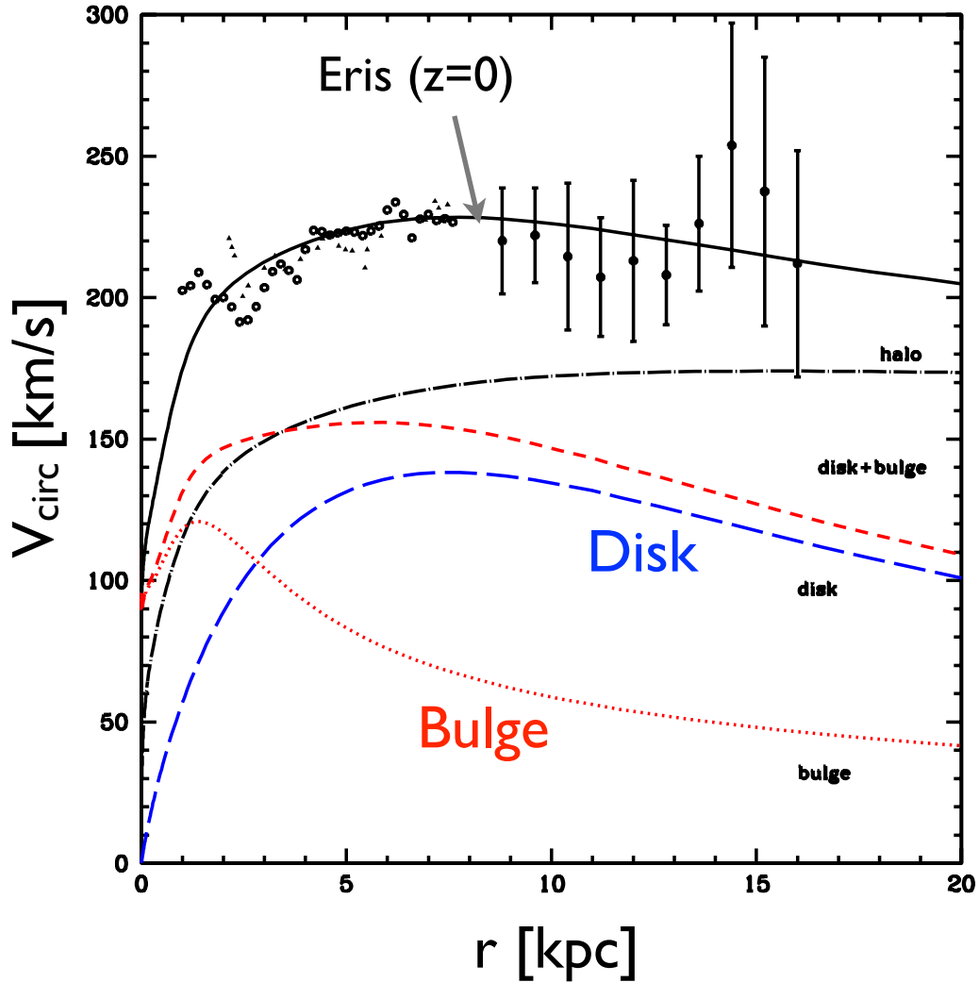

Total

Halo

Disk+Bulge

Solution:

* Mimic star formation as occurs in real galaxies, i.e. localized, on high-density peaks only.
* Feedback from SN becomes more efficient in removing gas from high-density regions.

These outflows remove preferentially low angular momentum material, suppressing the formation of large bulges.

Guedes, Callegari, Madau, Mayer 2011 ApJ

Dependence of Halo Concentration on Mass and Redshift

Profiles of dark haloes: evolution, scatter, and environment

J. S. Bullock[1,2], T. S. Kolatt[1,3], Y. Sigad[3], R.S. Somerville[3,4], A. V. Kravtsov[2,5⋆], A. A. Klypin[5], J. R. Primack[1], and A. Dekel[3] 2001 MNRAS 321, 559

ABSTRACT

We study dark-matter halo density profiles in a high-resolution N-body simulation of a ΛCDM cosmology. Our statistical sample contains ∼5000 haloes in the range $10^{11} - 10^{14} h^{-1} M_{\odot}$ and the resolution allows a study of subhaloes inside host haloes. The profiles are parameterized by an NFW form with two parameters, an inner radius r_s and a virial radius R_{vir}, and we define the halo concentration $c_{vir} \equiv R_{vir}/r_s$. We find that, for a given halo mass, the redshift dependence of the median concentration is $c_{vir} \propto (1+z)^{-1}$. This corresponds to $r_s(z) \sim$ constant, and is contrary to earlier suspicions that c_{vir} does not vary much with redshift. The implications are that high-redshift galaxies are predicted to be more extended and dimmer than expected before. Second, we find that the scatter in halo profiles is large, with a 1σ $\Delta(\log c_{vir}) = 0.18$ at a given mass, corresponding to a scatter in maximum rotation velocities of $\Delta V_{max}/V_{max} = 0.12$. We discuss implications for modelling the Tully-Fisher relation, which has a smaller reported intrinsic scatter. Third, subhaloes and haloes in dense environments tend to be more concentrated than isolated haloes, and show a larger scatter. These results suggest that c_{vir} is an essential parameter for the theory of galaxy modelling, and we briefly discuss implications for the universality of the Tully-Fisher relation, the formation of low surface brightness galaxies, and the origin of the Hubble sequence. We present an improved analytic treatment of halo formation that fits the measured relations between halo parameters and their redshift dependence, and can thus serve semi-analytic studies of galaxy formation.

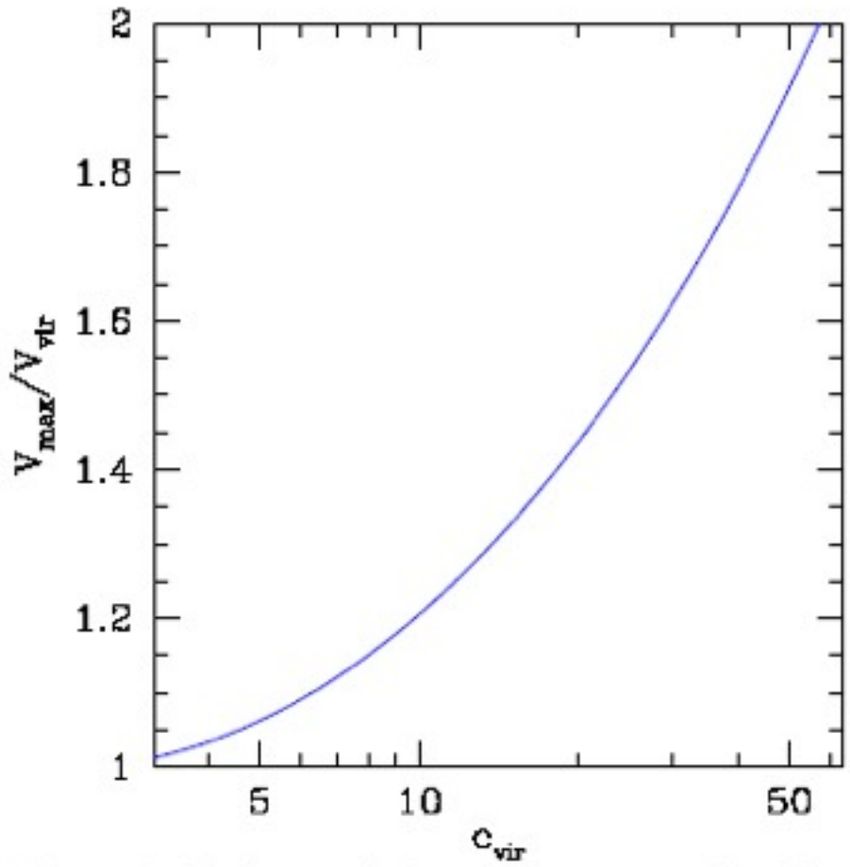

Figure 1. Maximum velocity versus concentration. The maximum rotation velocity for an NFW halo in units of the rotation velocity at its virial radius as a function of halo concentration.

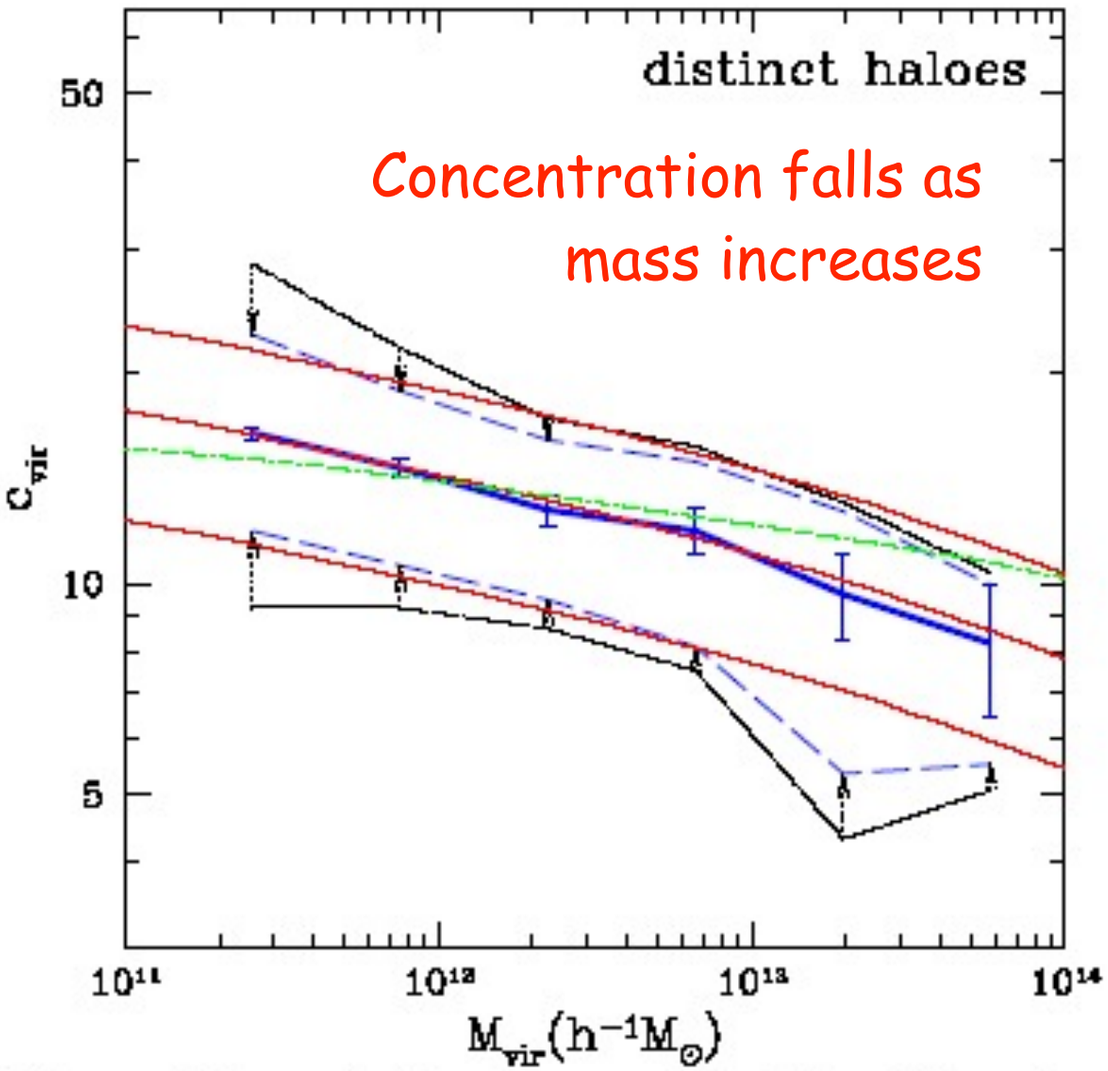

Figure 4. Concentration versus mass for distinct haloes at $z = 0$. The thick solid curve is the median at a given $M_{\rm vir}$. The error bars represent Poisson errors of the mean due to the sampling of a finite number of haloes per mass bin. The outer dot-dashed curves encompass 68% of the $c_{\rm vir}$ values as measured in the simulations. The inner dashed curves represent only the true, intrinsic scatter in $c_{\rm vir}$, after eliminating both the Poisson scatter and the scatter due to errors in the individual profile fits due, for example, to the finite number of particles per halo. The central and outer thin solid curves are the predictions for the median and 68% values by the toy model outlined in the text, for $F = 0.01$ and three different values of K. The thin dot-dashed line shows the prediction of the toy model of NFW97 for $f = 0.01$ and $k = 3.4 \times 10^3$.

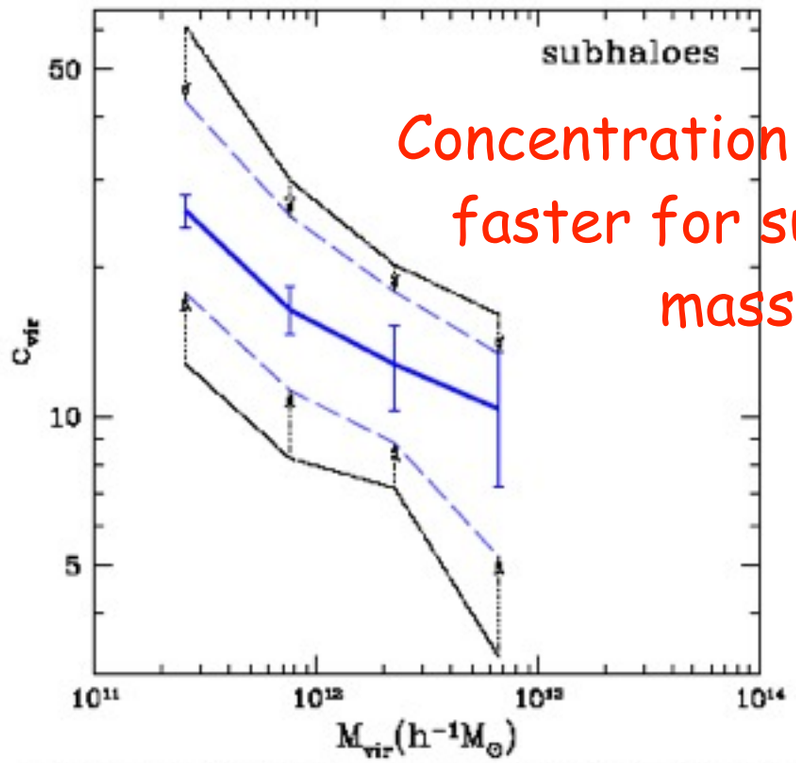

Figure 5. Concentration versus mass for subhaloes at $z = 0$. The curves and errors are the same as in Figure 4.

Bullock et al. 2001

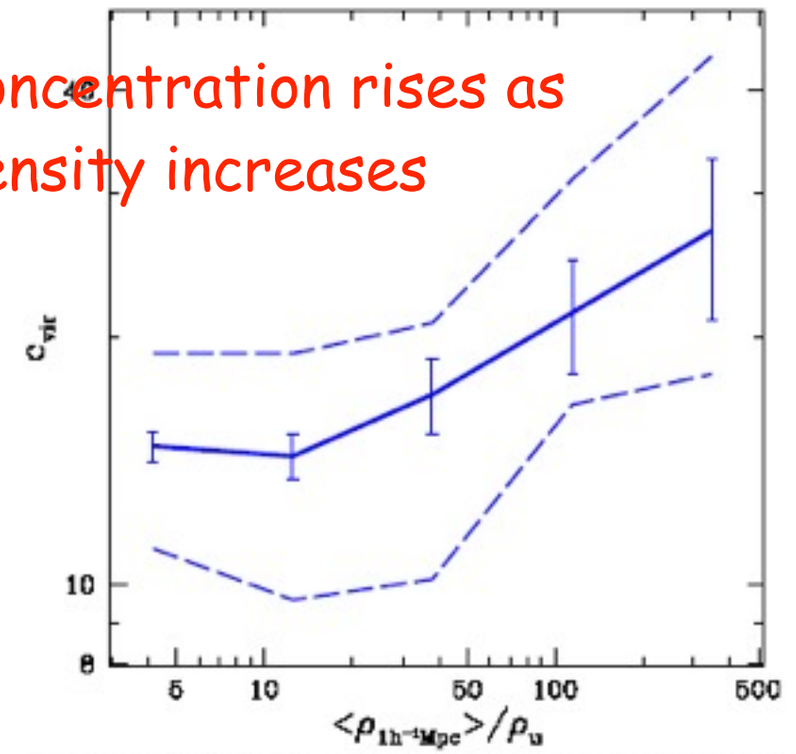

Figure 6. Concentrations versus environment. The concentration at $z = 0$ of all haloes in the mass range $0.5 - 1.0 \times 10^{12} h^{-1} M_\odot$ as a function of local density in units of the average density of the universe. The local density was determined within spheres of radius $1h^{-1}$Mpc. The solid line represents the median $c_{\rm vir}$ value, the error bars are Poisson based on the number of haloes, and the dashed line indicates our best estimate of the intrinsic scatter.

Spread of Halo Concentrations

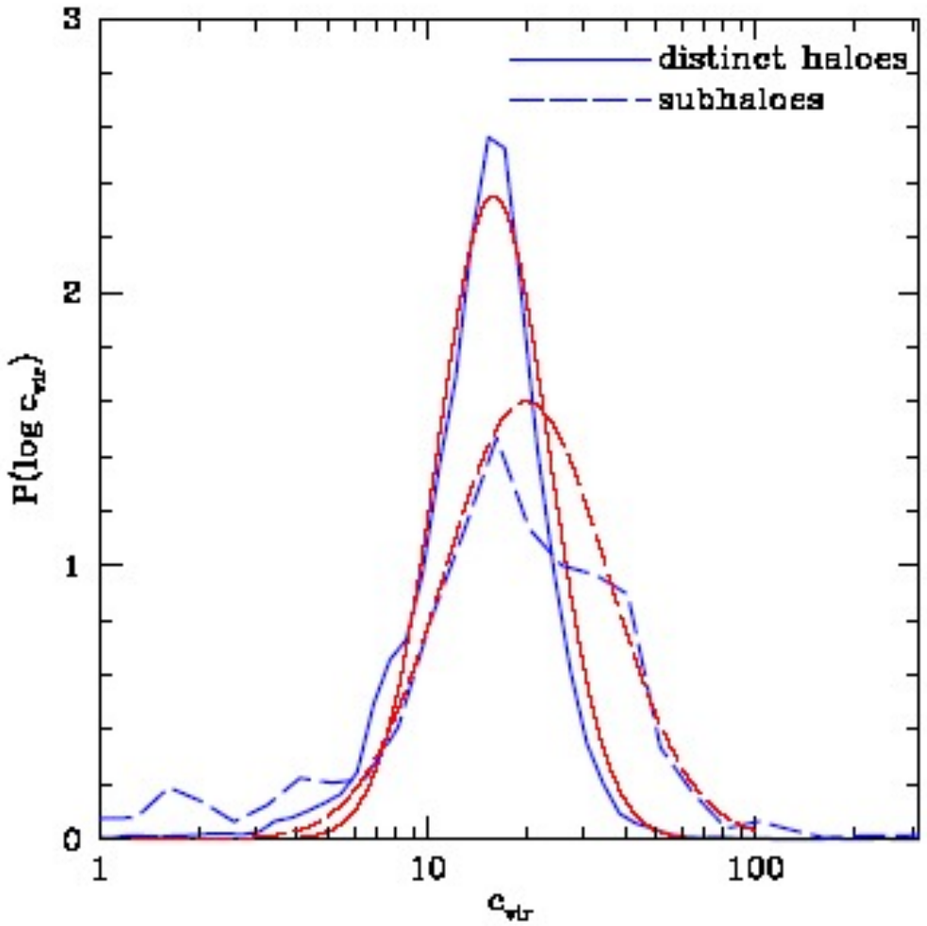

Figure 7. The probability distributions of distinct haloes (solid line) and subhaloes (dashed line) at $z = 0$ within the mass range $(0.5 - 1.0) \times 10^{12} h^{-1} M_{\odot}$. The simulated distributions (thick lines) include, the $\sim 2,000$ distinct haloes and ~ 200 subhaloes within this mass range. Log-normal distributions with the same median and standard deviation as the measured distributions are shown (thin lines). Subhaloes are, on average, more concentrated than distinct haloes and they show a larger spread.

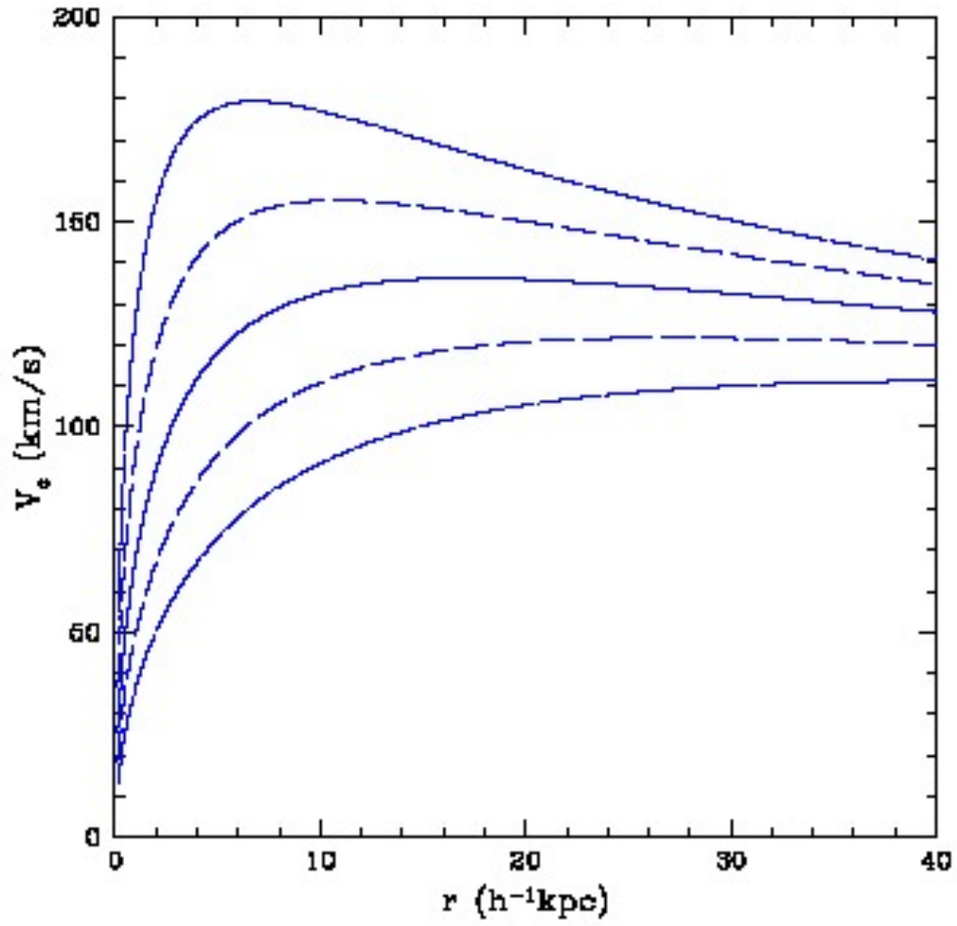

Figure 8. The spread in NFW rotation curves corresponding to the spread in concentration parameters for distinct haloes of $3 \times 10^{11} h^{-1} M_{\odot}$ at $z = 0$. Shown are the median (solid), $\pm 1\sigma$ (long dashed), and $\pm 2\sigma$ (dot-dashed) curves. The corresponding median rotation curve for subhaloes is comparable to the upper 1σ curve of distinct haloes.

Bullock et al. 2001

Evolution of Halo Concentration with Redshift

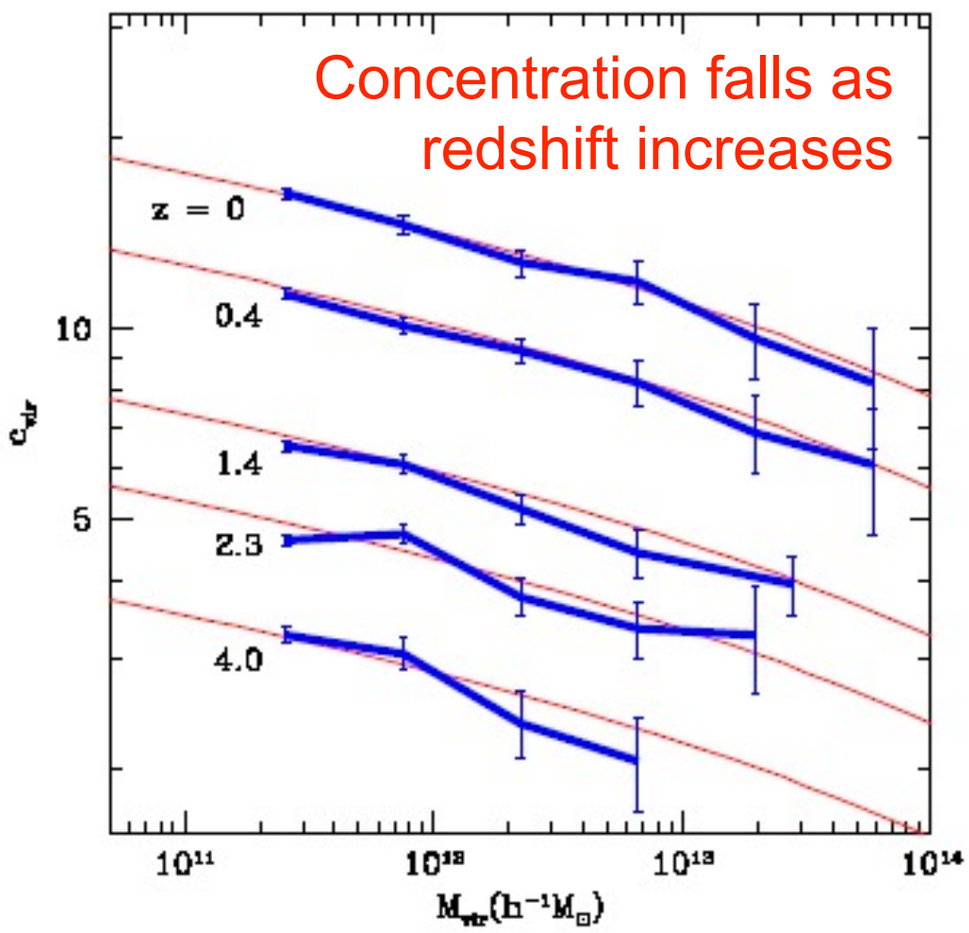

Figure 10. Median $c_{\rm vir}$ values as a function of $M_{\rm vir}$ for distinct haloes at various redshifts. The error bars are the Poisson errors due to the finite number of haloes in each mass bin. The thin solid lines show our toy model predictions.

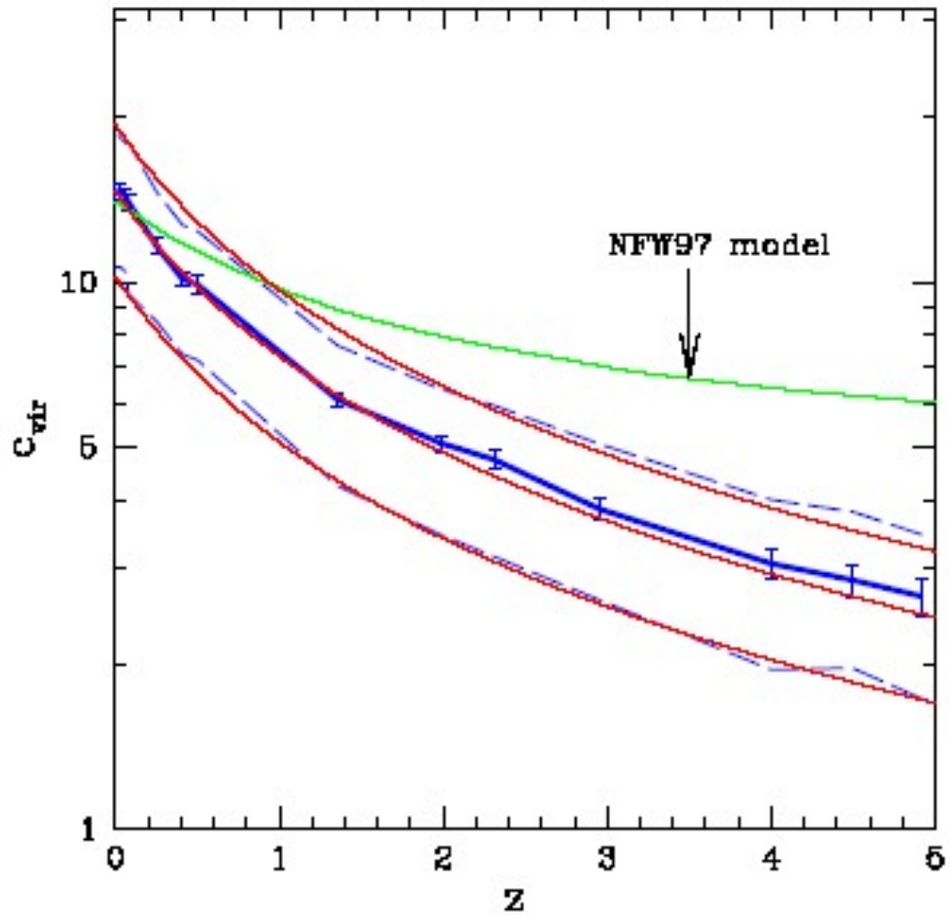

Figure 11. Concentration as a function of redshift for distinct haloes of a fixed mass, $M_{\rm vir} = 0.5 - 1.0 \times 10^{12} h^{-1} M_\odot$. The median (heavy solid line) and intrinsic 68% spread (dashed line) are shown. The behavior predicted by the NFW97 toy model is marked. Our revised toy model for the median and spread for $8 \times 10^{11} h^{-1} M_\odot$ haloes (thin solid lines) reproduces the observed behavior rather well.

$C_{vir} \propto 1/(1+z)$
at fixed mass

Bullock et al. 2001

Merger Trees

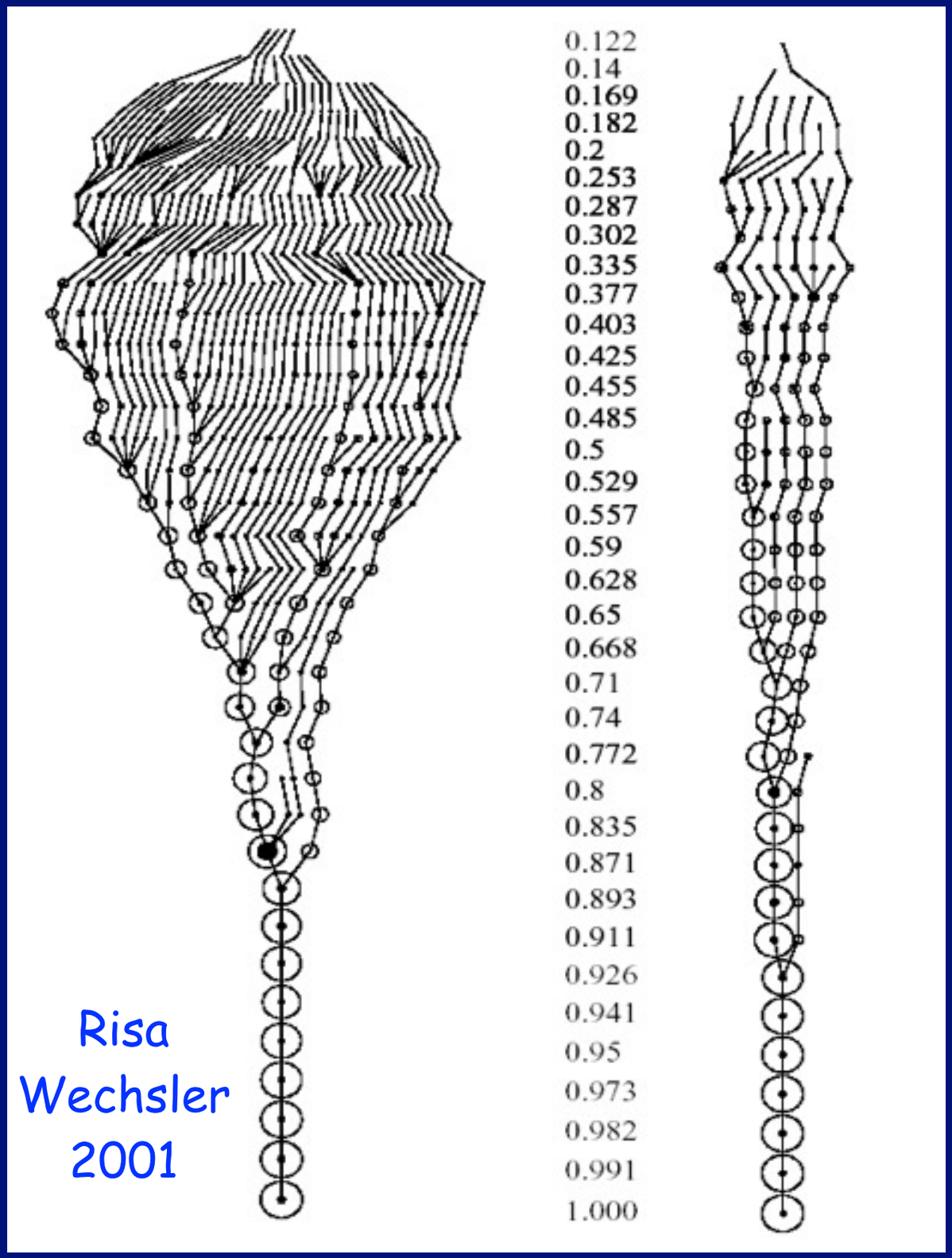

Based on our ART simulations, Risa Wechsler created the first structural merger trees tracing the merging history of thousands of halos with structural information on their higher-redshift progenitors, including their radial profiles and spins. This led to the discovery that a halo's merging history can be characterized by a single parameter a_c which describes the scale factor at which the halo's mass accretion slows, and that this parameter correlates very well with the halo concentration, thus showing that the distribution of dark matter halo concentrations reflects mostly the distribution of their mass accretion rates. We found that the radius of the inner part of the halo, where the density profile is roughly 1/r, is established during the early, rapid-accretion phase of halo growth (a result subsequently confirmed and extended by other groups, e.g., Zhao et al. 2003, Reed et al. 2004).

CONCENTRATIONS OF DARK HALOS FROM THEIR ASSEMBLY HISTORIES

Risa H. Wechsler[1], James S. Bullock[2], Joel R. Primack[1], Andrey V. Kravtsov[2,3], Avishai Dekel[4], ApJ 568 (2002) 52-70

$$\rho_{\rm NFW}(r) = \frac{\rho_{\rm s}}{(r/R_{\rm s})\,(1+r/R_{\rm s})^2}, \qquad (1)$$

where $R_{\rm s}$ is a characteristic "inner" radius, and $\rho_{\rm s}$ a corresponding inner density. One of the inner parameters can be replaced by a "virial" parameter, either the virial radius ($R_{\rm vir}$), mass ($M_{\rm vir}$), or velocity ($V_{\rm vir}$), defined such that the mean density inside the virial radius is $\Delta_{\rm vir}$ times the mean universal density ρ_u at that redshift:

$$M_{\rm vir} \equiv \frac{4\pi}{3}\Delta_{\rm vir}\rho_u {R_{\rm vir}}^3. \qquad (2)$$

The critical overdensity at virialization, $\Delta_{\rm vir}$, is motivated by the spherical collapse model; it has a value $\simeq 180$ for the Einstein-deSitter cosmology, and $\simeq 340$ for the ΛCDM cosmology assumed here. A useful alternative parameter for describing the shape of the profile is the concentration parameter $c_{\rm vir}$, defined as $c_{\rm vir} \equiv R_{\rm vir}/R_{\rm s}$.

(Bryan & Norman 1998) $\Delta_{\rm vir} \simeq (18\pi^2 + 82x - 39x^2)/\Omega(z)$ where $x \equiv \Omega(z) - 1$

By examining a range of full mass assembly histories for our sample of halos, we have found a useful parameterized form that captures many essential aspects of halo growth over time. Remarkably, we find that both average mass accretion histories and mass accretion histories for individual halos, as observed at $z = 0$, can be characterized by a simple function:

$$M(a) = M_{\rm o} e^{-\alpha z}, \quad a = (1+z)^{-1}. \qquad (3)$$

The single free parameter in the model, α, can be related to a characteristic epoch for formation, $a_{\rm c}$, defined as the expansion scale factor a when the logarithmic slope of the accretion rate, $\mathrm{d}\log M/\mathrm{d}\log a$, falls below some specified value, S. The functional form defined in Eq. 3 implies $a_{\rm c} = \alpha/S$. In what follows we have chosen $S = 2$.

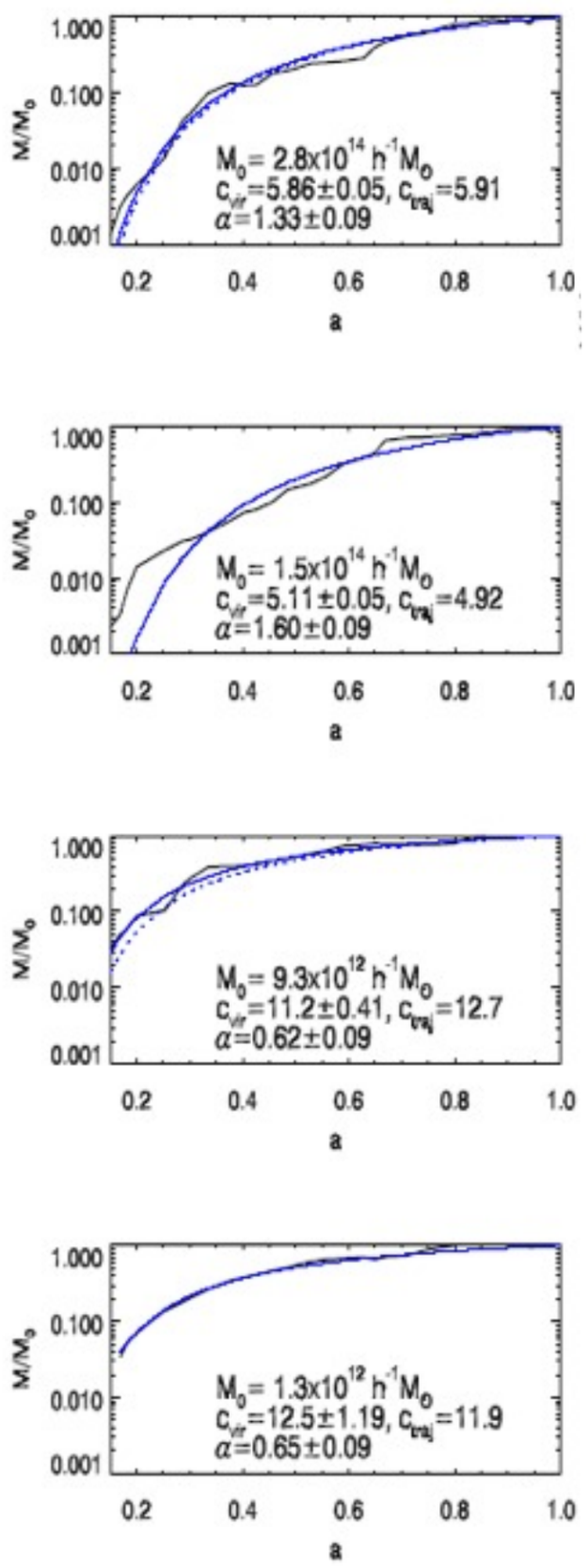

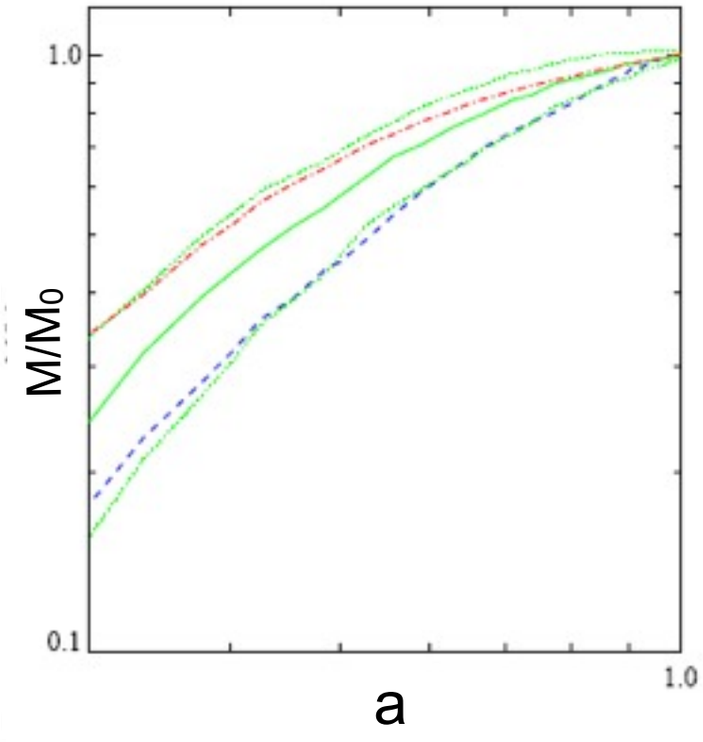

Average mass accretion histories, normalized at a = 1. The three green curves connect the averages of M(a)/M0 at each output time. The pair of dotted lines shows the 68% spread about the middle case. Red dot-dashed lines correspond to early formers (typically low mass halos), blue dashed lines to late formers (typically higher mass halos). We see that massive halos tend to form later than lower mass halos, whose mass accretion rate peaks at an earlier time.

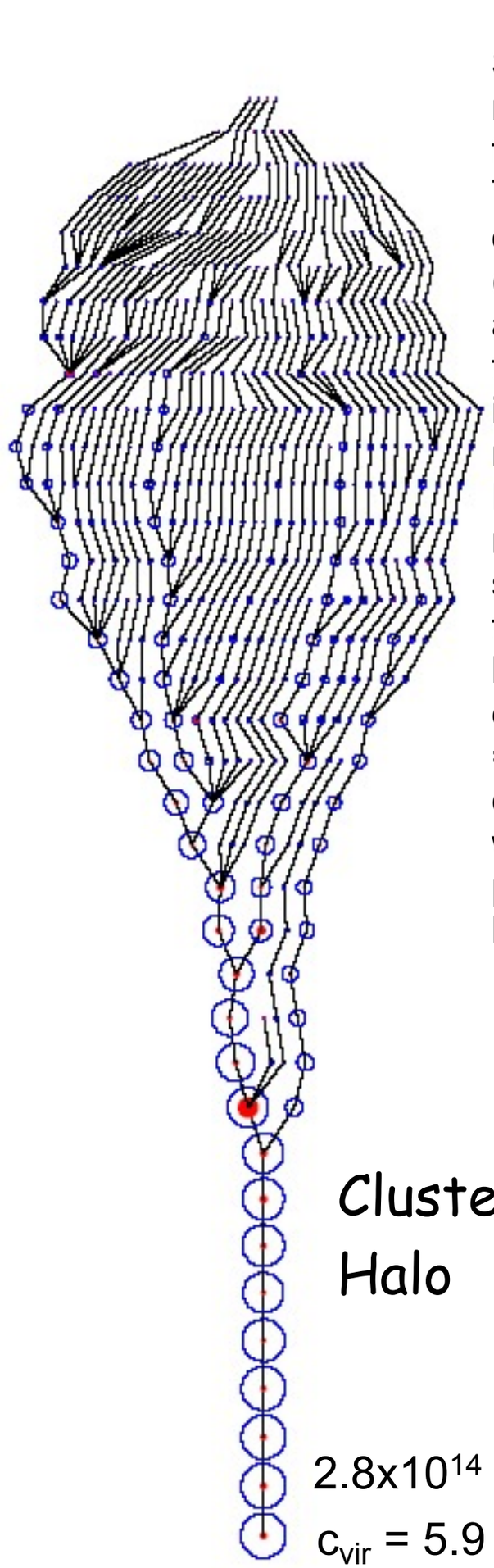

Structural merger trees for two halos. The radii of the outer and inner (filled) circles are proportional to the virial and inner NFW radii, R_{vir} and R_s, respectively, scaled such that the two halos have equal sizes at a = 1. Lines connect halos with their progenitor halos.

a

0.122
0.14
0.169
0.182
0.2
0.253
0.287
0.302
0.335
0.377
0.403
0.425
0.455
0.485
0.5
0.529
0.557
0.59
0.628
0.65
0.668
0.71
0.74
0.772
0.8
0.835
0.871
0.893
0.911
0.926
0.941
0.95
0.973
0.982
0.991
1.000

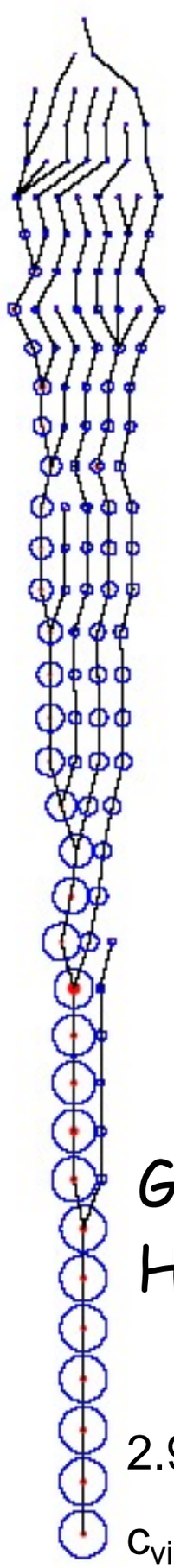

Cluster Halo

$2.8 \times 10^{14}\ M_{sun}/h$

$c_{vir} = 5.9$

Galaxy Halo

$2.9 \times 10^{12}\ M_{sun}/h$

$c_{vir} = 12.5$

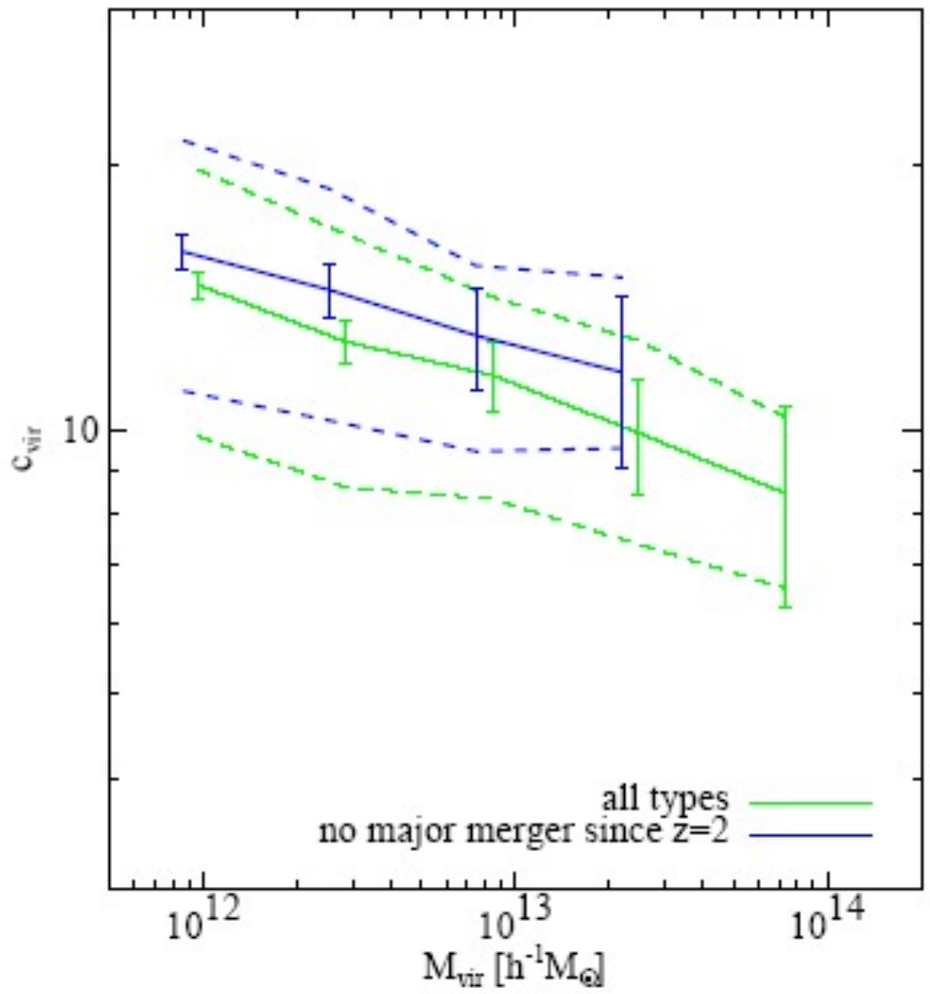

For halos without recent mergers, c_{vir} is higher and the scatter is reduced to log c_{vir} ≈ 0.10.

Wechsler et al. 2002

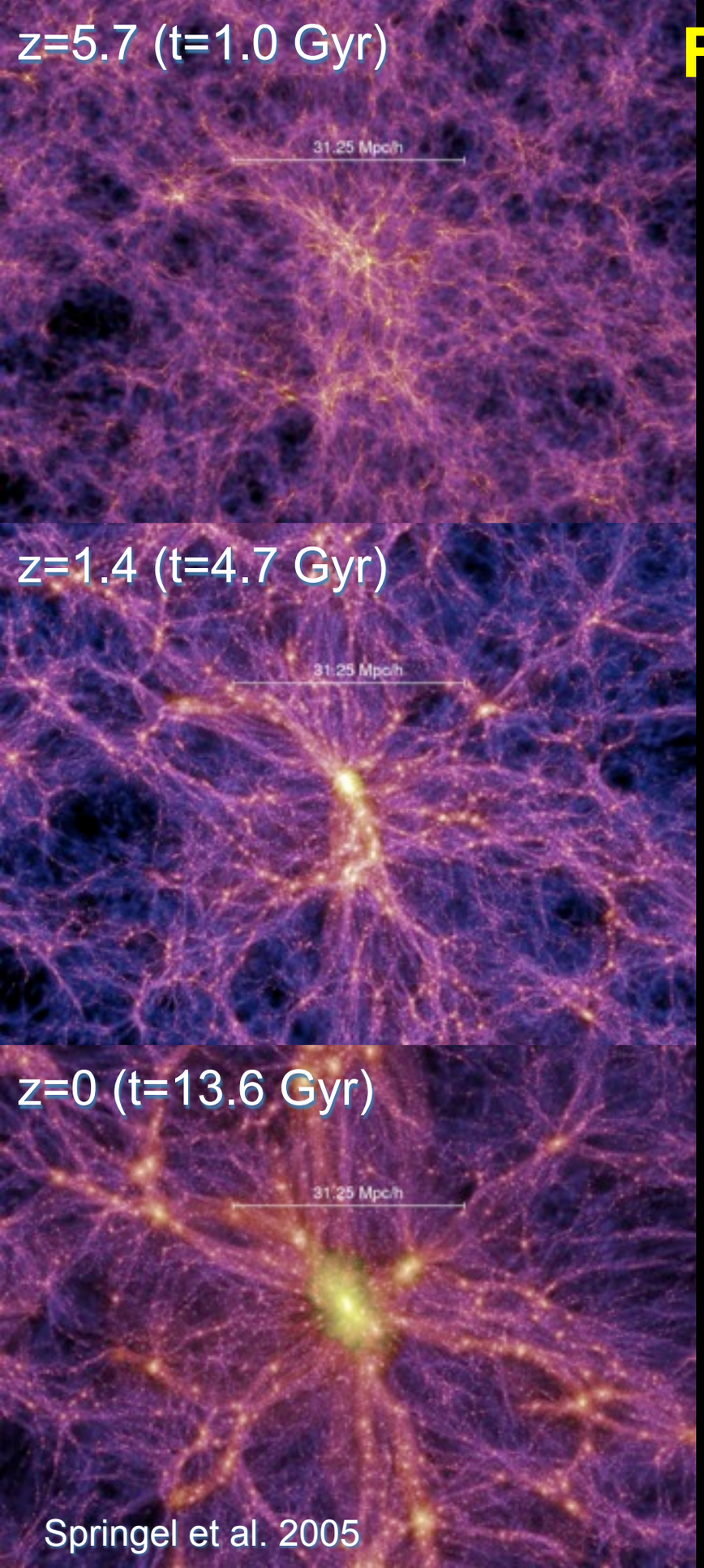

Forward Evolution

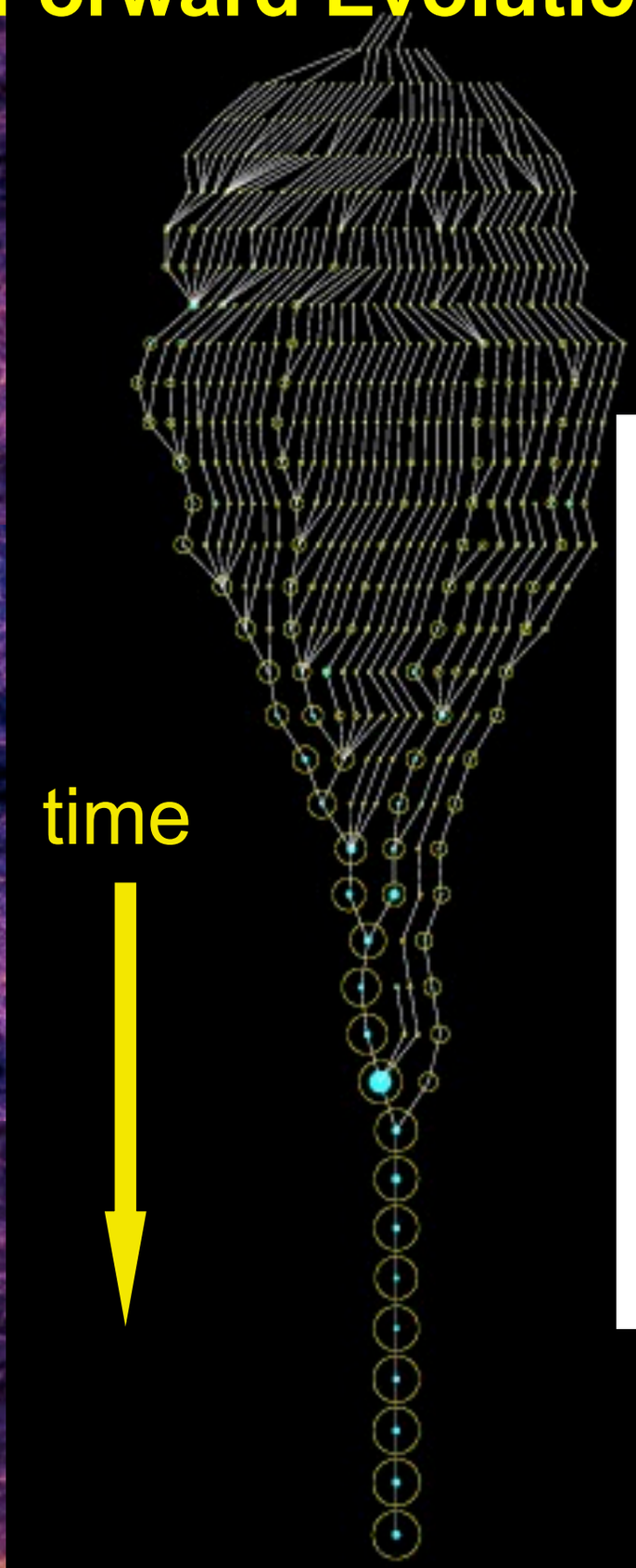

Present status of ΛCDM "Double Dark" theory:

- cosmological parameters are now well constrained by observations

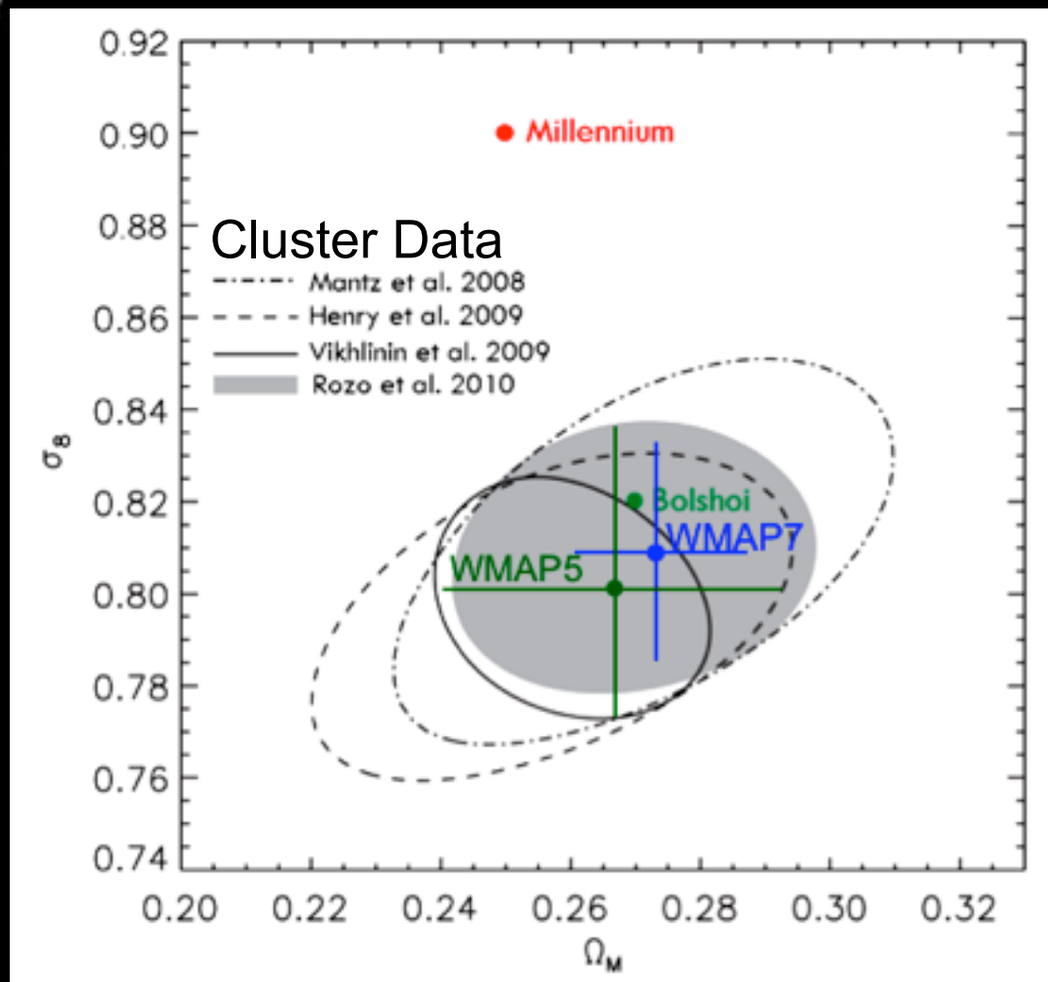

- mass accretion history of dark matter halos is represented by 'merger trees' like the one at left

Semi-Analytic Models of Galaxy Formation

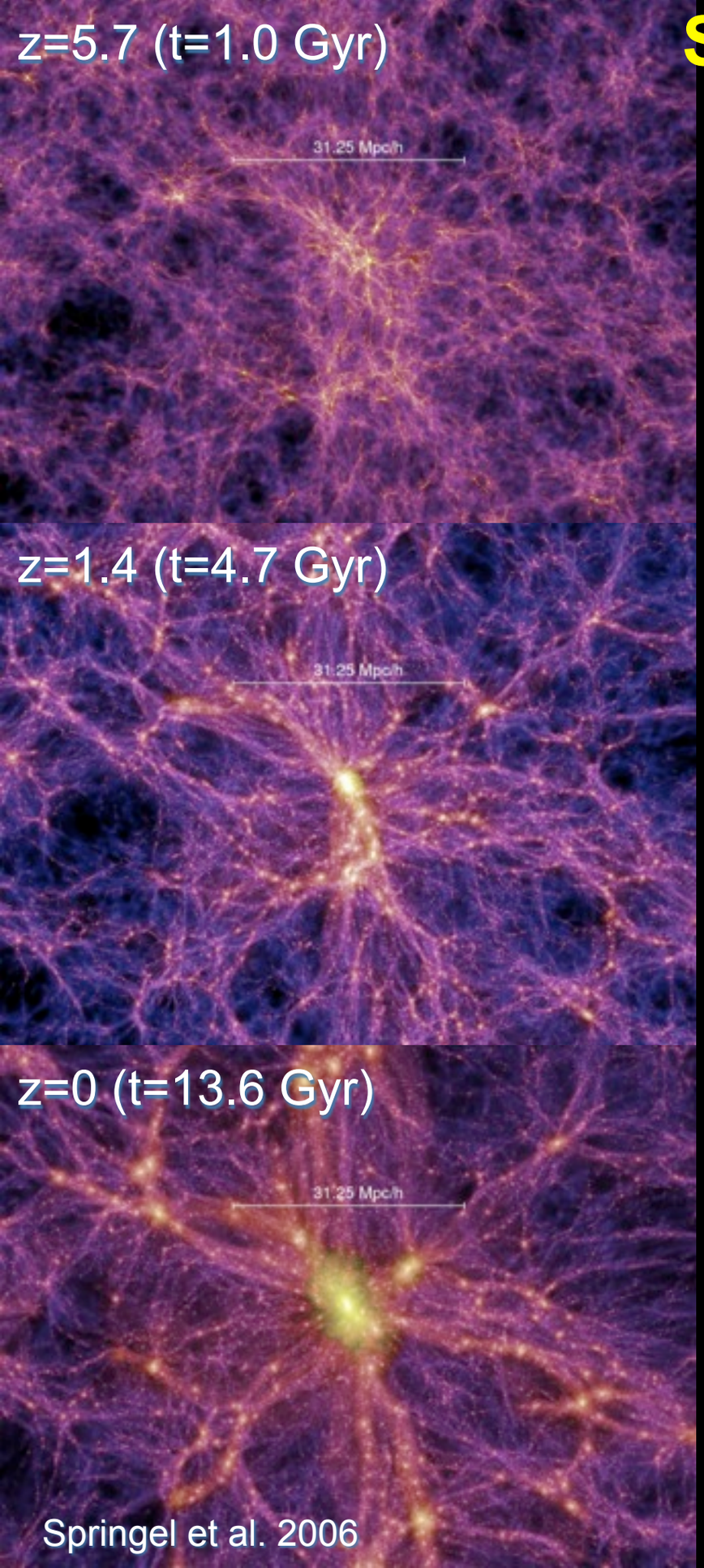

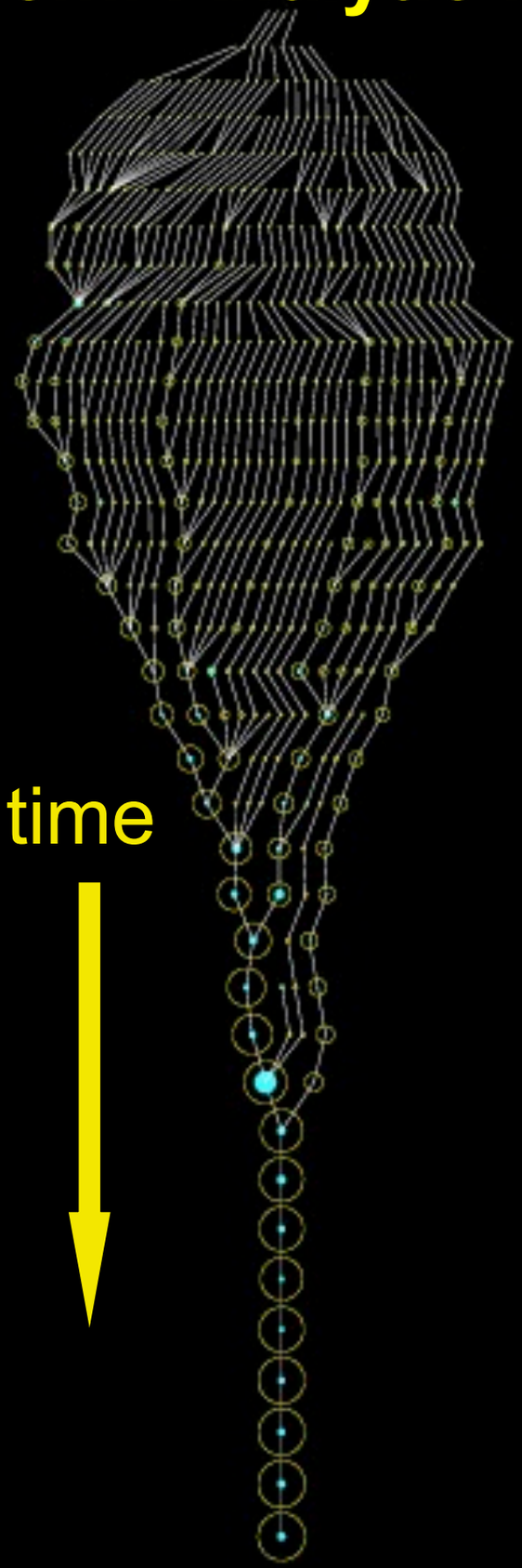

Astrophysical processes modeled:

- shock heating & radiative cooling
- photoionization squelching
- merging
- star formation (quiescent & burst)
- SN heating & SN-driven winds
- AGN accretion and feedback
- chemical evolution
- stellar populations & dust

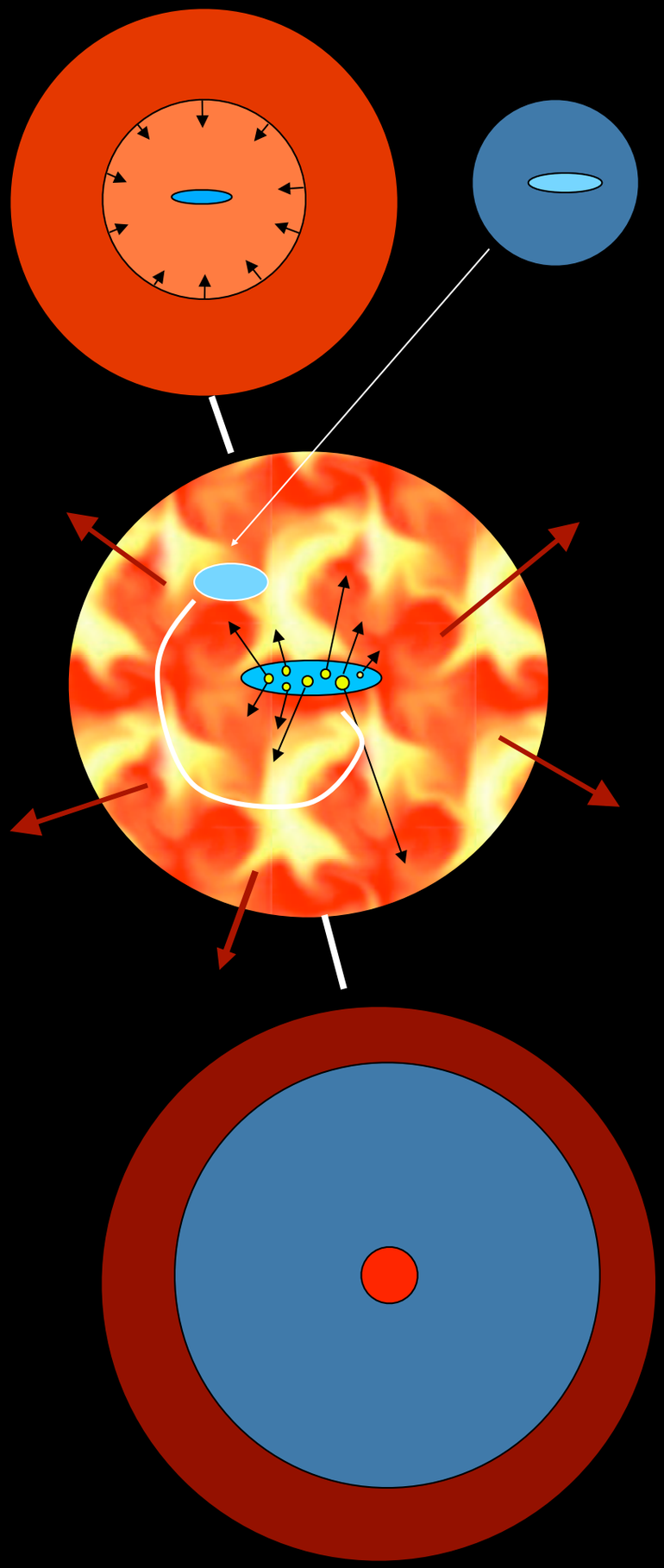

Galaxy Formation in ΛCDM

- gas is collisionally heated when perturbations ‘turn around’ and collapse to form gravitationally bound structures
- gas in halos cools via atomic line transitions (depends on density, temperature, and metallicity)
- cooled gas collapses to form a rotationally supported disk
- cold gas forms stars, with efficiency a function of gas density (e.g. Schmidt-Kennicutt Law)
- massive stars and SNae reheat (and in small halos expel) cold gas and some metals
- galaxy mergers trigger bursts of star formation; ‘major’ mergers transform disks into spheroids and fuel AGN
- AGN feedback cuts off star formation

White & Frenk 91; Kauffmann+93; Cole+94; Somerville & Primack 99; Cole+00; Somerville, Primack, & Faber 01; Croton et al. 2006; Somerville +08; Fanidakis+09; Somerville, Gilmore, Primack, & Dominguez 11

Frank Summers, STScI: “Cosmic Collisions Galore”

http://hubblesite.org/newscenter/archive/releases/2008/16/video/d/

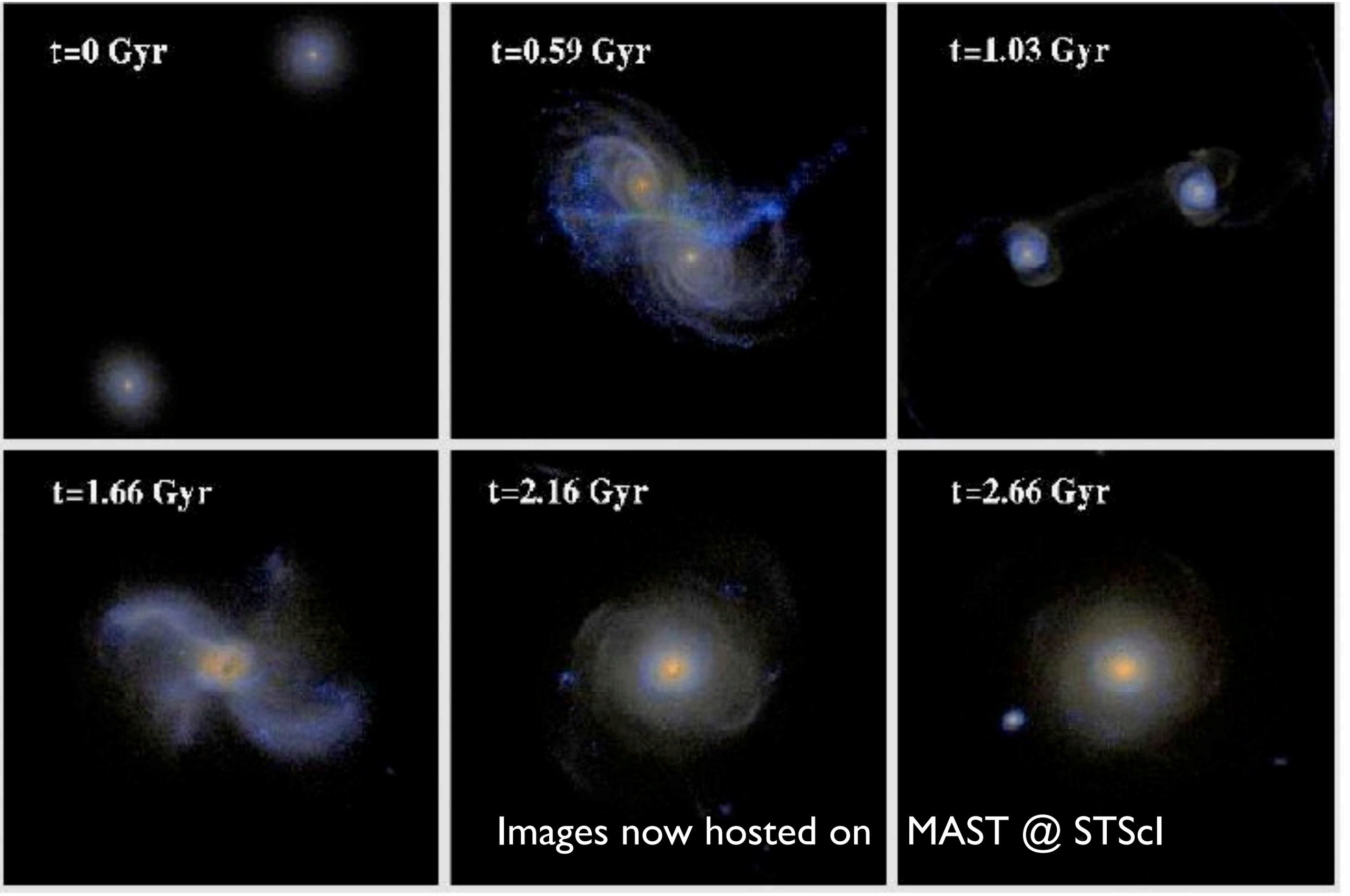

Lotz, Jonsson, Cox, Primack 2008 Galaxy Merger Morphologies and Time-Scales from Simulations analyzed to determine observability timescales using CAS, G-M_{20}, pairs ➙ merger rates

The Astrophysical Journal, 742:103 (22pp), 2011 December 1

THE MAJOR AND MINOR GALAXY MERGER RATES AT $z < 1.5$

Jennifer M. Lotz[1,2,9], Patrik Jonsson[3], T. J. Cox[4,10], Darren Croton[5], Joel R. Primack[6], Rachel S. Somerville[2,7], and Kyle Stewart[8,11]

ABSTRACT

Calculating the galaxy merger rate requires both a census of galaxies identified as merger candidates and a cosmologically averaged "observability" timescale $\langle T_{\rm obs}(z)\rangle$ for identifying galaxy mergers. While many have counted galaxy mergers using a variety of techniques, $\langle T_{\rm obs}(z)\rangle$ for these techniques have been poorly constrained. We address this problem by calibrating three merger rate estimators with a suite of hydrodynamic merger simulations and three galaxy formation models. We estimate $\langle T_{\rm obs}(z)\rangle$ for (1) close galaxy pairs with a range of projected separations, (2) the morphology indicator $G - M_{20}$, and (3) the morphology indicator asymmetry A. Then, we apply these timescales to the observed merger fractions at $z < 1.5$ from the recent literature. When our physically motivated timescales are adopted, the observed galaxy merger rates become largely consistent. The remaining differences between the galaxy merger rates are explained by the differences in the ranges of the mass ratio measured by different techniques and differing parent galaxy selection. The major merger rate per unit comoving volume for samples selected with constant number density evolves much more strongly with redshift ($\propto (1+z)^{+3.0\pm1.1}$) than samples selected with constant stellar mass or passively evolving luminosity ($\propto (1+z)^{+0.1\pm0.4}$). We calculate the minor merger rate (1:4 $< M_{\rm sat}/M_{\rm primary} \lesssim$ 1:10) by subtracting the major merger rate from close pairs from the "total" merger rate determined by $G - M_{20}$. The implied minor merger rate is ~3 times the major merger rate at $z \sim 0.7$ and shows little evolution with redshift.

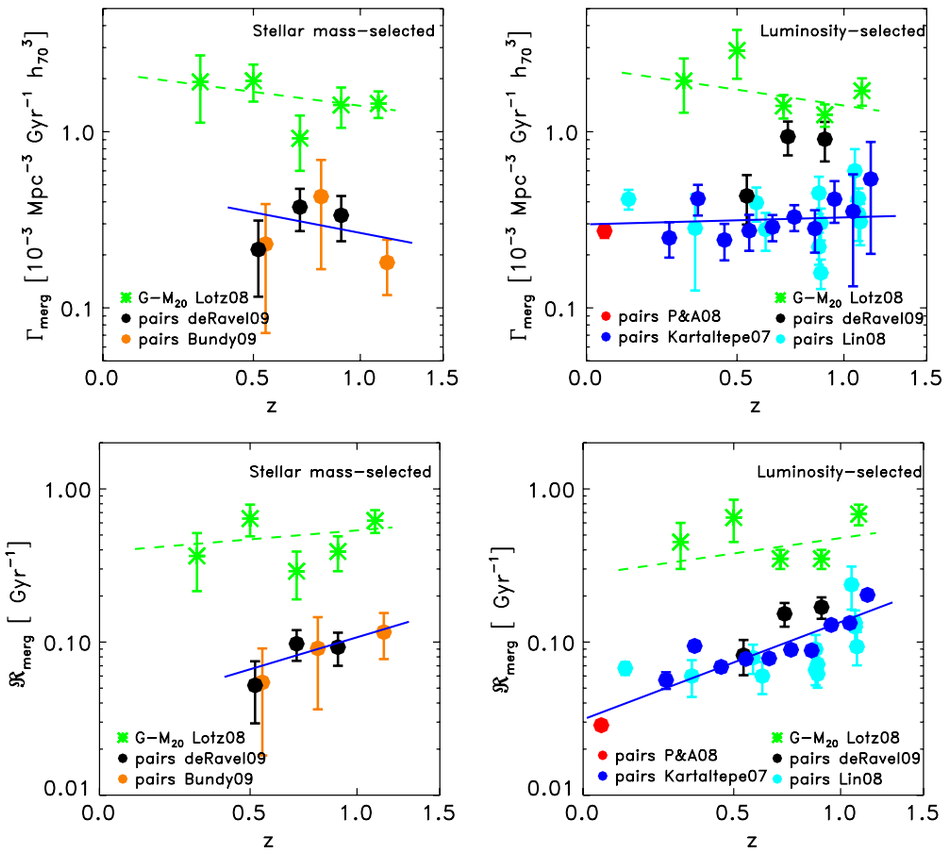

Figure 10. Top: $\Gamma_{\rm merg}$, the merger rate per comoving unit volume, for close pairs (circles) and G – M20 (asterisks), for stellar-mass-selected (left) and rest-frame luminosity-selected samples. Bottom: $R_{\rm merg}$, the fractional merger rate, for close pairs (circles) and G – M20 (asterisks), for the same samples. The error bars are computed using the observational uncertainties on $f_{\rm merg}$, $f_{\rm pair}$, and $n_{\rm gal}$ and do not include uncertainties in $\langle T_{\rm obs}\rangle$. G – M20 probes both major and minor mergers, and therefore captures a "total" merger rate, which is several times higher than the major merger rate probed by these close pair studies. The evolution in $\Gamma_{\rm pairs}(z)$ is weaker than in $R_{\rm pairs}(z)$ because $f_{\rm pairs}$ increases with redshift (Figure 1) while the corresponding $n_{\rm gal}$ decreases with redshift for fixed stellar mass and PLE galaxy selections (Figure 2). The best-fit slopes for the close pair (major) merger rates (blue solid lines) are given in Section 5.1 and the best slopes for the G – M20 (total) merger rates (green dashed lines) are given in Section 5.2.

Baryons in Dark Matter Halos

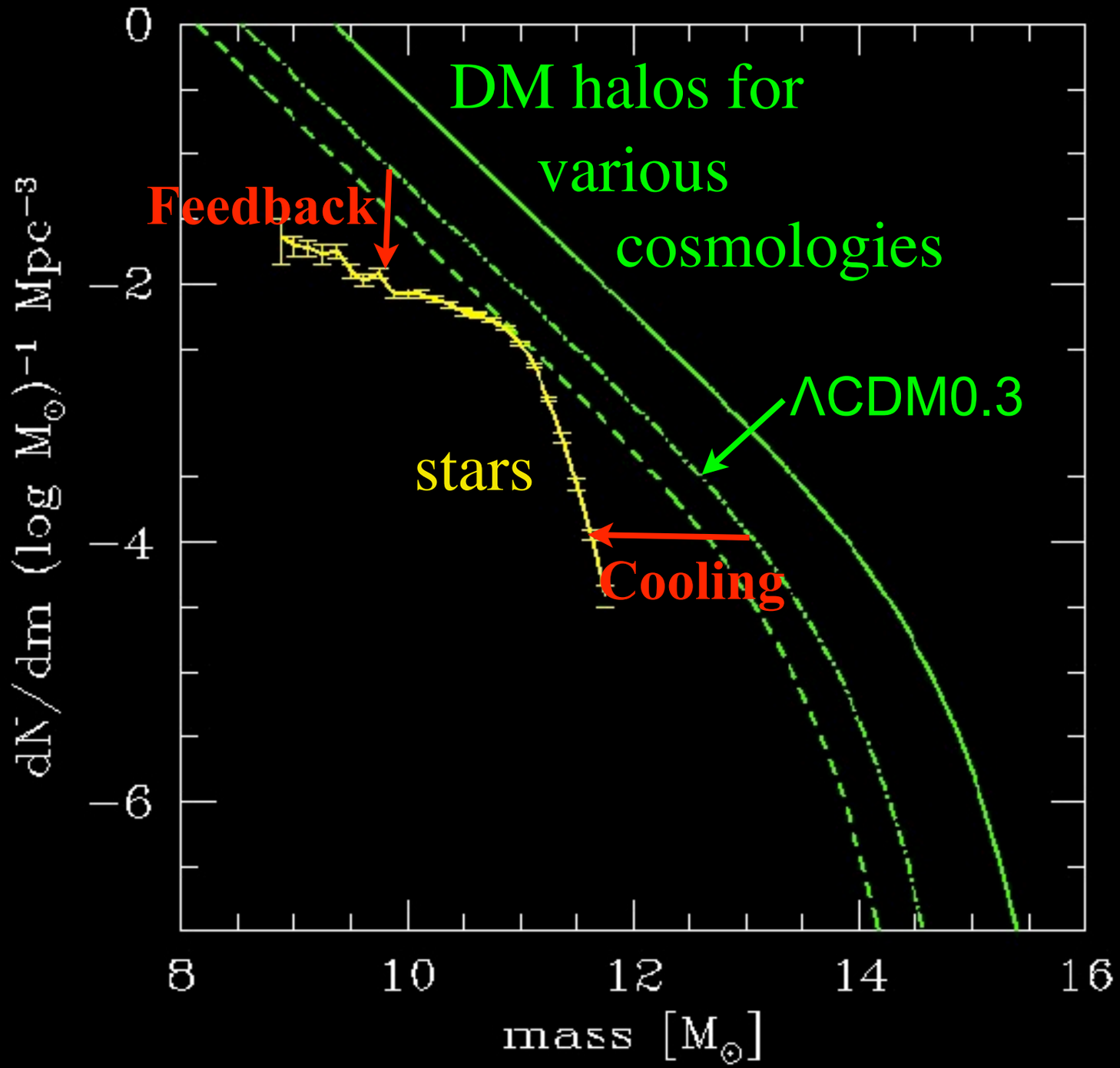

- in order to reconcile CDM (sub)halo mass function with galaxy LF or stellar MF, cooling/star formation must be inefficient overall, most efficient at $M_{halo} \sim 10^{11}\ M_{sun}$
- baryon/DM ratio must be a strongly non-linear (& non-monotonic) function of halo mass

Somerville & Primack 1999; cf. Benson et al. 2003

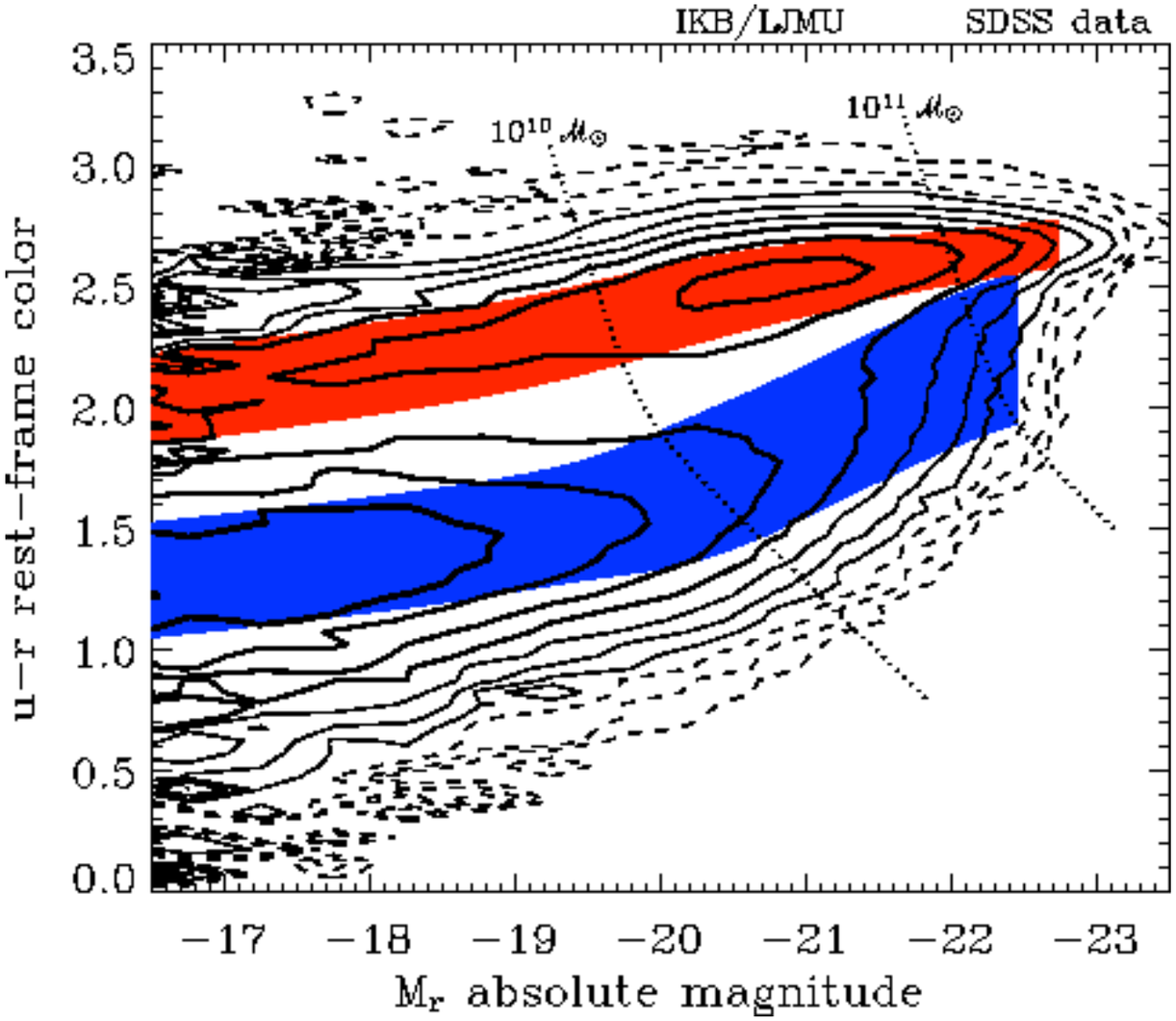

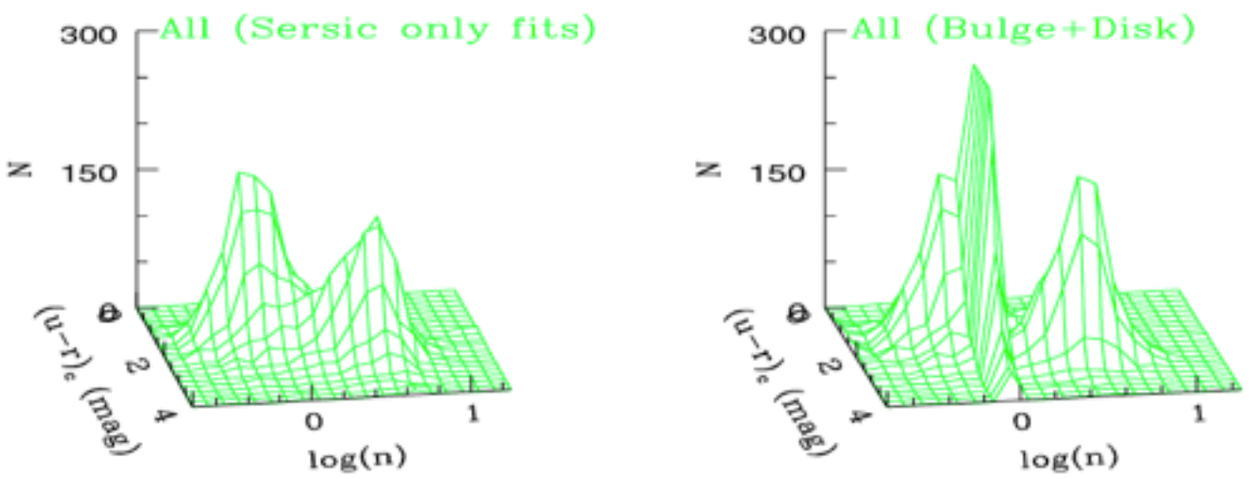

Galaxy bimodality in the color-structure plane (S. Driver et al. 2006)

Color bimodality of galaxies on color-magnitude plot from Baldry et al. (2004). The black solid and dashed contours represent the number density of galaxies: logarithmically spaced with four contours per factor of ten. The distribution is bimodal: there are two peaks corresponding to a red sequence (generally early types) and a blue sequence (late types).

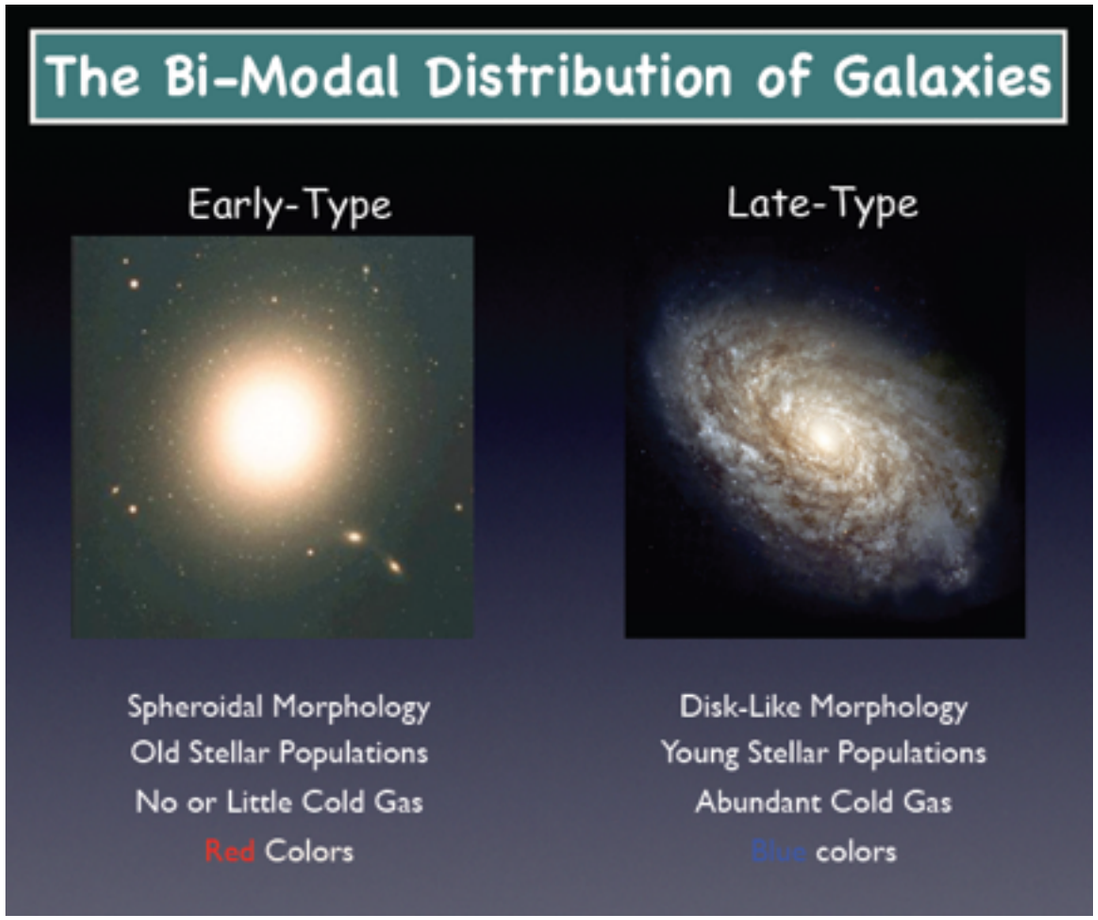

Flow through the color-mass diagram for "central" galaxies

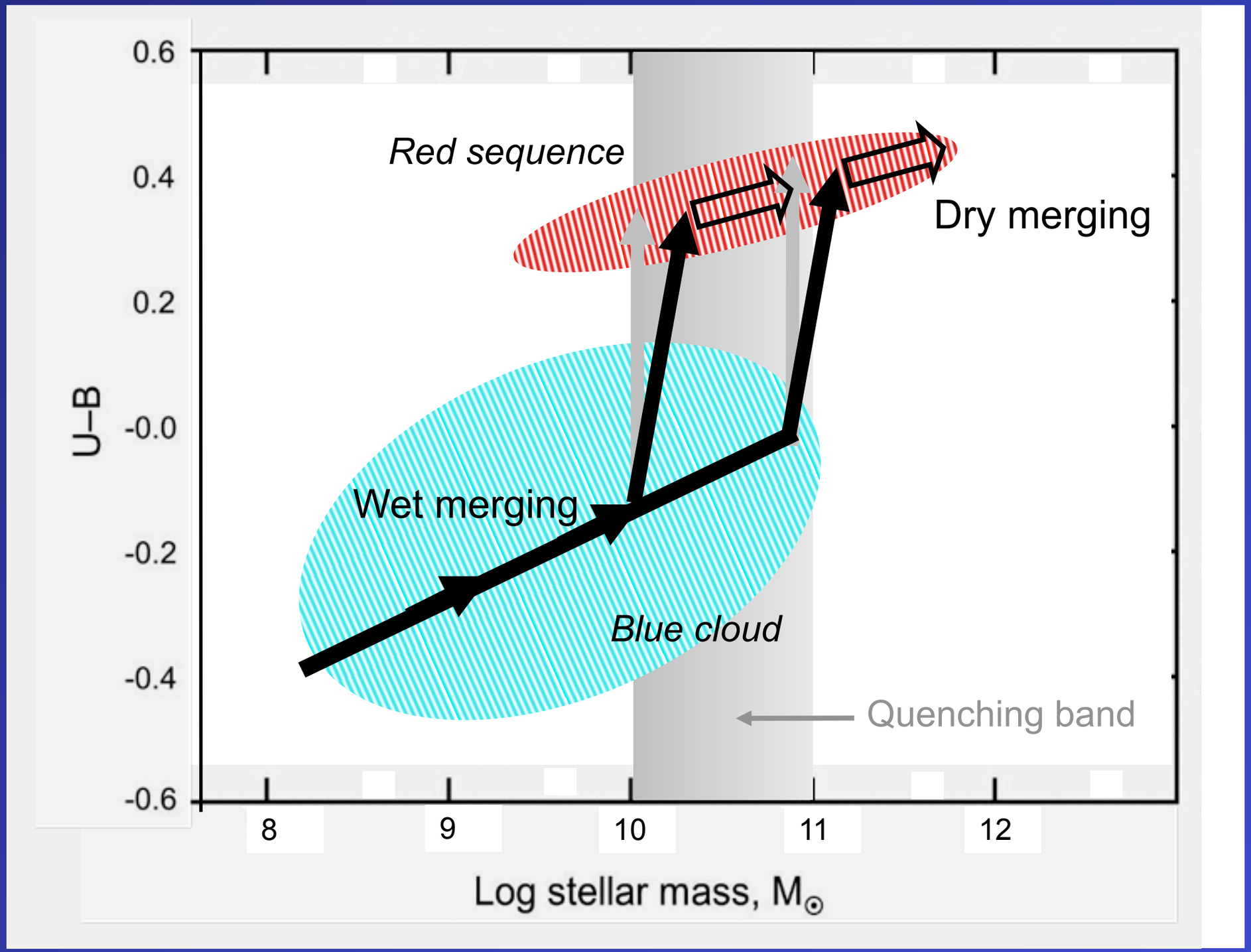

Sandra Faber

Flow through the color-mass diagram for "satellite" galaxies

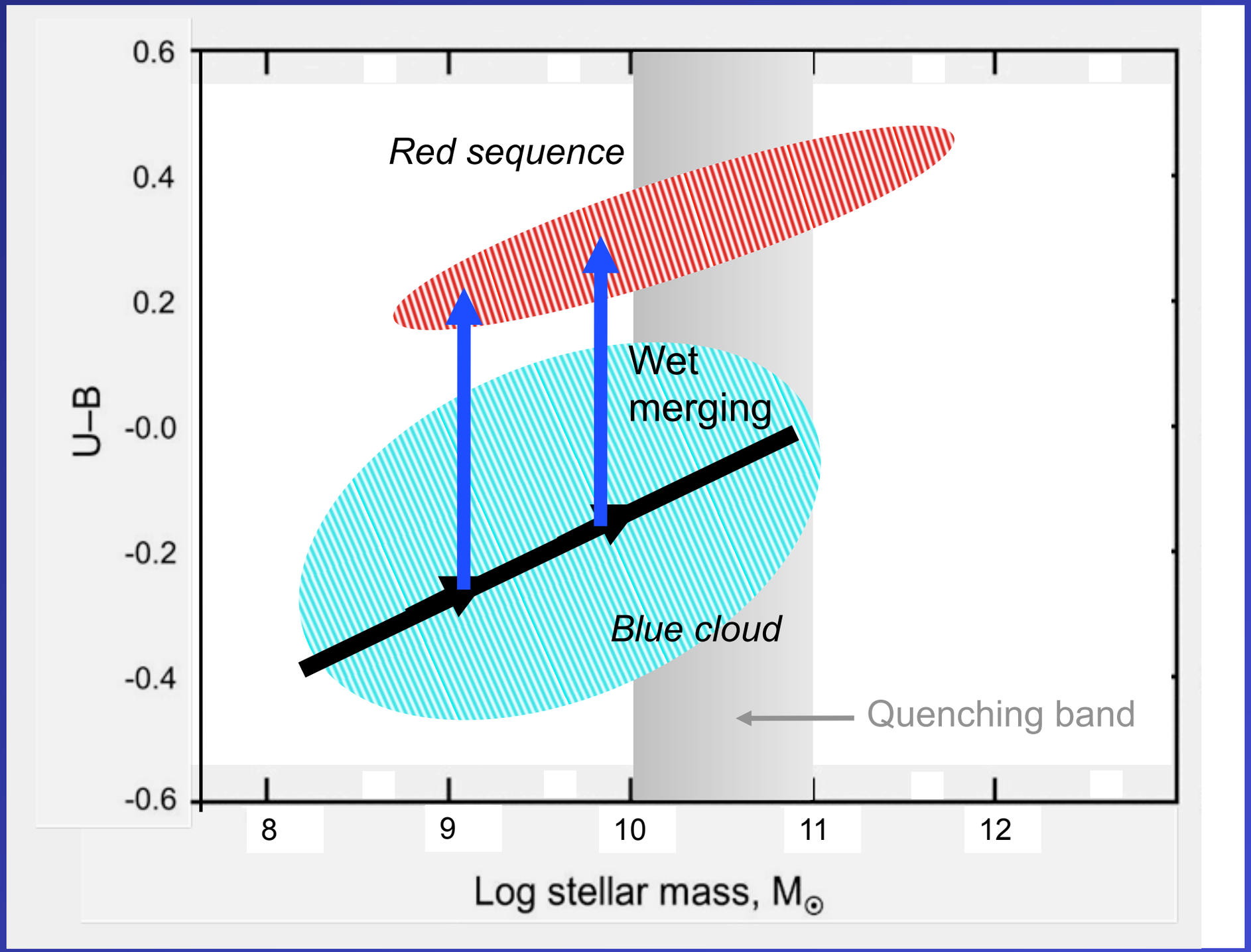

Sandra Faber

Flow through the CM diagram versus environment

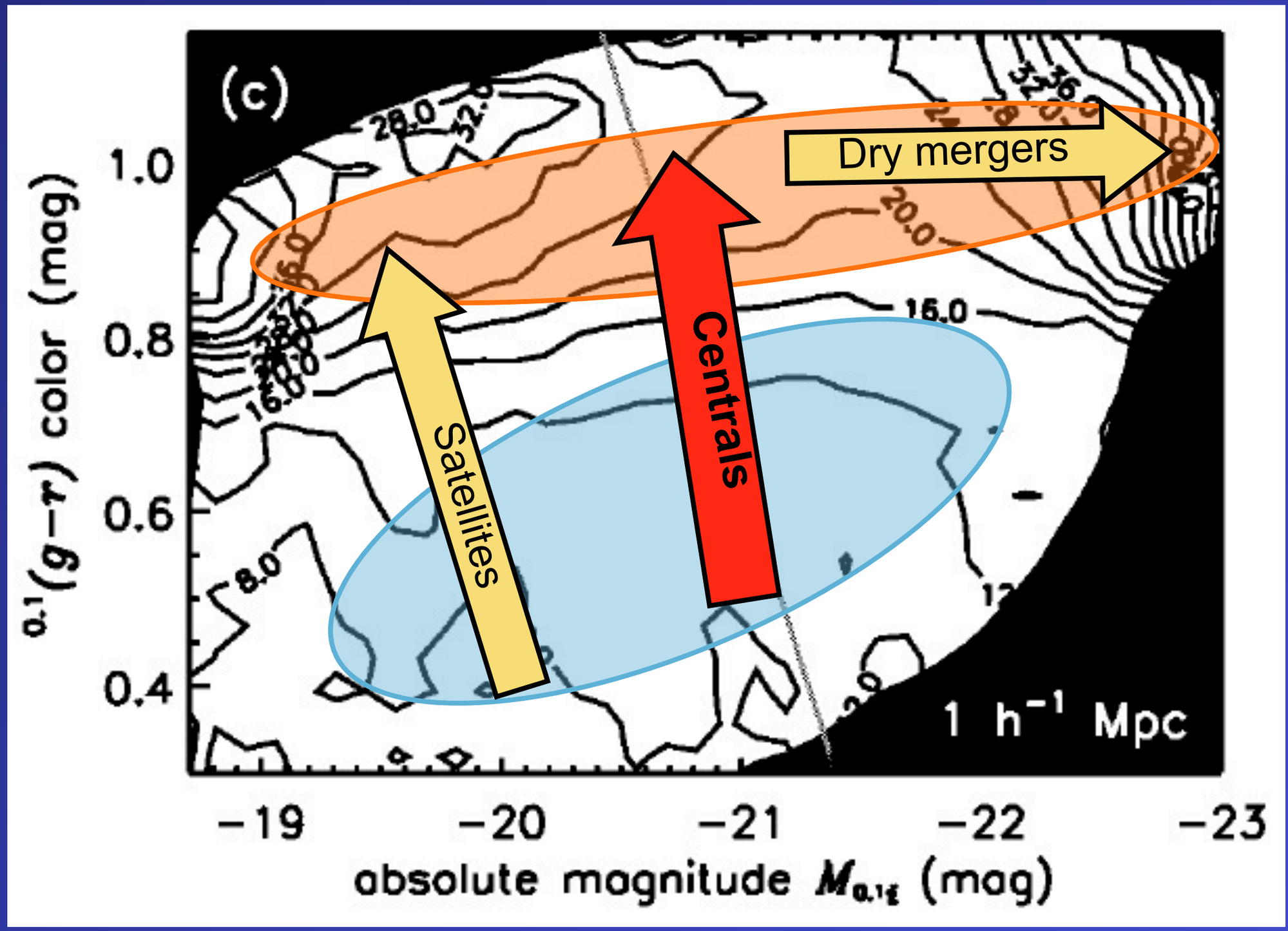

Hogg et al. 2003: Sloan Survey

All formed by environment

BH not avail?

$M_i^{0.1} = -19.3$

Transition mass $3 \times 10^{10}\ M_\odot$

$M_i^{0.1} \sim -21.0$

Satellite/Central wet/dry transition

$M_i^{0.1} > -22.1$

All boxy/dry

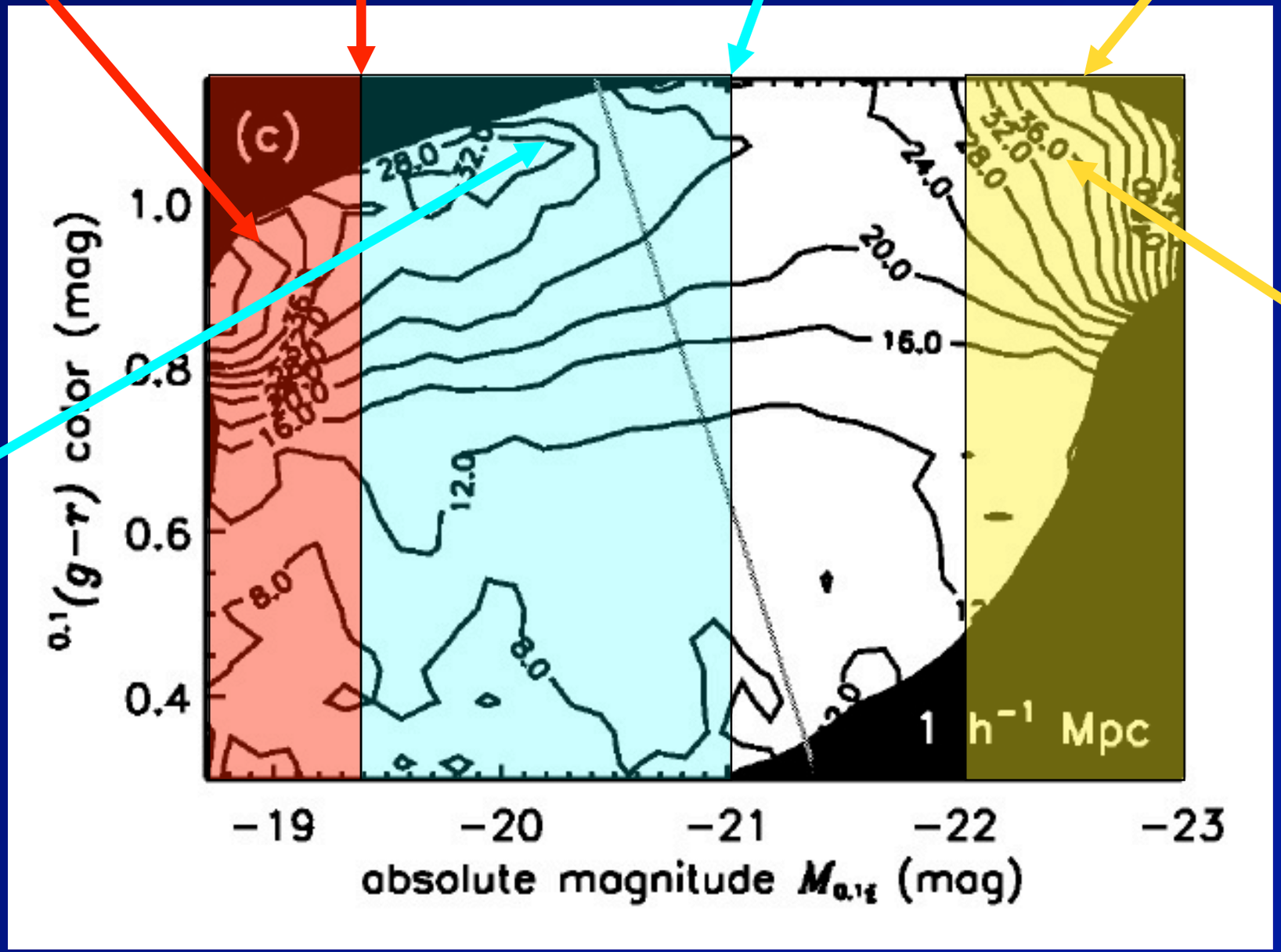

Some by env, some by wet mergers

All by dry mergers

Sandra Faber

New Improved Semi-Analytic Models Work!

- Earlier CDM-based galaxy formation models suffered from a set of interlinked problems
  - overcooling/cooling flow problems in galaxies and clusters
  - failure to produce observed color bimodality
- 'Bright mode' AGN feedback may regulate BH formation & temporarily quench star formation, but is not a viable 'maintenance' mechanism
- Low-accretion rate 'radio mode' feedback is a promising mechanism for counteracting cooling flows over long time scales
- New self-consistent 'hybrid' models based on physical scaling from numerical simulations and calibrated against empirical constraints now enable us to predict/ interpret the relationship between galaxies, BH, and AGN across cosmic history

-- Rachel Somerville

Some Results from our Semi-Analytic Models

z=0-2 Luminosity Density

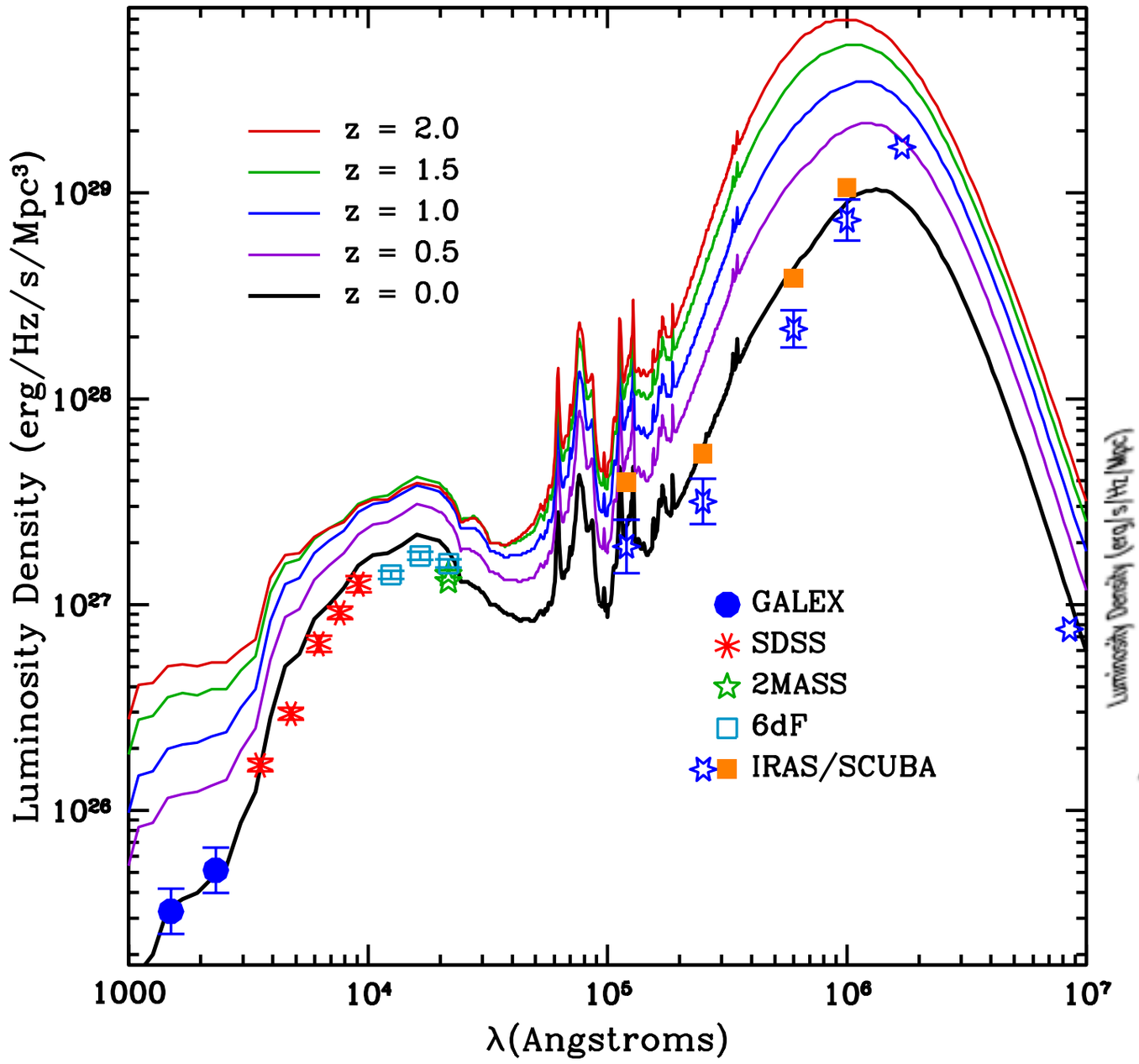

Somerville, Gilmore, Primack, & Dominguez (2012)

z=0-8 Luminosity Density

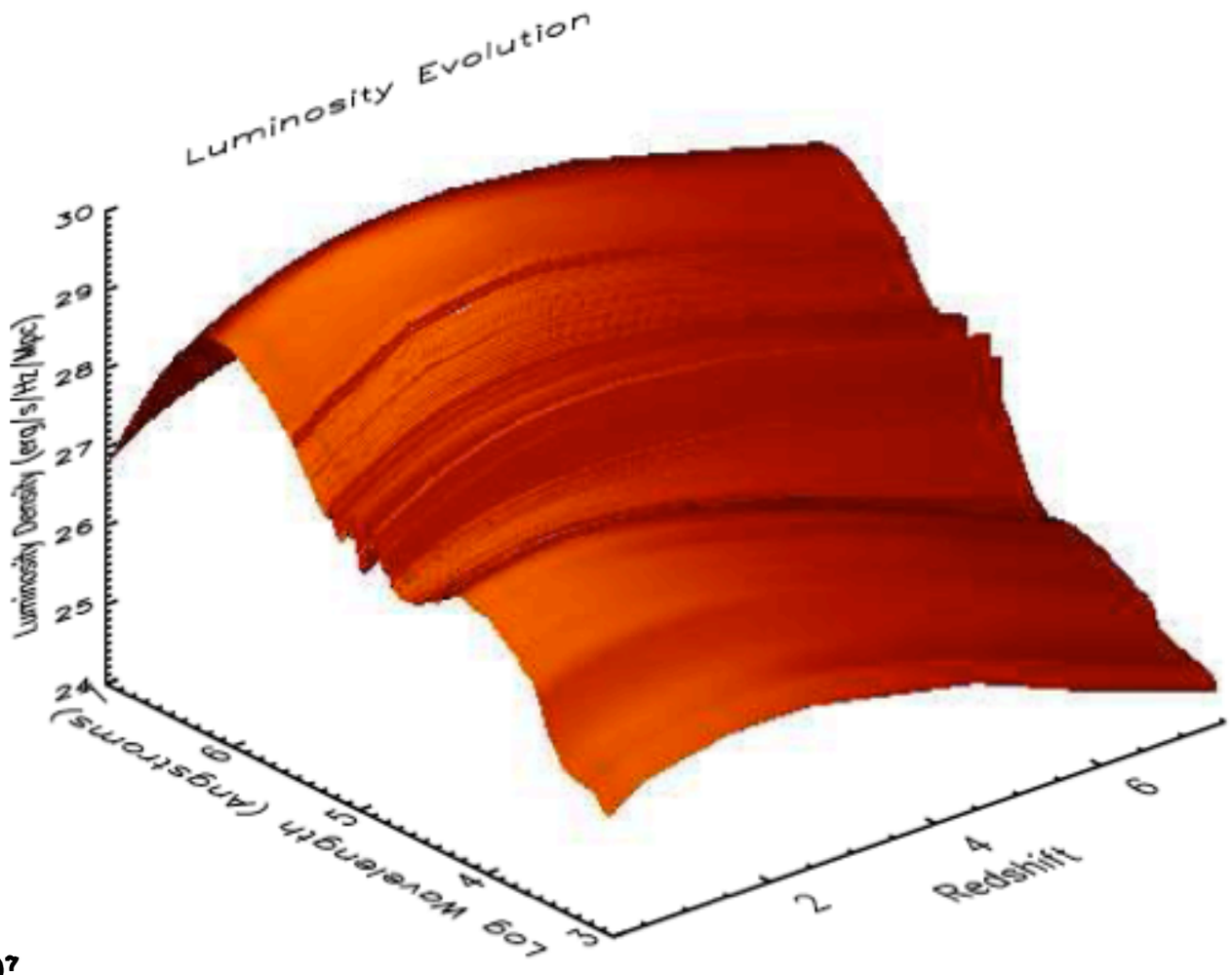

Gilmore, Somerville, Primack, & Dominguez (2012)

Results from our Semi-Analytic Models

An advantage of the SAM approach is that it is possible to compare predictions with observations at all redshifts and in all spectral bands.

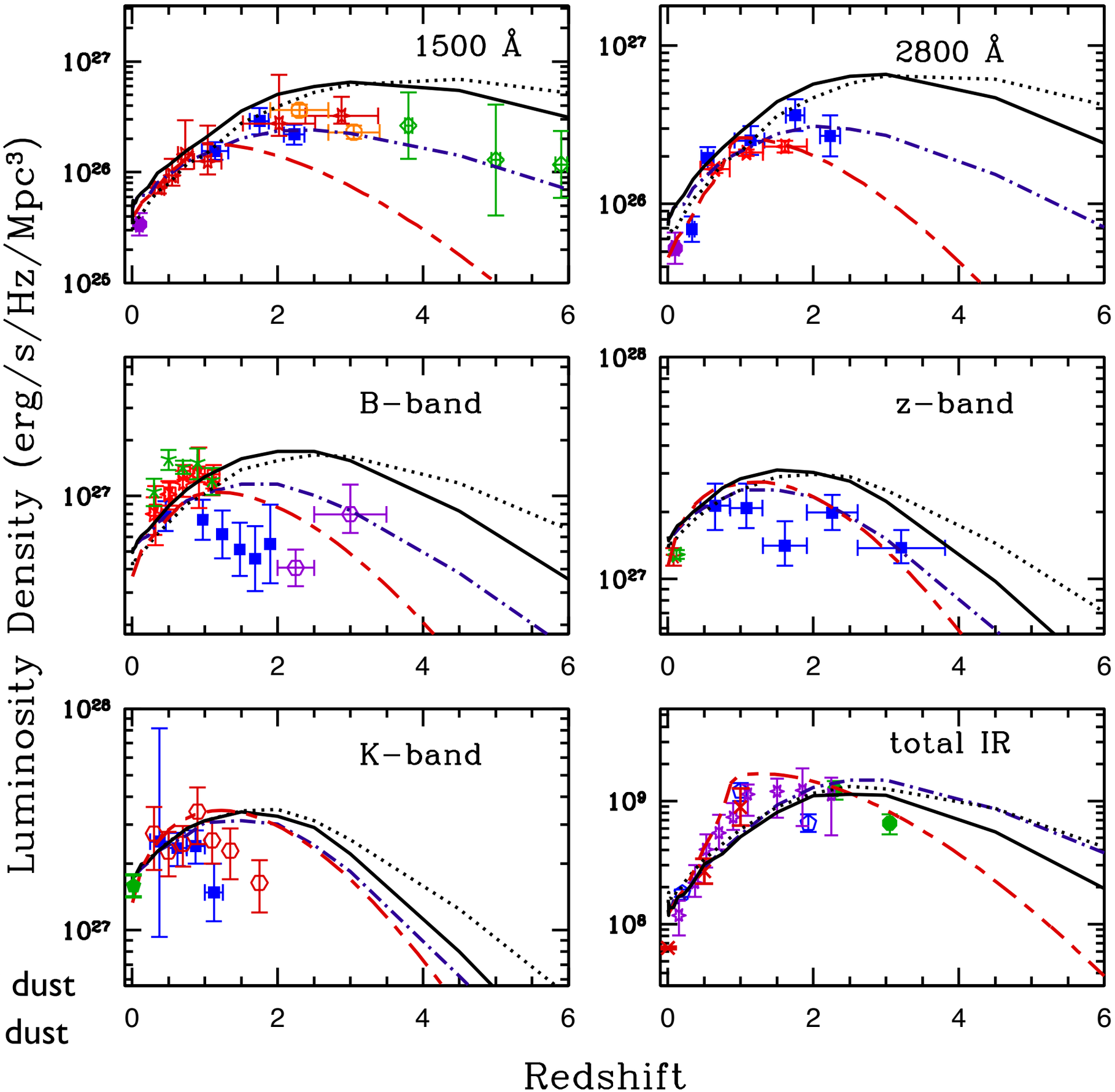

Gilmore, Somerville, Primack, & Dominguez (2012)

Some Results from our Semi-Analytic Models

z=0 Luminosity Functions

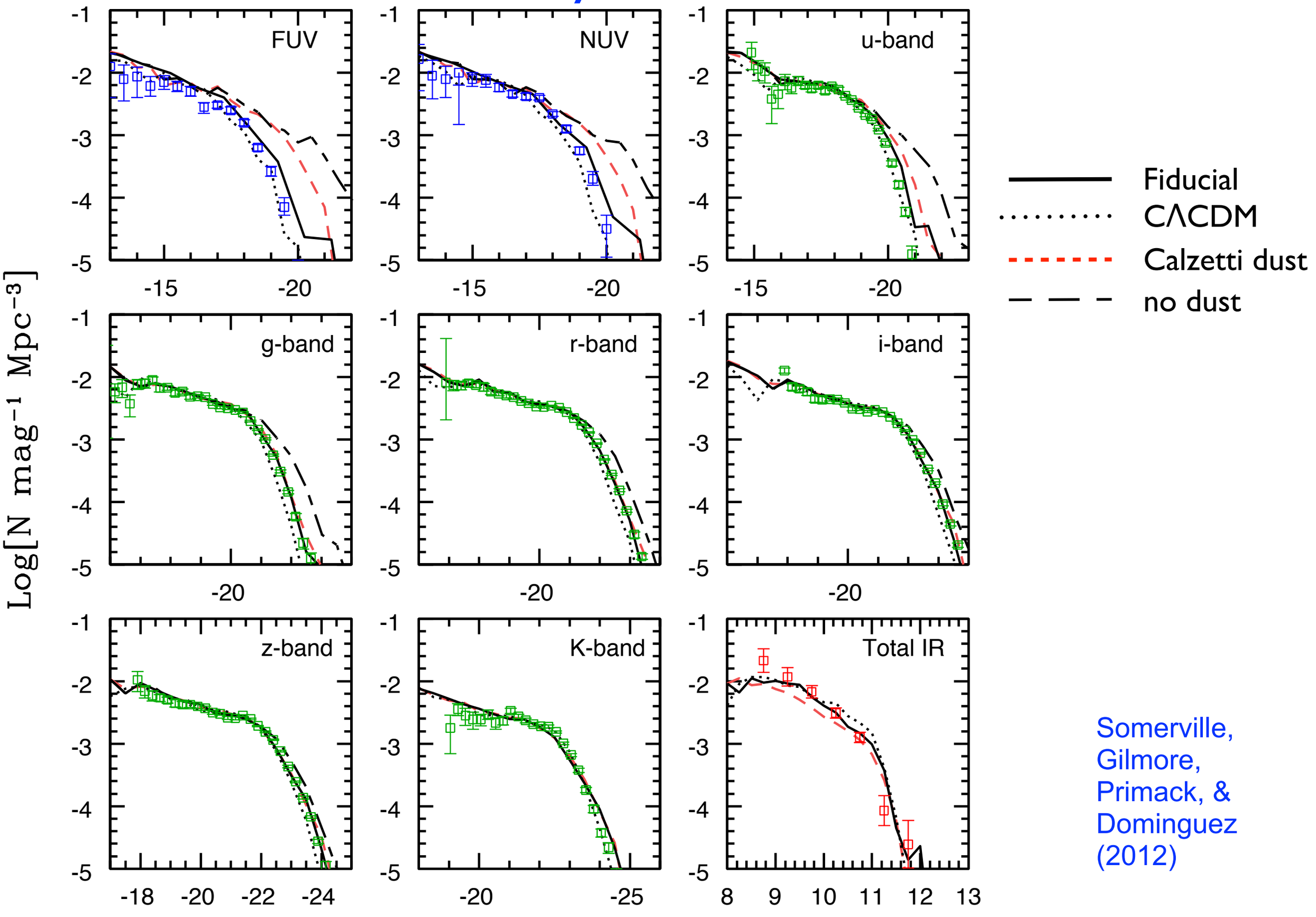

Somerville, Gilmore, Primack, & Dominguez (2012)

Some Results from our Semi-Analytic Models

Number Counts in UV, b, i, z, K Bands

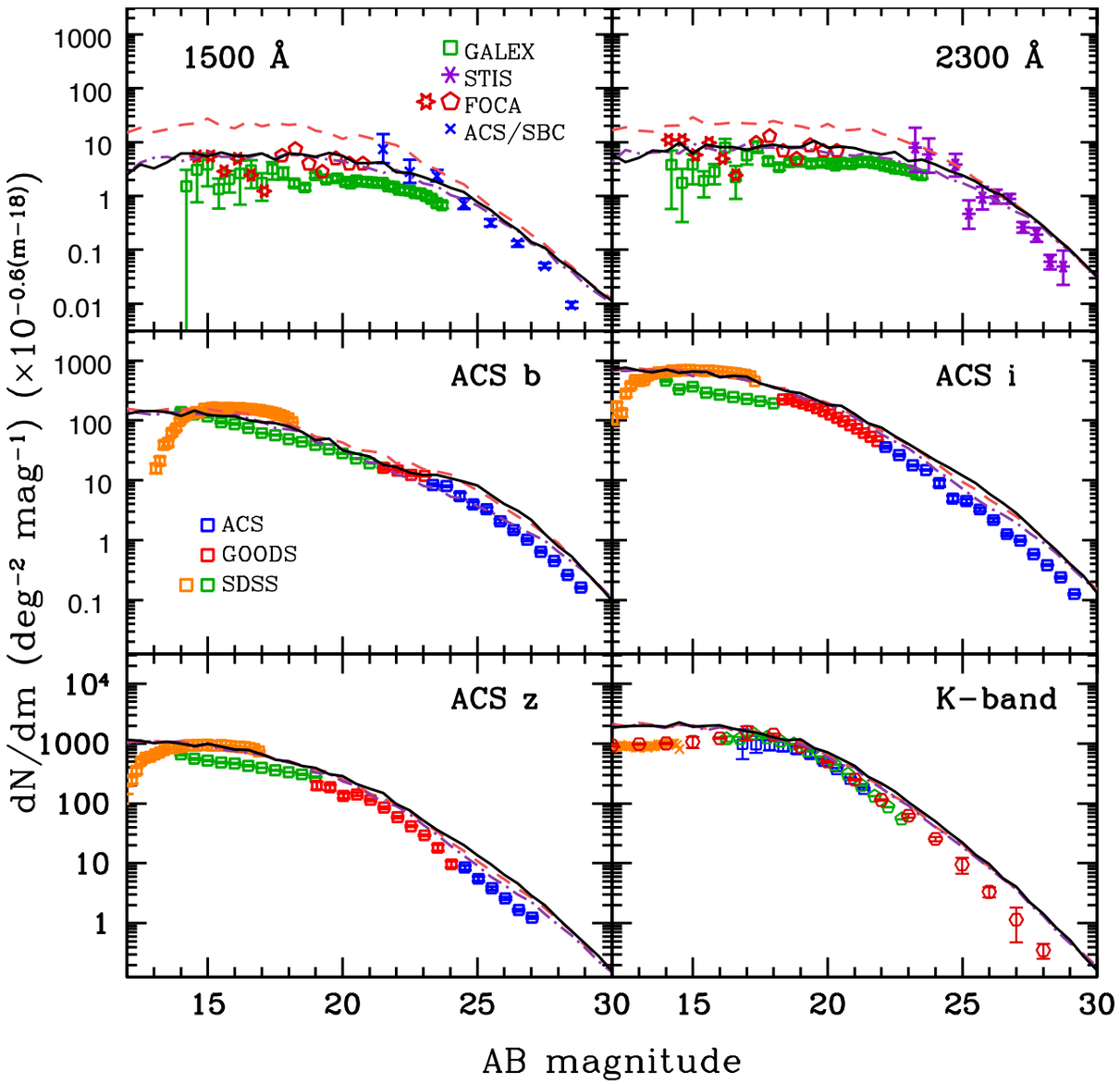

Number Counts in 3.6, 8, 24, 70, 250, & 850 μm Bands

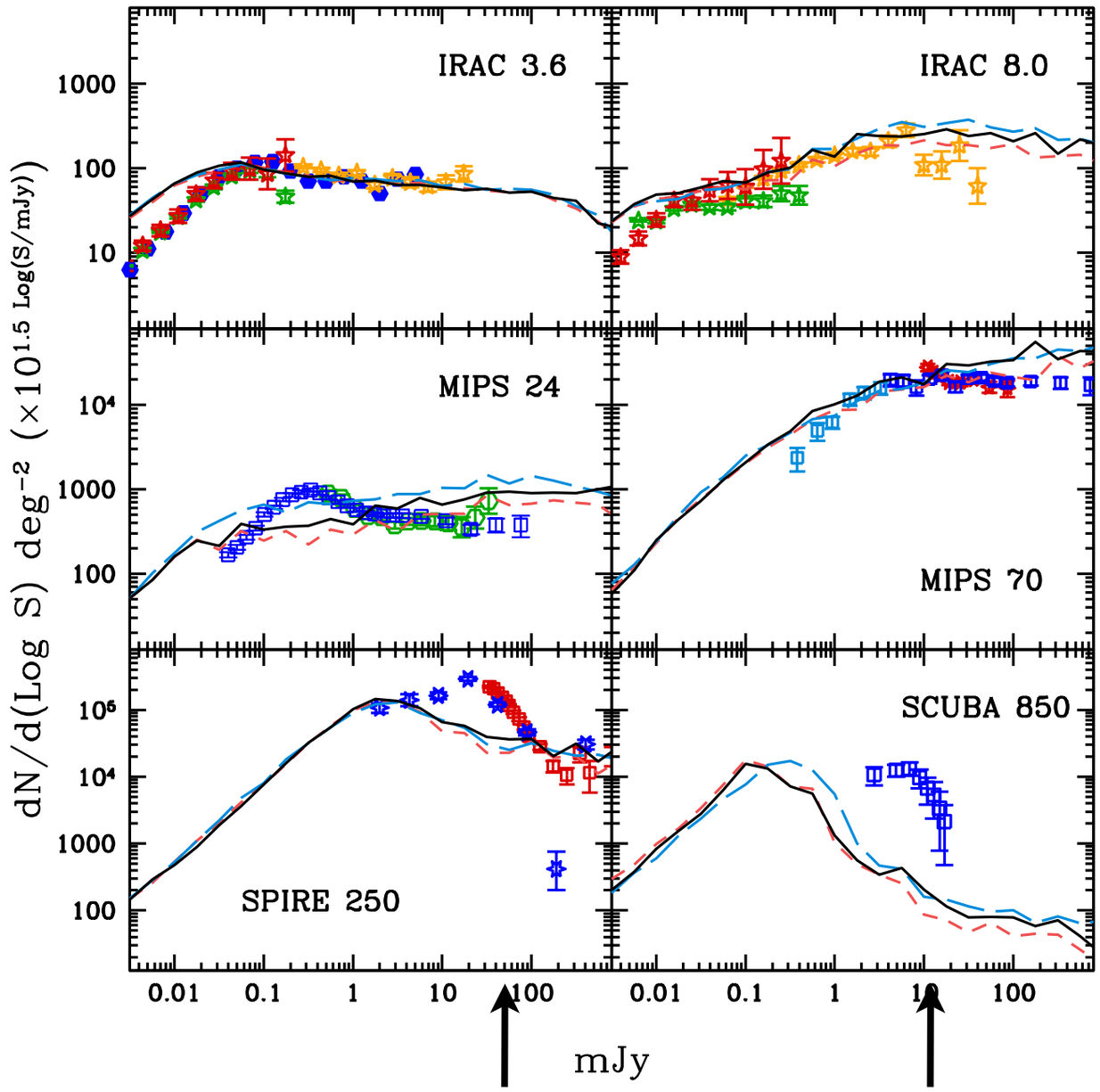

Somerville, Gilmore, Primack, & Dominguez (2012)

Far-IR problems

EBL Observations & Theory

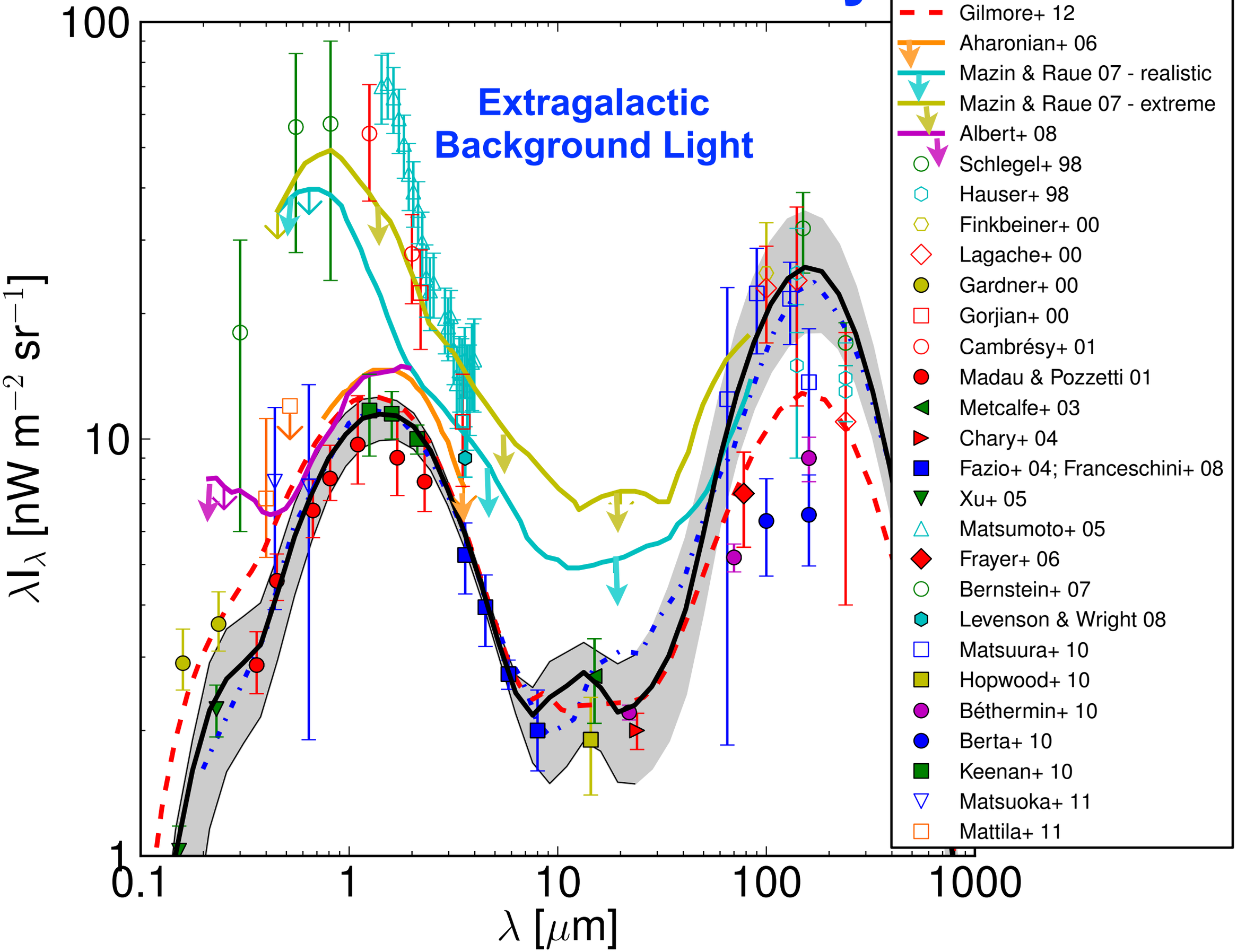

EBL Evolution

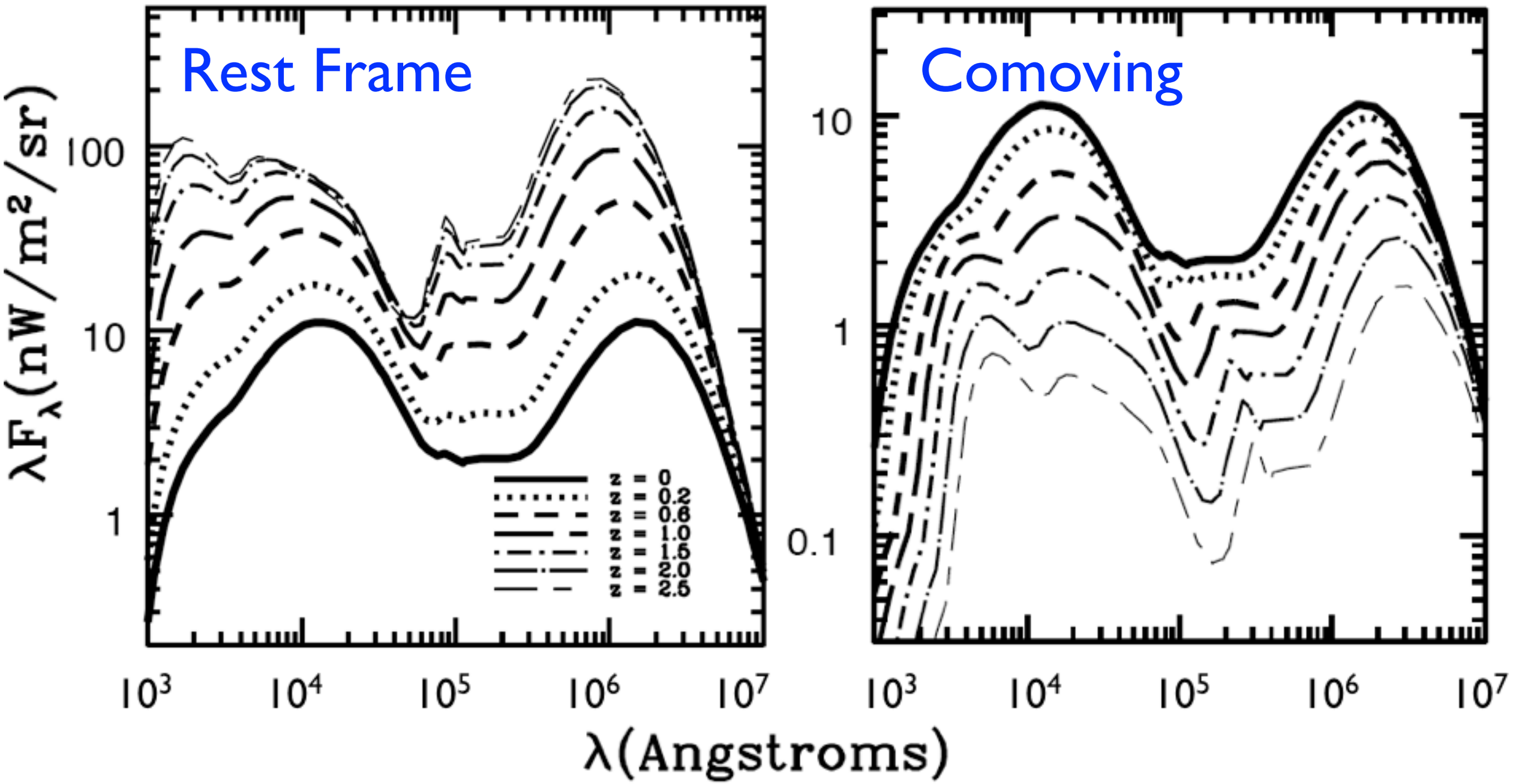

The evolution of the EBL in our WMAP5 Fiducial model. This is plotted on the left panel in standard units. The right panel shows the build-up of the present-day EBL by plotting the same quantities in comoving units. The redshifts from 0 to 2.5 are shown by the different line types in the key in the left panel.

Gilmore, Somerville, Primack, & Dominguez (2012)